Aalborg **UNIVERSITY**

Diffusion a

Diffusion and Evaporation-Controlled Emission in Ventilated Rooms

Claus Topp

Thesis No 11

Indoor Environmental Engineering

Department of Building Technology and Structural Engineering

ISSN 1395-7953 R9917

This thesis is accepted for the degree of Doctor of Philosophy at the Faculty of Engineering and Science, Aalborg University, Denmark. Defended publicly at Aalborg University March 17, 1999.

Supervisors:
Peter V. Nielsen, Professor, Aalborg University, Denmark
Per Heiselberg, Associate Professor, Aalborg University, Denmark

Adjudication Committee:
Alois Schälin, Eidgenössische Technische Hochschule, Zürich, Switzerland
Peter A. Nielsen, Senior Researcher, Danish Building Research Institute, Denmark
Kjeld Svidt, Research Associate Professor, Aalborg University, Denmark

Printed at Aalborg University

Diffusion and Evaporation-Controlled Emission in Ventilated Rooms

Claus Topp

Thesis No 11

Indoor Environmental Engineering

Department of Building Technology and Structural Engineering

ISSN 1395-7953 R9917

PREFACE

This thesis is submitted in accordance with the conditions for attaining the Danish PhD degree.

It represents the conclusion of my Ph.D.-study at the Department of Building Technology and Structural Engineering, Aalborg University. Professor Peter V. Nielsen and associate professor Per Heiselberg supervised the study.

The study was carried out from December 1, 1995 to November 30, 1998 and has been supported financially by Aalborg University.

I would like to express my thanks to professor Peter V. Nielsen and associate professor Per Heiselberg for their guidance and advice which I highly appreciated.

I also extend my thanks to Dr. Leslie E. Sparks, Elizabeth M. Howard, Mark A. Mason, Kelly W. Leovic and the rest of the staff at the Indoor Environmental Management Branch for their hospitality and support during my stay at the United States Environmental Protection Agency, Research Triangle Park, North Carolina.

I want to thank colleagues and members of the technical staff at the Department of Building Technology and Structural Engineering, Aalborg University, for their assistance during my study. Especially, I want to thank Bente Jul Kjærgaard for linguistic support.

Finally, I want to thank Mette for her patience and support.

Claus Topp

February 1999

ABSTRACT

In emission studies reported in literature little effort has been made to investigate the emission from building materials in ventilated enclosures from a fluid dynamics point of view. Furthermore, most of the existing emission models are empirical relations that are based on specific pollutants and sources.

This work provides an investigation based on fundamental fluid dynamics and mass transfer theory to obtain a general understanding of the mechanisms involved in the emission from building materials in ventilated rooms. In addition, a generally applicable model for prediction of surface emission is proposed.

The interest has been focused on the emission of vapours and gases as no particulate emissions have been considered. The methods used are numerical calculations by computational fluid dynamics (CFD) and full-scale laboratory experiments.

It was found that the emission is a strong function of air change rate, local air velocity and local turbulence intensity as the mass transfer coefficient increases in proportion to these parameters. The experimental results moreover exhibit the behaviour of a diffusion-controlled emission process at the end of the experiments.

A simplified version of the model proposed was applied to investigate the influence of source diffusion coefficient and air velocity on the concentration distribution. The findings show that the mass transfer coefficient increases in proportion to the velocity when the emission is controlled by evaporation from the surface. As to diffusion-controlled emission the mass transfer coefficient is unaffected by the velocity.

CONTENTS

Chapter 1

INTRODUCTION

1.1 BACKGROUND

Nowadays people spend the majority of their time in an indoor environment (home, workplace, transportation, recreational buildings, etc.). Therefore, it is of great importance that buildings provide a healthy, safe and comfortable indoor environment. However, occupants in many indoor environments experience the Sick Building Syndrome, a relatively recent phenomenon, caused by poor ventilation, increased tightness of buildings and extended use of synthetic materials.

The Sick Building Syndrome is related to the indoor air quality and is often caused by the release of volatile organic compounds (VOCs) from materials, furniture, office equipment and, in industry, production equipment. Materials tend to give off high levels of vapour at normal temperature that may cause general symptoms such as headache and tiredness. Further symptoms are nasal irritation, dryness and irritation of the skin, throat and the mucous membranes of the eyes. Although none of these symptoms are potentially lethal they are very important to the people affected.

Robertson et al. (1985) and Ashley (1986) report that more complaints about the indoor air quality are found in buildings with mechanical ventilation than in buildings with natural ventilation and it is believed (Bishop, Custer and Vogel, 1985) that the pollutants are generated in the buildings. Furthermore, building materials and furnishings have been identified as major sources of indoor air contamination (Haghighat and Donini, 1993, Wolkoff, 1995 and Fanger et al., 1988) due to the large surface area and the permanent exposure to indoor air.

In a ventilated environment the pollutants emitted from building materials are transported across the boundary layer along the material and is then mixed into the bulk air flow by convection and diffusion (Nielsen, 1995). The presence of a person locally changes the air flow pattern as the person obstructs the

general flow pattern and generates a convective ascending boundary layer flow along the body that may transport pollutants to the breathing zone. Brohus (1997) presents different tools for the assessment of personal exposure in ventilated rooms and proposes a personal exposure model for a displacement ventilated room. When more persons are present the exhalation from one person might penetrate the breathing zone of another person and cause personal exposure (Bjørn and Nielsen, 1996, 1998).

An acceptable air quality in an indoor environment can be achieved by increasing the ventilation rate and thereby diluting the contaminant concentration. This is, however, an expensive solution in terms of energy consumed by the ventilation system. Alternatively, the ventilation system can be controlled by the contaminant concentration so that the ventilation system is only operating when fresh air is required to dilute the contaminant concentration.

The dilution principle can also be combined with heat supply to accelerate the contaminant release. This is the so-called bake-out procedure (Girman, 1989), which is applied prior to the initial building occupancy to reduce the amount of emittable contaminants in the building. In a bake-out study of an office building Girman et al. (1989) found that the VOC concentration increased to more than four times the original concentration during the 24-hours' bake-out and was reduced to 71 % of the original concentration after the bake-out. Girman et al. (1989) suggest longer bake-out time to obtain a further reduction of the VOC concentration and that different procedures should be applied to individual buildings.

Another way of reducing the emission of contaminants to the indoor air is through source control. As building materials and furnishings have been identified as major sources of indoor air pollutants (Haghighat and Donini, 1993, Wolkoff, 1995 and Fanger et al., 1988) selection of low emitting products is of great importance. In recent years emphasis has been placed on source control. In Denmark a certification organisation, the Danish Indoor Climate Labelling, has been established for labelling indoor properties of building materials (Larsen, Funch, and Mortensen, 1995, Larsen, Wolkoff and Nielsen, 1995, Nielsen and Wolkoff, 1995 and Wolkoff and Nielsen 1995-a and 1995-b). The labelling declare the products in terms of application, storage, transport and installation.

When ventilating with respect to indoor air quality the amount of fresh air is important but the efficiency of the air distribution system also has to be considered. This implies the importance of knowing the air flow pattern and the concentration distribution within the building.

1.2 EMISSION FROM BUILDING MATERIALS AND FURNISHINGS

Several researchers have addressed the topic of VOC emission from building materials and furnishings in ventilated enclosures. Some researchers have focused on modelling the emission to predict concentrations without performing lengthy experiments, others have concentrated their effort on the influence of environmental parameters. The following sections give a brief review of recently relevant studies.

1.2.1 EMISSION MODELLING AND CHARACTERISTICS

Although most emission processes involve both diffusion through the material and evaporation from the surface they are often characterised as being either evaporative or diffusion-controlled depending on which of the two is the limiting process. Emission of VOCs from carpets and other flooring materials is mainly controlled by internal diffusion while emission from freshly applied liquid films is typically evaporative. After an initial period of evaporation the emission from the applied liquid films become diffusion-controlled.

When modelling emission of VOCs the empirical first order decay model is often used

$$J = J_0 e^{-kt} \tag{1.1}$$

The model is applicable to many sources but experiments are necessary to obtain the model constants J_0 and k.

Tichenor, Guo and Sparks (1993) developed a model for surface emission based on fundamental mass transfer and boundary layer theory. The model has been compared to dynamic test chamber experiments as well as measurements in a test house. Conclusions are that good agreement is achieved although there is a difference in the last part (tail) and that scaling problems may occur when translating results from small-scale test chambers to full scale. The model relies

on the mass transfer coefficient, which is obtained through fitting experimental data.

Sparks et al. (1996) developed a gas phase limited model based on fundamental mass transfer theory. For reasons of simplicity a linear relationship was assumed between the mass remaining in the source and the concentration in the room air which corresponds to the linear adsorption isotherm. Results from test chamber experiments as well as a test house have been correlated to overcome scaling problems.

Chang and Guo (1992) investigated the emission characteristics of four organic compounds and found that the emission process can be divided into two phases. Phase one contains the initial increase, the peak and the rapid decrease in concentration and phase two is the slow decline period. In phase one the emission process is mainly controlled by evaporation from the surface and in phase two the emission is controlled by diffusion through the material. Clausen (1993) confirmed this behaviour.

Clausen et al. (1993) conclude that the first order decay model is insufficient for diffusion-controlled emission and therefore developed a new model. This model assumes that the diffusion coefficient depends exponentially on the concentration in the source. Good agreement with FLEC and small chamber experiments is achieved for vinyl floor covering. In another study Clausen (1993) reports that the emission rate of volatile and semivolatile organic compounds from waterborne paints is decreased with increasing film thickness, i.e. the emission is reduced as the mass transfer coefficient is decreased.

Little, Hodgson and Gadgil (1994) developed a model based on Fick's second law of diffusion. The model assumes equilibrium between the concentration in the air and in the solid material and accounts for the phase change. The model provides a reasonable fit to experimental chamber data for most compounds but it is computational intensive.

A model for VOC emission from PVC flooring was proposed by Christiansson, Yu and Neretnieks (1993). The model is based on diffusion theory and requires knowledge of the diffusion coefficient and the concentration in the source. Dunn (1987) developed two models for diffusion-controlled emission. One for diffusion through thin films like adhesives and varnish and one for deep sources such as particleboard and plywood. Both models

nevertheless, are complicated and require parameters obtained from experiments.

Yang, Chen and Bluyssen (1998) demonstrated a specific model based on computational fluid dynamics (CFD) for short-term predictions of VOC emission from a carpet. The model accounts for the internal diffusion through the carpet. An analytical model was also developed for long term predictions.

1.2.2 INFLUENCE OF ENVIRONMENTAL PARAMETERS

Zhang and Haghighat (1997) studied the influence of air movement on material emission rates in a velocity controlled test chamber. The pollutant sources used were water, varnish and paint. For a constant source the results indicate increased emission as the velocity increases. Increased turbulence intensity also yields higher emission but the influence is weaker compared to the velocity. Consistent results were obtained by J.S. Zhang et al. (1996) and Low et al. (1998) in studies of emission from wood stain and carpet-adhesive assemblies, respectively. Low et al. (1998) further suggested that the early stage emission behaviour has some characteristics of wet materials as convective effects are predominant.

Gunnarsen (1997) performed experiments in a test chamber to investigate the influence of a specific ventilation rate (ventilation rate per source area) on VOC emissions from linoleum, waterborne acrylic paint, nylon carpet and sealant. The results show that at low specific ventilation rate the emission was proportional to the specific ventilation rate. For higher specific ventilation rates the emission became independent of ventilation. Tichenor (1991) also studied the effect of ventilation rate on emission and found that the initial emission rate for wood stain and polyurethane was increased with ventilation rate, while no effect was observed for floor wax.

Several investigations have been carried out to investigate the influence of temperature on material emissions. Wolkoff (1996, 1998) studied the emission of VOCs from carpet, PVC flooring, sealant, floor varnish and wall paint, and Van der Wal et al. (1997) studied the PVC flooring, carpet and paint. The results show that the temperature has a strong effect as the emission increases significantly with temperature, which is also reported in an interlaboratory comparison by De Bortoli and Colombo (1993). In another study Haghighat and De Bellis (1998) investigated the emission of VOCs from varnish and paint. The results are consistent with those obtained by Wolkoff (1996), De Bellis and

Haghighat (1996), Van der Wal et al. (1997) and De Bortoli and Colombo (1993). Haghighat and De Bellis (1998) also found that the emission of individual VOCs might not necessarily follow the same trend as the total volatile organic compounds (TVOCs).

Testing and characterisation of VOC emission from materials are often performed in small-scale test chambers as they provide a tool that is limited in size and is cheaper to establish and operate than full-scale chambers. Care should be taken though when using small-scale test chambers as a difference in scale may lead to different emission rates (Topp, Nielsen and Heiselberg, 1997).

For evaporative emissions the flow conditions over the emitting surface are important as they are subject to change with scale and thus affect the emission rate. Furthermore, the velocity referred to in small-scale test chambers is often measured in one single point. The velocity is therefore unlikely to reflect the flow conditions and to allow for comparison of test results from one investigation to another. For instance an interlaboratory comparison by De Bortoli and Colombo (1993) showed that the air velocity varied from 0.01 m/s to 0.5 m/s in the participating laboratories. There is thus a need for a standardised procedure in terms of control and measurement of air velocity, which is also recommended by Guo et al. (1996).

J.S. Zhang and Shaw (1996) and Y. Zhang and Haghighat (1996) developed small-scale test chambers for investigation of material emissions. Both chambers allow for velocity control but do not suggest how to overcome scaling problems.

1.3 OBJECTIVES AND SCOPE OF WORK

In general, the existing emission models are empirical relations that require parameters obtained from experiments. The models assume either diffusion-controlled or evaporation-controlled emission as they are based on specific compounds and materials.

There is thus a need for a thorough investigation based on fundamental fluid dynamics and mass transfer theory to obtain general understanding of the mechanisms involved in the emission from building materials in ventilated rooms.

Its is the objective of the present work to provide such an investigation, i.e. investigate the emission from surfaces in ventilated enclosures from a fluid dynamics point of view. The interest has been focused on the emission of vapours and gases as no particulate emissions have been considered. The methods used are numerical calculations by computational fluid dynamics (CFD) and full-scale laboratory experiments.

The general mechanisms that affect the emission have been studied, as the investigation has not been aimed on any specific compound or material. This implies studying the influence of the local environment, i.e. the boundary layer flow, on the emission from a surface at different geometries and set-ups. A method to transfer results from small-scale test chambers to full-scale ventilated rooms is also proposed.

Furthermore, the diffusion through a solid material has been investigated and by means of CFD a general model for prediction of emission from building materials is proposed. The model is capable of dealing with pollutant transport across the boundary layer as well as internal diffusion without prior knowledge of which is the limiting process. The model is generally applicable as no particular source or pollutant has been studied and it provides detailed information on the pollutant distribution in both the room air and the source.

Chapter 2

THEORETICAL BACKGROUND

2.1 INTRODUCTION

In this chapter the theoretical background for the present work is outlined, i.e. the fundamental equations for fluid dynamics and mass transfer.

2.2 CONSERVATION EQUATIONS

The governing equations for a fluid of motion are based on the conservation principle i.e., conservation of mass, momentum, energy and species. In the following the equations for an incompressible fluid are expressed in cartesian co-ordinates using tensor notation.

Considering a control volume of a fluid, conservation of mass requires that the total mass flux into the volume balance the outgoing mass flux. The conservation of mass, the so-called continuity equation, can be expressed as

$$\frac{\partial u_i}{\partial x_i} = 0 \tag{2.1}$$

As the fluid is assumed incompressible the density has been cancelled out.

The conservation of momentum also called the Navier-Stokes equations can be obtained by applying Newton's second law to a control volume of fluid, expressing the proportionality between the applied force and the acceleration. Thus the conservation of momentum is given by the equilibrium between momentum forces and body and surface forces

$$\rho\left[\frac{\partial u_i}{\partial t}+\frac{\partial}{\partial x_j}(u_i u_j)\right]=\rho g_i-\frac{\partial p}{\partial x_i}+\frac{\partial}{\partial x_j}\left[\mu\left(\frac{\partial u_i}{\partial x_j}+\frac{\partial u_j}{\partial x_i}\right)\right]+S_m \qquad (2.2)$$

The left-hand side expresses the supply of momentum from the surroundings on the fluid and the first term on the right side represents the body forces due to gravity, acting on the entire control volume. The next two terms on the right side describe the influence of the pressure gradient due to normal forces and the shear stresses respectively, i.e. surface forces due to external stresses. The last term is the source term.

From the first law of thermodynamics the equation for conservation of energy can be derived, expressing that the sum of heat and work added to a system equals the rate of change of energy. This leads to an equation that describes the temperature throughout the fluid

$$\frac{\partial T}{\partial t}+\frac{\partial}{\partial x_j}(u_j T)=\frac{\partial}{\partial x_j}\left(\alpha\frac{\partial T}{\partial x_j}\right)+S_T \qquad (2.3)$$

By analogy to the energy equation the conservation of species (concentration equation) is given by

$$\frac{\partial c}{\partial t}+\frac{\partial}{\partial x_j}(u_j c)=\frac{\partial}{\partial x_j}\left(D\frac{\partial c}{\partial x_j}\right)+S_c \qquad (2.4)$$

Equations 2.1-2.4 constitute the governing equations for motion of, and transport of energy and species throughout, an incompressible fluid. It is a set of coupled non-linear partial differential equations for which analytical solutions exist only in a few very simple cases. Therefore, numerical solution procedures are often applied.

2.3 BOUNDARY LAYER FLOW

In the bulk airflow far from any boundary the influence of shear stresses is insignificant and the flow can be regarded as frictionless. However, close to a

solid wall there exists a thin region, the boundary layer (see Figure 2.1), where viscous forces are non-negligible as the flow adheres to the wall which gives rise to shear stress.

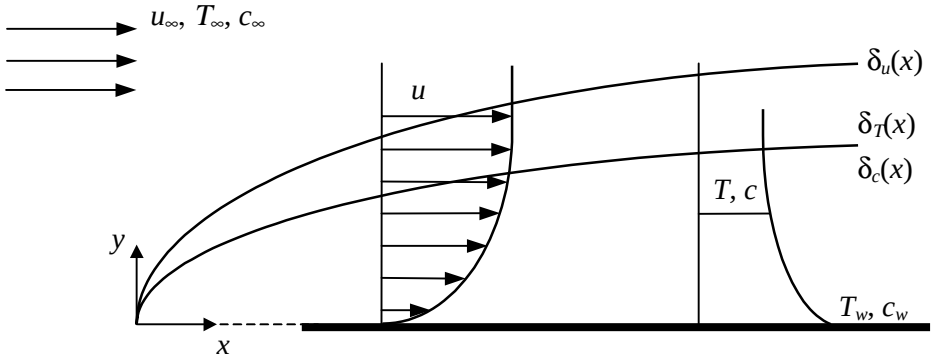

Figure 2.1 Outline of boundary layer flow over a flat plate with typical profiles for velocity, temperature and concentration. The Prandtl and Schmidt numbers are assumed to be equal and the profiles for temperature and concentration are therefore identical.

Across the boundary layer there are large variations in velocity, as the velocity changes from zero at the wall (no slip condition) to the bulk flow velocity, u_∞. The temperature and concentration changes from T_w and c_w at the wall to T_∞ and c_∞, respectively. The case illustrated in Figure 2.1 corresponds to forced convective flow over a flat plate releasing heat and mass.

In all viscous flows the controlling parameter is the Reynolds number which links the inertial force to the viscous force

$$Re_L = \frac{uL}{\nu} \tag{2.5}$$

For a given geometry the flow pattern changes from laminar through transitional to turbulent as Re_L increases.

A fundamental parameter in momentum and heat transfer is the Prandtl number, *Pr*, which can be interpreted as the ratio of viscous (momentum) diffusion to thermal diffusion and is thus a dimensionless diffusion ratio

$$Pr = \frac{\nu}{\alpha} \tag{2.6}$$

In mass transfer the corresponding dimensionless ratio is the Schmidt number, *Sc*, which relates the viscous diffusion to diffusion of mass

$$Sc = \frac{\nu}{D} \tag{2.7}$$

When either of *Pr* or *Sc* is unity the process is said to diffuse in the same ratio as the momentum and the boundary layers are identical.

The thickness, δ_u, of the velocity boundary layer is defined as the distance from the wall where the velocity is $u \approx 0.99u_\infty$. For the temperature and concentration boundary layers the thickness is defined in a similar way. The boundary layer grows in thickness along the wall in the downstream direction.

2.3.1 THE TURBULENT BOUNDARY LAYER

Due to the low viscosity of air room airflows are normally turbulent, as the critical Reynolds number, based on the transverse thickness of the flow, is of the order of 1000 (White 1991-b).

The boundary layer along a solid wall always has an initial laminar section but due to instabilities it soon becomes turbulent. The turbulent boundary layer is much thicker and consists of a very thin laminar sublayer, a buffer layer and a turbulent layer (see Figure 2.2).

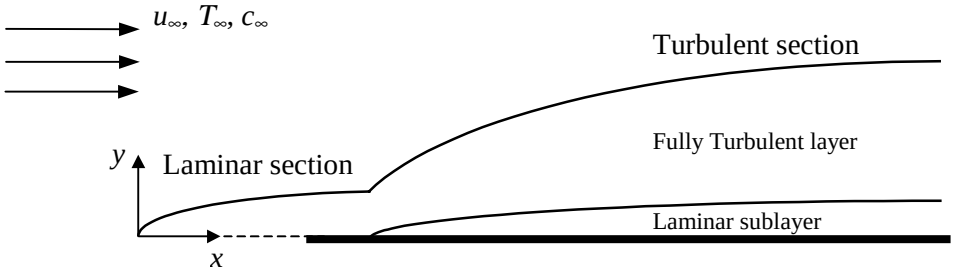

Figure 2.2 Development of turbulent boundary layer along a solid wall.

In the laminar sublayer the flow is dominated by viscous shear due to the damping effect of the wall while the boundary layer is fully turbulent farther from the wall as turbulent shear predominates. In the buffer layer both types of shear occur and the flow is neither laminar nor turbulent but a merge between the two.

There exist a set of universal profiles, the so-called wall-laws or wall functions for velocity, temperature and concentration in the turbulent boundary layer. These profiles are defined in terms of dimensionless variables

$$u_\tau = \left(\frac{\tau_w}{\rho} \right)^{1/2} \tag{2.8}$$

$$y^+ = \frac{y u_\tau}{\nu} \tag{2.9}$$

$$u^+ = \frac{u}{u_\tau} \tag{2.10}$$

$$T^+ = \frac{\rho c_p u_\tau (T_w - T)}{q_w} \tag{2.11}$$

$$c^+ = \frac{u_\tau (c_w - c)}{E_w} \tag{2.12}$$

The non-dimensional concentration, c^+, has been defined by analogy to the non-dimensional temperature, T^+.

Assuming that the laminar sublayer is a region of constant shear stress the profiles for velocity, temperature and concentration can be approximated as linear functions of distance from the wall (White 1991-a and 1991-b)

$$u^+ = y^+ \tag{2.13}$$

$$T^+ = Pr\, y^+ \tag{2.14}$$

$$c^+ = Sc\, y^+ \tag{2.15}$$

Farther from the wall the boundary layer is fully turbulent as turbulent shear predominates and the profiles are logarithmic (White 1991-a and 1991-b)

$$u^+ = \frac{1}{\kappa} ln\ y^+ + B \tag{2.16}$$

$$T^+ = \frac{Pr_t}{\kappa} ln\, y^+ + A(Pr) \tag{2.17}$$

$$c^+ = \frac{Sc_t}{\kappa} ln\, y^+ + A(Sc) \tag{2.18}$$

The above expressions for the non-dimensional concentration, c^+, has been established by analogy to the non-dimensional temperature, T^+.

White (1991-a and 1991-b) suggests $B \approx 5.0$ for turbulent flow past smooth impermeable walls and the Kármán constant is $\kappa \approx 0.41$. The functions *A(Pr)* and *A(Sc)* are given by (White 1991-a)

$$A(x) = 12.7x^{2/3} - 7.7 \tag{2.19}$$

where x denotes *Pr* or *Sc* respectively and $0.7 \le x \le 10^5$.

The cross over point between the laminar sublayer and the fully turbulent layer is at $y^+ \approx 11$. Figure 2.3 shows the velocity wall functions for the turbulent boundary layer along a flat plate. The profiles for temperature and concentration are similar in shape.

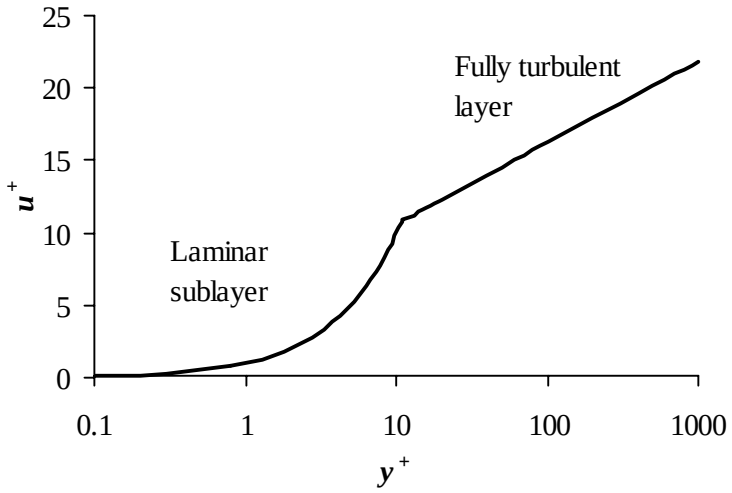

Figure 2.3 Velocity wall functions for the turbulent boundary layer along a flat plate.

2.4 MASS TRANSFER

Like heat transfer, mass transfer tends toward making a mixture uniform through diffusion from a region with high concentration to a region of low

concentration. Diffusion is defined as a process of random molecular motions and is often the result of a concentration gradient. Other driving forces exist such as thermal and pressure gradients. The present work deals with diffusion arising from a concentration gradient.

Emission of pollutants from solid materials is a chain-like process involving internal diffusion through the solid, transport across the boundary layer at the surface and mixing into the bulk air (see Figure 2.4).

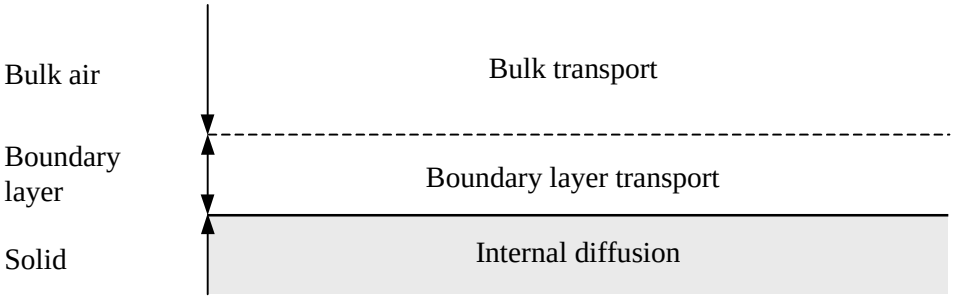

Figure 2.4 Processes involved in emission of pollutants from building materials and furnishings.

Mixing into the bulk air is usually rapid due to the low concentrations in the bulk air compared to the boundary layer and thus not a limiting process. As the processes act in series the slower process of internal diffusion through the solid and transport across the boundary layer will be the controlling mechanism.

In case of internal diffusion being the limiting process the emission is often referred to as diffusion-controlled and if transport across the boundary layer is limiting the emission is said to be evaporative. However, no matter which of the two is the controlling mechanism the emission from building materials or furnishings always involve transport across the boundary layer.

The fundamental equations in mass transfer are Fick's laws of diffusion. Assuming diffusion in only one direction, Fick's first law expressing direct proportionality between the concentration gradient and the species flux, is given by

$$J = -D_{AB} \frac{\partial c}{\partial y} \tag{2.20}$$

and the second law expresses conservation of species

$$\frac{\partial c}{\partial t} = D_{AB} \frac{\partial^2 c}{\partial y^2} + S_c \tag{2.21}$$

It is seen that Fick's first law is analogous to Fourier's equation for one-dimensional heat conduction. The second law corresponds to the one-dimensional form of equation (2.4) without the convection term.

The proportionality factor, D_{AB}, in Fick's laws is the molecular diffusion coefficient and it describes the diffusion of component A into component B. In a binary system D_{AB}=D_{BA} and the diffusion coefficient is thus independent of concentration but a property of the combination of components A and B. The diffusion coefficient is also a function of pressure, temperature and component composition (Bird, Stewart and Lightfoot 1960).

As a matter of convenience D_a and D_s is used henceforward to denote the molecular diffusion coefficient for air and solid material, respectively.

2.4.1 SURFACE EMISSION

For freshly applied liquid films, e.g. paint and lacquer, resistance in the gas-phase limits the mass transfer and the emission is generally controlled by evaporation from the surface as the drying process progresses. In analogue to heat transfer the emission can be described in terms of the convective mass transfer coefficient, k_c, and the difference between the concentration at the surface, c_w and the bulk air concentration, c_∞

$$E_w = k_c (c_w - c_\infty) \tag{2.22}$$

In a very thin layer close to the wall the air is moving slowly and can be considered stagnant. Throughout this layer, often referred to as the diffusion boundary layer, the only flow normal to the surface is that corresponding to

mass transfer by molecular diffusion. Farther from the surface the flow becomes turbulent and the emission is thus a combined process of both molecular and turbulent diffusion. Figure 2.5 shows typical velocity and concentration profiles for turbulent boundary layer flow.

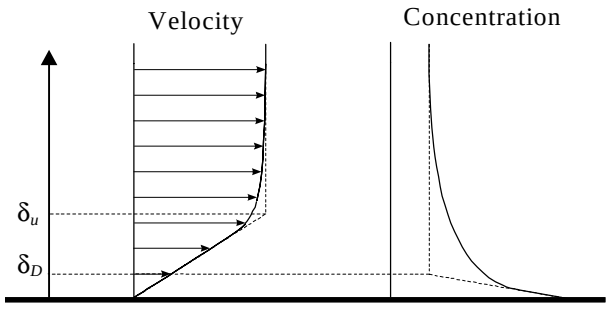

Figure 2.5 Typical velocity and concentration profiles for turbulent boundary layer flow.

The thickness of the diffusion boundary, δ_D, layer is defined so that the layer offers the same resistance to diffusion as encountered in the combined process of molecular and turbulent diffusion (Sissom and Pitts, 1972). Evaluating Fick's first law (equation 2.20) at $y=\delta_D$ yields

$$E_w = \frac{D_a}{\delta_D}(c_w - c_\infty) \tag{2.23}$$

Consequently, the mass transfer coefficient can be written in terms of the diffusion coefficient and the diffusion boundary layer thickness

$$k_c = \frac{D_a}{\delta_D} \tag{2.24}$$

As the mass transfer coefficient is related to the boundary layer flow through the diffusion boundary layer thickness it depends on local airflow parameters

such as velocity and temperature. It also depends on the source represented by the molecular diffusion coefficient.

In analogue to heat transfer the mass transfer can be described by a non-dimensionless parameter, the Sherwood number

$$Sh_L = \frac{k_c L}{D_a} \tag{2.25}$$

From boundary layer theory (White 1991-a and Sissom and Pitts 1972) the Sherwood number for laminar flow past a flat plate can be correlated with the Reynolds number and the Schmidt number by

$$Sh_L = 0.664\, Re_L^{1/2}\, Sc^{1/3} \tag{2.26}$$

and for turbulent flow by

$$Sh_L = 0.0365\, Re_L^{4/5}\, Sc^{1/3} \tag{2.27}$$

The mass transfer coefficient thus increases with Re_L and varies with $u^{1/2}$ for laminar flow and $u^{4/5}$ for turbulent flow. Figure 2.6 depicts the correlations in graphical form for a Schmidt number of unity.

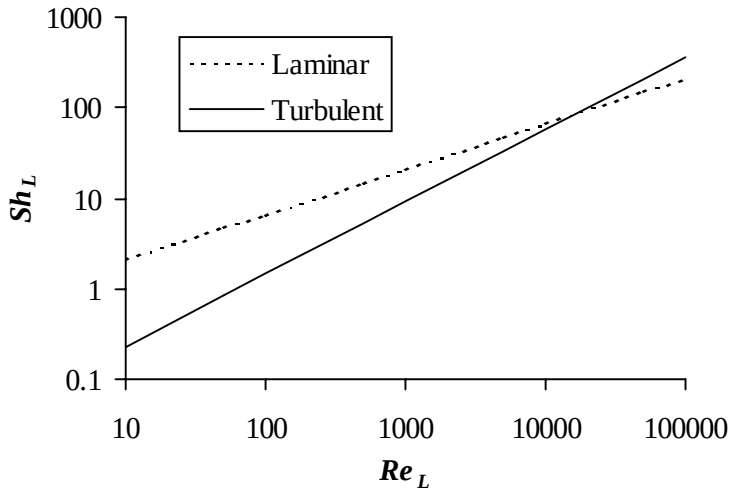

Figure 2.6 Correlation between Sherwood number and Reynolds number for flow past a flat plate with a Schmidt number of unity.

2.4.2 INTERNAL DIFFUSION

Most emission processes become diffusion-controlled after an initial period of evaporative emission. Different compound phases must be taken into account as the compound undergoes a change in phase after crossing the physical barrier at the surface-air interface by adsorption or desorption. In the solid material the compound assumes a solid or adsorbed phase and in the air the compound assumes a vapour or gas phase.

In steady state the rate of internal diffusion balances the emission from the surface and there is thus a relation between the compound concentration in the solid phase, c_s, and the gas phase concentration of the compound, c_a. Under isothermal conditions this relation is referred to as an adsorption isotherm. The far simplest relation is the linear model (Slejko 1985)

$$c_s = K_p c_a \tag{2.28}$$

The model expresses direct proportionality between phase concentrations by the linear partition coefficient, K_p. Little, Hodgson and Gadgil (1994) report

partition coefficients in the range from 1 to 450000 for VOC emission from carpets. A more sophisticated model is the Langmuir model (Slejko 1985, Ruthven 1984)

$$c_s = \frac{c_{s0} K_L c_a}{1 + K_L c_a} \tag{2.29}$$

The model assumes a single layer of compounds at the surface and accounts for the surface capacity through the concentration, c_{s0}, corresponding to complete surface coverage. For low gas phase concentrations the Langmuir model approximates the linear model as the denominator approaches unity.

Further adsorption isotherms exist but for compound adsorption on or desorption from building materials the linear or Langmuir models are the most applicable (Axley, 1993).

In principle the models are valid at the surface only but for reasons of convenience they are applied throughout the solid material henceforward.

2.5 COMPUTATIONAL FLUID DYNAMICS (CFD)

Computational Fluid Dynamics (CFD) is a numerical tool for solution of the governing equations of fluid flow and heat and mass transfer. To account for turbulent flow any variable is resolved into a mean and a fluctuating component.

As only steady state and isothermal problems are considered in the present work the governing equations are given for steady state, incompressible, isothermal and turbulent (or laminar) flow. Substituting any variable by a mean and a fluctuating component the continuity, momentum and concentration equations respectively, yields

$$\frac{\partial \bar{u}_j}{\partial x_j} = 0 \tag{2.30}$$

$$\rho\frac{\partial(\bar{u}_i\bar{u}_j)}{\partial x_j}=-\frac{\partial\bar{p}}{\partial x_i}+\frac{\partial}{\partial x_j}\left[\mu\left(\frac{\partial\bar{u}_i}{\partial x_j}+\frac{\partial\bar{u}_j}{\partial x_i}\right)\right]-\rho\frac{\partial(\overline{u_i'u_j'})}{\partial x_j}+S_m \qquad (2.31)$$

$$\frac{\partial(\bar{u}_j\bar{c})}{\partial x_j}=\frac{\partial}{\partial x_j}\left(D\frac{\partial\bar{c}}{\partial x_j}\right)-\frac{\partial(\overline{u_j'c'})}{\partial x_j}+S_c \qquad (2.32)$$

The substitution has thus produced a number of additional terms in the equations. In the momentum equations the terms $\overline{u_i'u_j'}$ are the turbulent or Reynolds stresses, which represent the transport of momentum due to the fluctuating motion of the flow. In the concentration equation the terms $\overline{u_j'c'}$ represent the turbulent transport of species.

To solve the set of equations it is necessary to find a suitable description of the turbulent correlations $\overline{u_i'u_j'}$ and $\overline{u_j'c'}$. This fundamental problem is often referred to as the closure-problem in turbulence.

2.5.1 THE EDDY VISCOSITY CONCEPT

In 1877 Boussinesq introduced the concept of an eddy viscosity based on the assumption that the turbulent stresses, in analogy to the viscous stresses in laminar flow, are proportional to the velocity gradient. The coefficient of proportionality is the eddy or turbulent viscosity and in general form the eddy viscosity concept gives (Rodi 1980)

$$-\overline{u_i'u_j'}=\frac{\mu_t}{\rho}\left(\frac{\partial\overline{u_i}}{\partial x_j}+\frac{\partial\overline{u_j}}{\partial x_i}\right)-\frac{2}{3}k\delta_{ij} \qquad (2.33)$$

Although the eddy viscosity, μ_t, has the same dimensions as the laminar viscosity, μ_l, it is not a fluid property but instead it varies with flow conditions and geometry.

By Reynolds analogy the turbulent mass flux is related to the temperature gradient and the concentration gradient, respectively. Corresponding to the eddy

viscosity the eddy diffusion coefficient is introduced. The turbulent mass transfer is approximated by

$$-\overline{u_j' c'} = \frac{\mu_t}{\rho Sc_t}\frac{\partial \bar{c}}{\partial x_j} \tag{2.34}$$

The turbulent Schmidt number, Sc_t, is given by

$$Sc_t = \frac{\nu_t}{D_t} \tag{2.35}$$

Introducing the effective viscosity as the sum of the laminar and turbulent viscosity, i.e. $\mu_{eff}=\mu_l+\mu_t$ the momentum equation gives

$$\rho\frac{\partial(\bar{u}_i\bar{u}_j)}{\partial x_j} = -\frac{\partial \bar{p}}{\partial x_i} + \frac{\partial}{\partial x_j}\left[\mu_{eff}\left(\frac{\partial \bar{u}_i}{\partial x_j} + \frac{\partial \bar{u}_j}{\partial x_i}\right)\right] + S_m \tag{2.36}$$

In a similar way the effective diffusion coefficient can be introduced as $D_{eff}=D_l+D_t$. Substitution into the concentration equation yields

$$\frac{\partial(\bar{u}_j\bar{c})}{\partial x_j} = \frac{\partial}{\partial x_j}\left(D_{eff}\frac{\partial \bar{c}}{\partial x_j}\right) + S_c \tag{2.37}$$

The problem has now been shifted from a description of the turbulent correlations $\overline{u_i' u_j'}$, $\overline{u_j' c'}$ to the eddy properties and necessitates the introduction of a turbulence model.

In the present work the k-ε turbulence model has been applied in both a standard and a low Reynolds number (LRN) formulation. For further details of the turbulence models see appendix A.

2.5.2 NUMERICAL SOLUTION OF THE GOVERNING EQUATIONS

The solution procedure used is the finite volume method (FVM) but before applying the procedure the governing equations must be put on a discrete form. The computational domain is divided into a number of control volumes each surrounding one grid point. Discrete equations are then obtained by integrating the equations over each control volume to connect the variable at a cell centre to its neighbours.

For discretisation of the convection terms the hybrid difference scheme (Patankar, 1980) has been used and the SIMPLEC algorithm (CFX-4.2 User manuals), which is a variant of the SIMPLE algorithm (Patankar, 1980) has been used for coupling of velocity and pressure.

In the present work the commercial CFD software package CFX-4.2 from AEA Technology has been used for the numerical solution. The software uses the FVM solution procedure.

Chapter 3

NUMERICAL EXPERIMENTS BY CFD – METHODS AND RESULTS

3.1 INTRODUCTION

A series of numerical experiments by CFD (Topp, Nielsen and Heiselberg, 1997) have been performed to investigate the influence of velocity and turbulence on the evaporative emission in a ventilated room. All calculations have been performed for steady-state two-dimensional airflow with the LRN turbulence model developed by Launder and Sharma (1974) (see Appendix A).

3.2 GEOMETRY AND SET-UP

The experiments have been performed for a full-scale ventilated room as well as a small-scale test chamber to allow evaluation of the influence of scale. For reasons of comparison typical geometries have been chosen.

3.2.1 FULL-SCALE ROOM

The geometry of the full-scale room was chosen similar to the two-dimensional test room used in the International Energy Agency, Annex 20 programme (Nielsen, 1990) as it is well known in terms of velocity and airflow pattern. The room is ventilated by a supply opening at the ceiling and a return opening at the floor (see Figure 3.1).

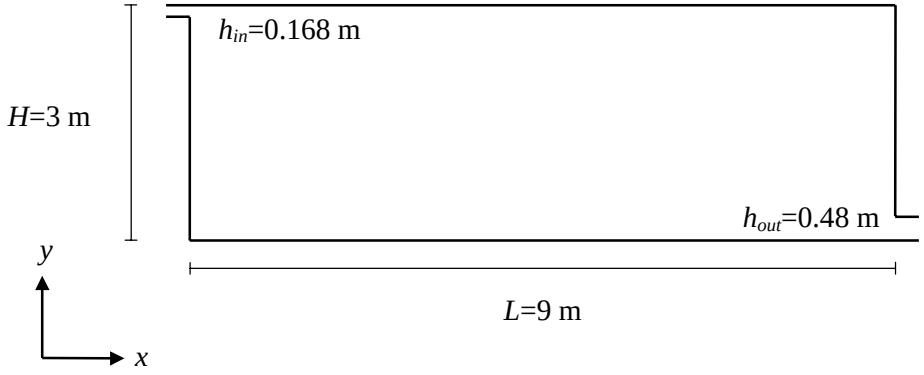

Figure 3.1 Outline of the two-dimensional test room.

The pollutant source has been located either at the ceiling or the floor. To avoid disturbances from the inlet and reattachment to the floor an area of 3 m from the inlet or outlet respectively, is not emitting. A wall (partition) has been added to the room to increase the level of turbulence. A total of four different set-ups have been investigated (see Figure 3.2) for different air change rates.

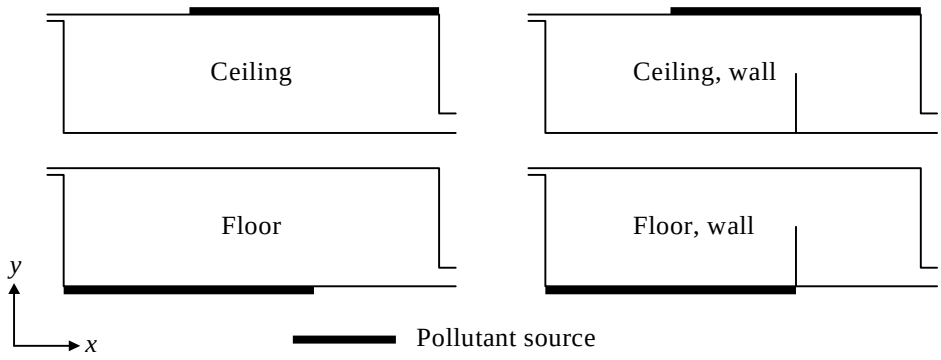

Figure 3.2 The investigations were performed for four different set-ups in the full-scale room. In two of the set-ups a wall (height 1.5 m) was located at x=6 m to increase the level of turbulence.

Five different air change rates (1, 2, 5, 8 and 10 h^{-1}) were investigated for the two source locations with and without the wall, thus yielding a total of 20 combinations.

In the CFD calculations the full-scale room was resolved into a total of 4250 cells with a high resolution of the boundary regions. Two slightly different grid distributions were used depending on the whether the wall was included or not.

3.2.2 SMALL-SCALE TEST CHAMBER

The computational model of the small-scale test chamber is based on the CLIMPAQ (Chamber for Laboratory Investigations of Materials, Pollution and Air Quality) test chamber developed by Gunnarsen, Nielsen and Wolkoff (1994). Figure 3.3 shows an outline of the CLIMPAQ test chamber.

In the test chamber various materials can be tested simultaneously. Each material sample consists of a plate with the dimension 0.8 m by 0.2 m. The maximum loading is 12 plates corresponding to a distance of approximately 2 cm between the material samples. An internal fan generates airflow over the material samples (Gunnarsen, Nielsen and Wolkoff, 1994).

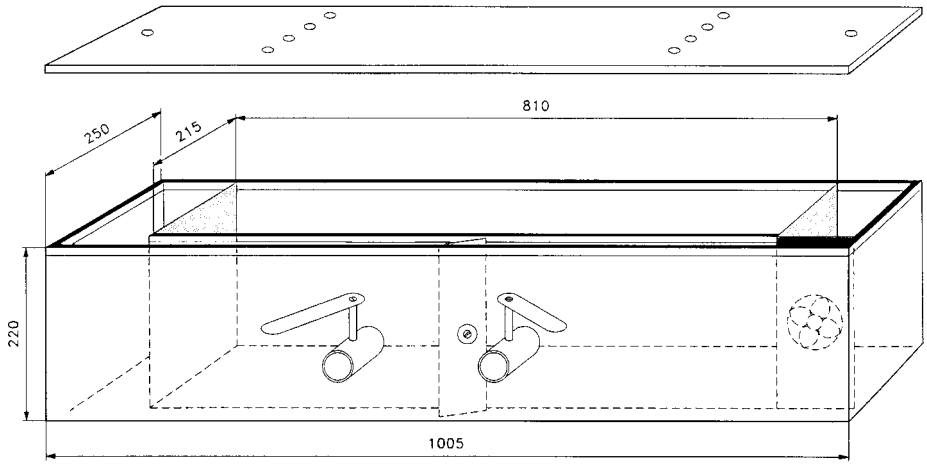

Figure 3.3 The CLIMPAQ test chamber with main dimensions in mm (Gunnarsen, Nielsen and Wolkoff, 1994).

The small-scale geometry has been modelled as two parallel emitting surfaces with length and spacing based on the dimensions of the CLIMPAQ test chamber (see Figure 3.4) and airflow between the surfaces.

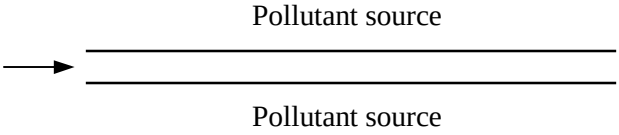

Figure 3.4 Computational model of the small-scale geometry. The length of the emitting surfaces is 0.8 m and the spacing is 0.02 m.

Emissions at five different inlet velocities, u_0, were investigated and the model was resolved into a total of 100 cells.

3.2.3 BOUNDARY CONDITIONS

Different air change rates, N, were obtained by changing the inlet velocity, u_0. Further inlet parameters were concentration, c_0, turbulent kinetic energy, k_0, and dissipation rate, ε_0, given by (Nielsen, 1990)

$$\begin{aligned} u_0 &= \frac{H\,L}{h_{in}}\,\frac{N}{3600} \\ c_0 &= 0 \\ k_0 &= 1.5(0.04u_0)^2 \\ \varepsilon_0 &= \frac{10k_0^{1.5}}{h_{in}} \end{aligned} \tag{3.1}$$

No parameters were specified for the outlet opening.

The pollutant source was modelled as an area of constant surface concentration, c_w=1000 mg/m^3. A hypothetical VOC was used and the molecular diffusion coefficient of the VOC in air is D=15.1E-6 m^2/s corresponding to a Schmidt number of unity.

3.3 RESULTS

In the following the results from the CFD calculations are presented. The calculated velocities have been compared to measurements (Nielsen, 1990) and good agreement has been achieved (see Appendix B for further details).

3.3.1 AIRFLOW PATTERN

In the set-up without the wall the incoming jet generates a recirculating flow as shown in Figure 3.5 (left). When a wall is added to the room the airflow pattern is altered and a recirculating zone is established behind the wall.

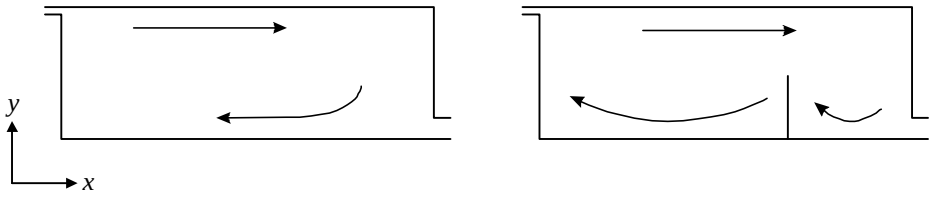

Figure 3.5 General airflow pattern in the full-scale ventilated room for the set-up without the wall (left) and the set-up with a wall located at x=6 m (right).

Figure 3.6 shows typical velocity profiles from the full-scale room. It is seen that the boundary layer at the ceiling is thinner than at the floor.

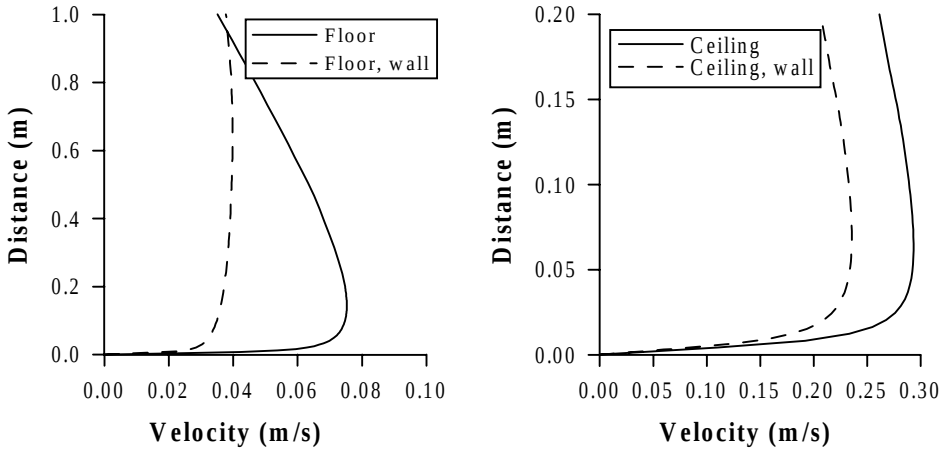

Figure 3.6 Typical velocity profiles from the full-scale room at x=3 m for the floor and x=6m for the ceiling. The profiles shown are for an air change rate of 10 h^{-1}.

The wall obstructs the flow and reduces the velocity level with the larger influence observed at the floor.

3.3.2 EMISSION RATE

The emission rate varies with position as it is influenced by the airflow over the surface. In Figure 3.7 - Figure 3.10 the non-dimensional emission, E^*, along the pollutant source is depicted for the four different set-ups. The non-dimensional emission rate is defined as the ratio of the local emission, E_x, to the average emission, E_w, that is

$$E^* = \frac{E_x}{E_w} \tag{3.2}$$

The calculation of the average emission rate is based on the local emission rates weighed by area.

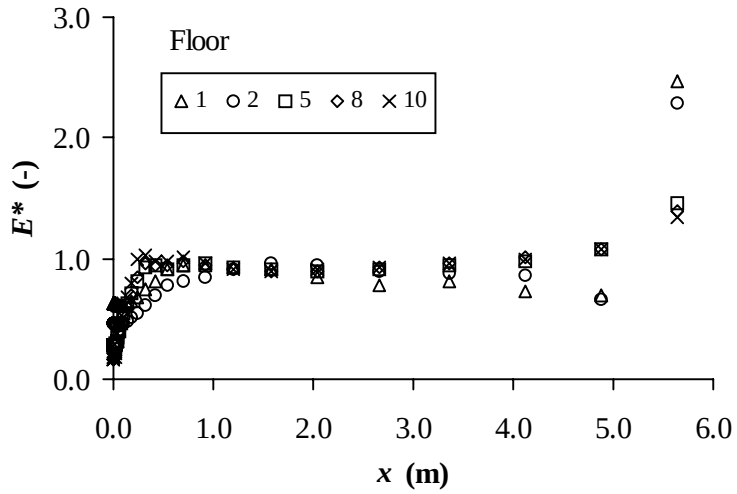

Figure 3.7 Non-dimensional emission rate versus horizontal distance with the air change rate per hour as parameter.

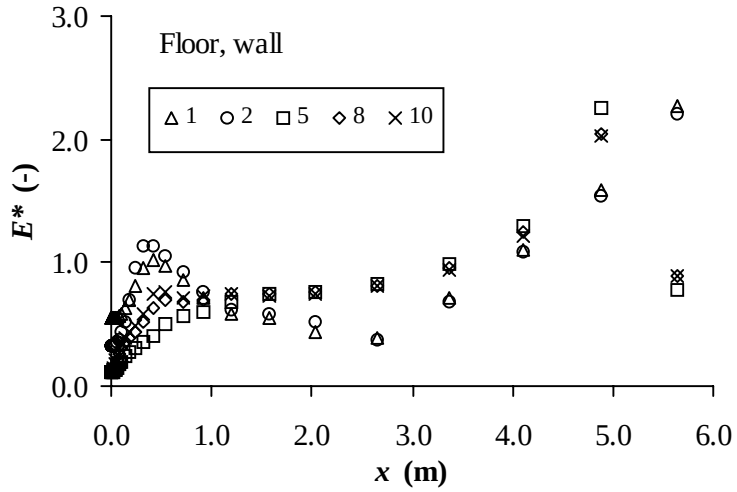

Figure 3.8 Non-dimensional emission rate versus horizontal distance with the air change rate per hour as parameter.

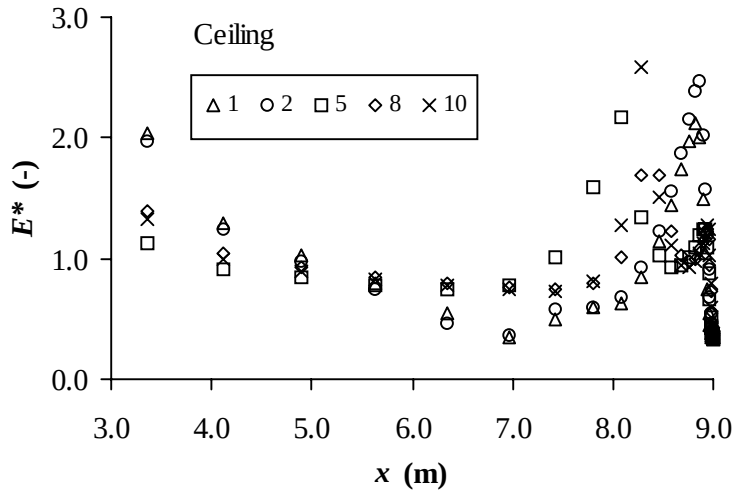

Figure 3.9 Non-dimensional emission rate versus horizontal distance with the air change rate per hour as parameter.

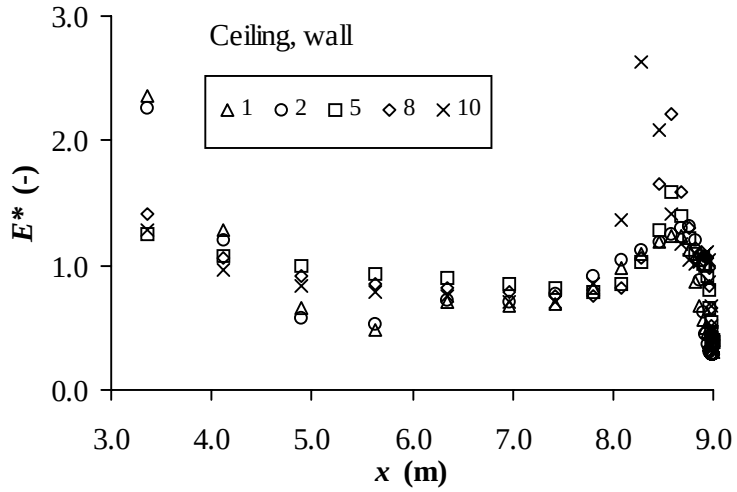

Figure 3.10 Non-dimensional emission rate versus horizontal distance with the air change rate per hour as parameter.

From the figures it is seen that the emission rate varies largely in horizontal direction. When the pollutant source is located at the floor the emission rate is increasing with distance as the velocity level decreases. Some discrepancy is observed for low air change rates though. When the ceiling is emitting the emission rate is also seen to increase in direction of lower velocity level except for a region within approximately 1.5 m from the right end wall.

For reasons of convenience the emission rate is represented by a single value. The emission rate referred to henceforward is the average value, E_w.

When the air change rate is increased the emission rate increases as a larger amount of VOCs is removed from the boundary layer flow. This is illustrated in Figure 3.11, which indicates a linear relationship between emission rate and air change rate. The figure also shows that the presence of a wall has no significant influence on the emission rate for a given source location and air change rate.

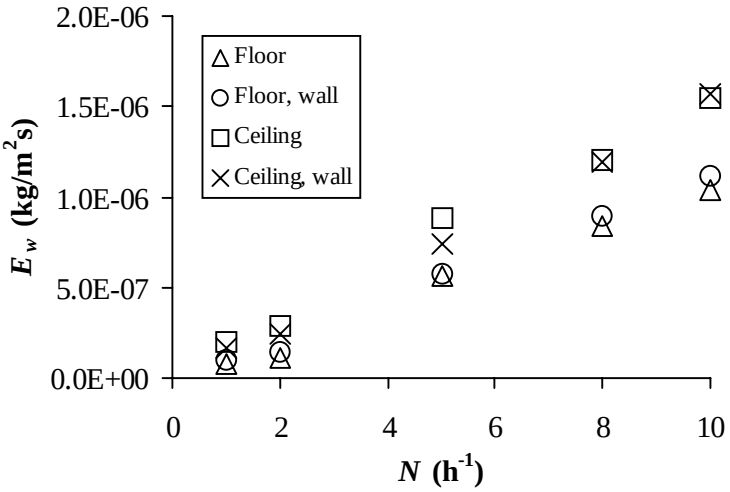

Figure 3.11 Emission rates in the full-scale test room from the CFD calculations at different air change rates and set-ups.

3.3.3 CONCENTRATION DISTRIBUTION

Different concentration distributions are observed for the different set-ups (see Figure 3.12 - Figure 3.15) as the airflow pattern affects the transport of

contaminants in the room. Further concentration distributions are shown in Appendix B.

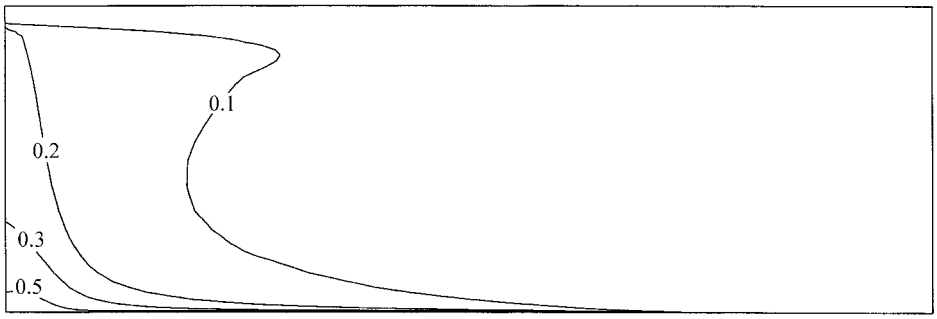

Figure 3.12 Concentration distribution in the empty room with the pollutant source located at the floor for N=10h^{-1}. The values represent the non-dimensional concentration c/c_w.

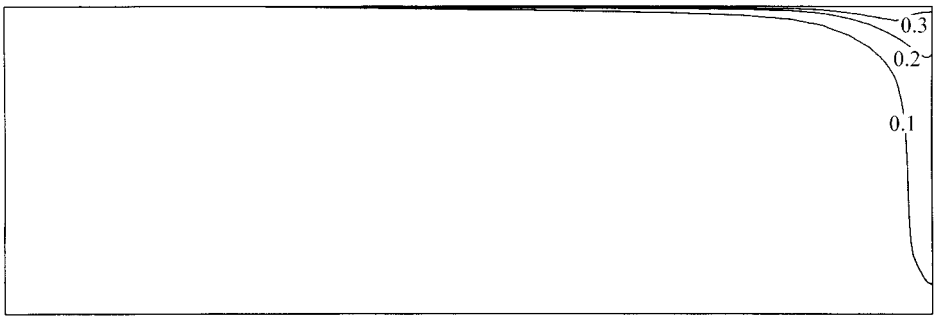

Figure 3.13 Concentration distribution in the empty room with the pollutant source located at the ceiling for N=10h^{-1}. The values represent the non-dimensional concentration c/c_w.

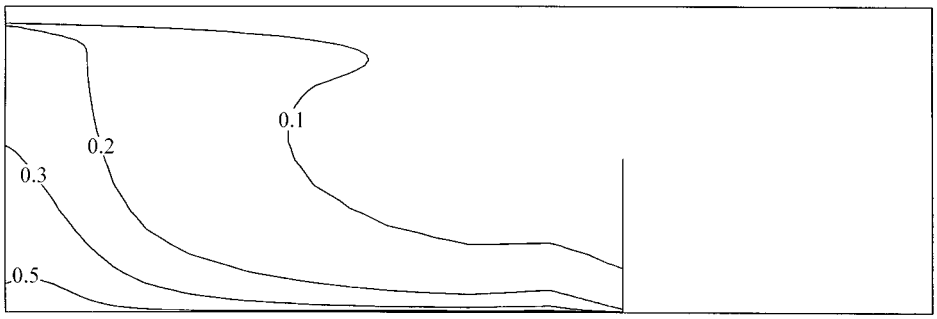

Figure 3.14 Concentration distribution in the room with a wall and the pollutant source located at the floor for N=10h^{-1}. The values represent the non-dimensional concentration c/c_w.

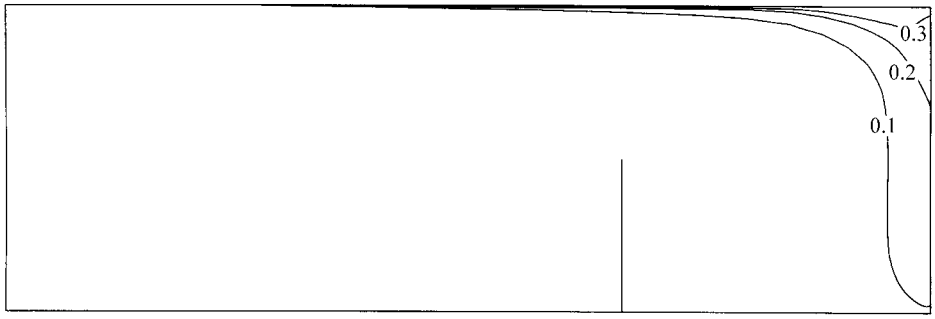

Figure 3.15 Concentration distribution in the room with a wall and the pollutant source located at the ceiling for N=10h^{-1}. The values represent the non-dimensional concentration c/c_w.

Typical concentration profiles close to the surface in the full-scale room are shown in Figure 3.16

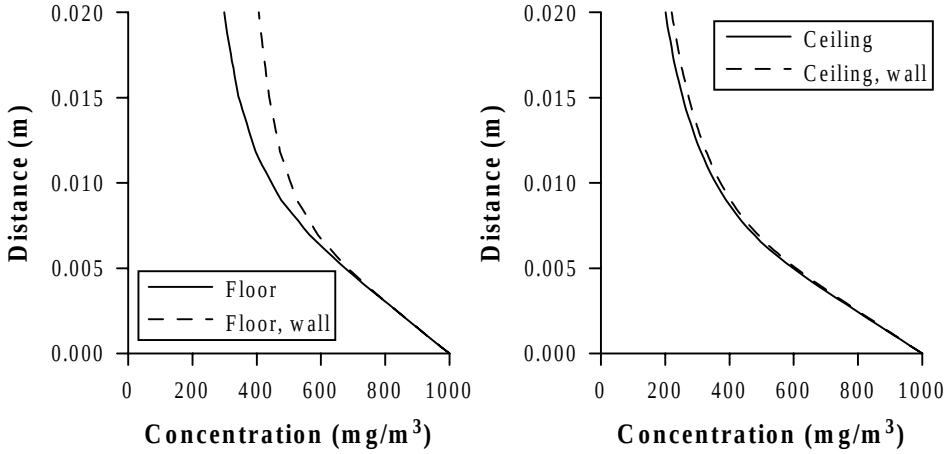

Figure 3.16 Typical concentration profiles from the full-scale room at x=3 m for the floor and x=6m for the ceiling. The profiles shown are for an air change rate of 10 h^{-1}.

From the figures it is seen that the wall has a low influence on the concentration distribution when the source is located on the ceiling. When the floor is emitting the influence of the wall becomes more significant due to the reduced velocities.

3.3.4 INFLUENCE OF VELOCITY

As the velocity over the emitting surface increases with air change the emission rate is expected to increase with velocity. The velocity referred to henceforward is the maximum velocity in the boundary layer evaluated at the centre of the emitting surface, i.e. at x=3m for the floor and at x=6m for the ceiling.

The emission rate can be conveniently expressed in terms of the mass transfer coefficient, k_c, or its non-dimensional equivalent, the Sherwood number, Sh_L.

The mass transfer coefficient referred to in the following is based on E_w and is thus the average mass transfer coefficient for the emitting surface. It is calculated from

$$k_c = \frac{E_w}{c_w - c_\infty} \tag{3.3}$$

The local concentration at y=1.5 m (x corresponding to the centre of the pollutant source) has been chosen to represent the concentration of the bulk air, c_∞.

From boundary layer theory (White, 1991-a and Sissom and Pitts, 1972) there exist a correlation between Sh_L and the Reynolds number, Re_L (see Chapter 2) according to which Sh_L correlates with Re_L raised to the power of 0.8 for turbulent flow and a Schmidt number, Sc, of unity.

When plotting Sh_L versus Re_L for the full-scale CFD calculations (see Figure 3.17) it appears that the turbulent correlation tends to underestimate the Sherwood number in particular when the floor is emitting. Furthermore, there is a difference from one set-up to another indicating that the data can not be represented by one single correlation.

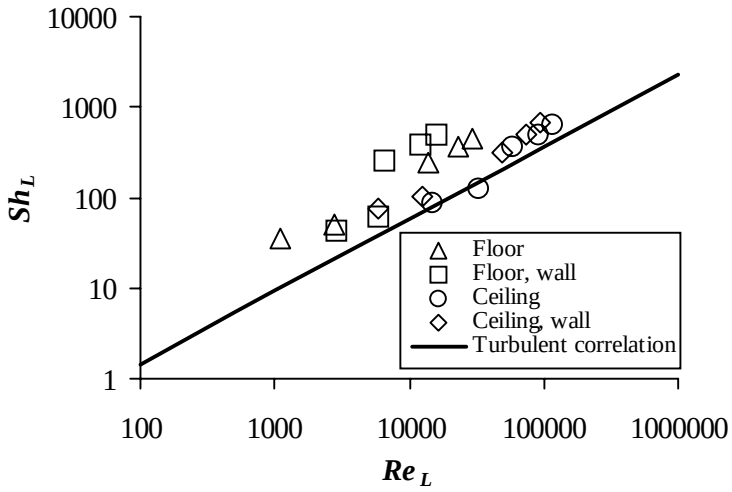

Figure 3.17 Relation between Sherwood number, Sh_L, and Reynolds number, Re_L. The solid line represents the turbulent correlation for a Schmidt number of unity (White, 1991-a and Sissom and Pitts, 1972).

The correlation of Sh_L and Re_L further implies that the mass transfer coefficient, k_c, varies with velocity raised to the power of 0.8. Figure 3.18 shows the mass transfer coefficient against velocity.

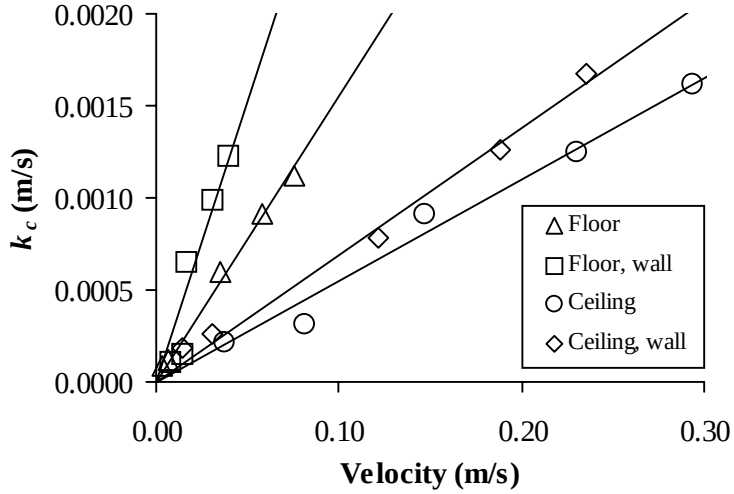

Figure 3.18 Relation between mass transfer coefficient, k_c, and velocity for the different set-ups. The solid lines have been obtained from linear regression.

From the figure it seems more likely that the relation is linear as linear regression applied to the individual data sets provides better correlations than the power fit. It is further seen that for a given set-up there is a substantial increase in mass transfer coefficient with velocity.

The thickness of the diffusion boundary layer, δ_D, is inverse proportional to the mass transfer coefficient and thus decreases with velocity (see Figure 3.19).

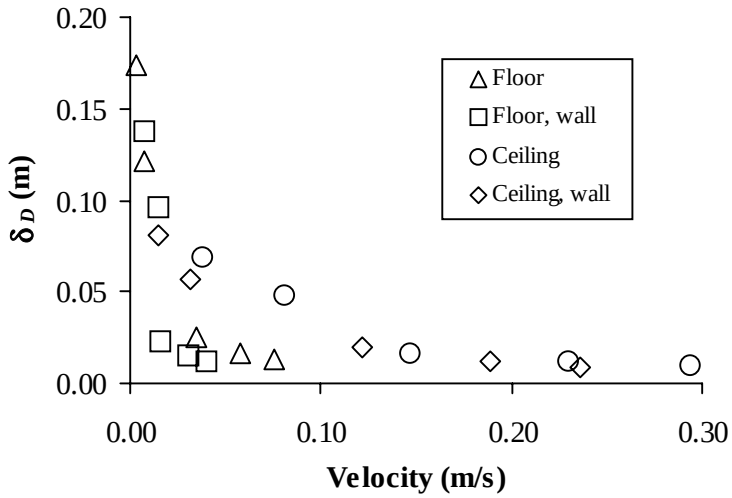

Figure 3.19 Relation between diffusion boundary layer thickness and velocity.

At low velocities the diffusion boundary layer is thick like the velocity boundary layer. In all cases the diffusion boundary layer is thinner than the velocity boundary layer.

3.3.5 INFLUENCE OF TURBULENCE

The different correlations of mass transfer coefficient and velocity are caused by the difference in set-up as the presence and location of the wall generates different levels of turbulence that have to be considered when evaluating the emission rate.

The turbulence level can be described in terms of the turbulence intensity, *Tu*. Further, the size of the turbulent eddies (length scale) might be important but it has not been considered in the present work.

The turbulence intensity is defined as the ratio of the root mean square (RMS) value of the fluctuating velocity to the mean velocity. For the two-dimensional room considered, the RMS value can be approximated by $k^{0.5}/1.1$ (Nielsen, 1990), where k is the turbulent kinetic energy. *Tu* is then given by

$$Tu = \frac{k^{0.5}}{1.1u} \tag{3.4}$$

The turbulence intensity is thus a relative measure of the turbulent kinetic energy in proportion to the velocity. Figure 3.20 shows the mass transfer coefficient as a function of the turbulent kinetic energy. It is seen that k_c increases in proportion to $k^{0.5}$ and that the wall has no significant influence on k. It should be noticed that the turbulent kinetic energy also is a function of velocity through the RMS value.

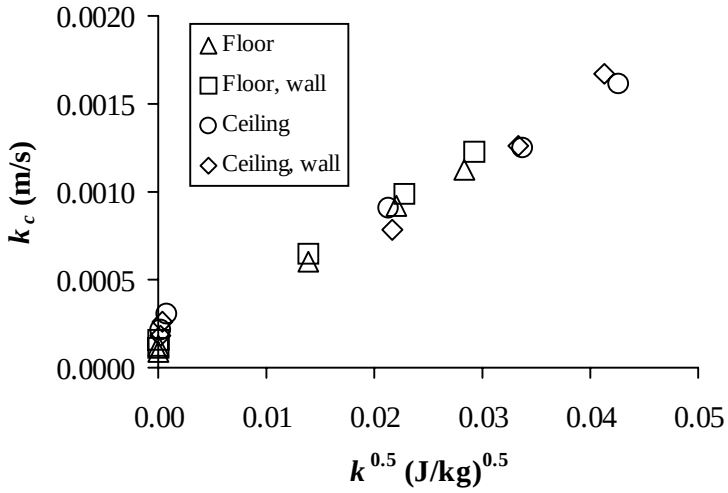

Figure 3.20 Relation between mass transfer coefficient and the square root of turbulent kinetic energy.

In the following the calculation of *Tu* is based on the reference velocity defined in Chapter 3.3.4 and the turbulent kinetic energy evaluated at the same position.

For each of the four set-ups the turbulence intensity is approximately constant and Figure 3.18 can then be replotted with *Tu* as parameter (Figure 3.21).

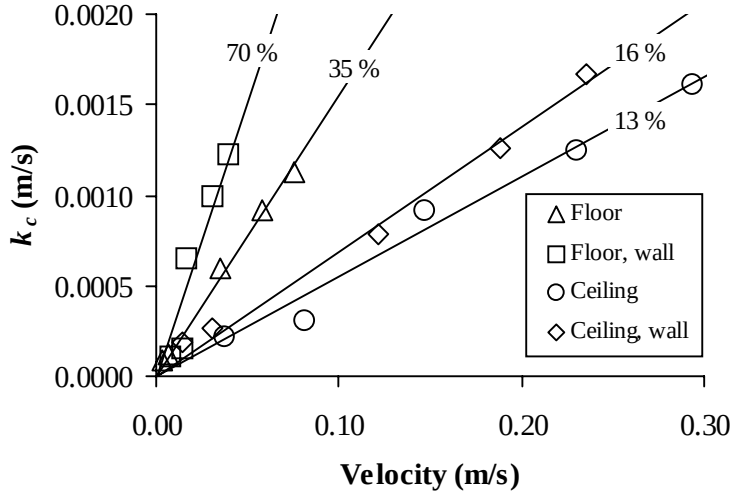

Figure 3.21 Relation between mass transfer coefficient and velocity, obtained from linear regression, with *Tu* as parameter.

For the calculations with low air change rates ($1h^{-1}$ and $2h^{-1}$) though, the turbulence intensity is less than 1.5 % and the flow is not considered turbulent. The flow close to a surface can be considered fully turbulent provided the turbulent Reynolds number, R_t>350 (Nielsen, 1998) corresponding to $f_\mu=f_2=1$ in the LRN turbulence model and it is assumed that this condition is valid also far from the wall. In the formulation of the LRN turbulence model the eddy viscosity is given by

$$\mu_t = f_\mu C_\mu \rho \frac{k^2}{\varepsilon} = f_\mu C_\mu R_t \mu_l \tag{3.5}$$

As C_μ=0.09, f_μ=1 and R_t>350 the condition for fully turbulent flow yields

$$\frac{\mu_t}{\mu_l} > 30 \tag{3.6}$$

In Figure 3.22 - Figure 3.25 the non-dimensional viscosity (μ_{eff}/μ_l) distributions are shown for $N=2h^{-1}$ and $N=5h^{-1}$.

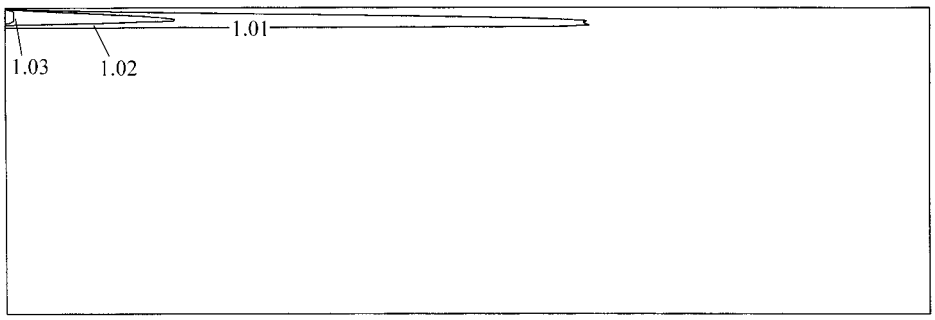

Figure 3.22 Viscosity distribution at $N=2h^{-1}$ in the empty room. The values represent the non-dimensional viscosity μ_{eff}/μ_l.

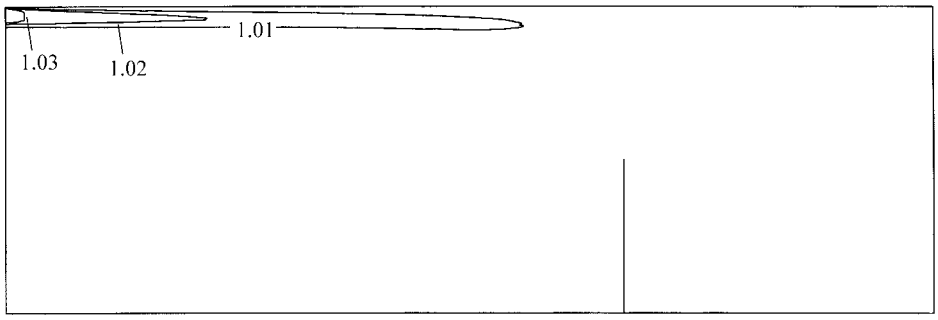

Figure 3.23 Viscosity distribution at $N=2h^{-1}$ in the room with a wall. The values represent the non-dimensional viscosity μ_{eff}/μ_l.

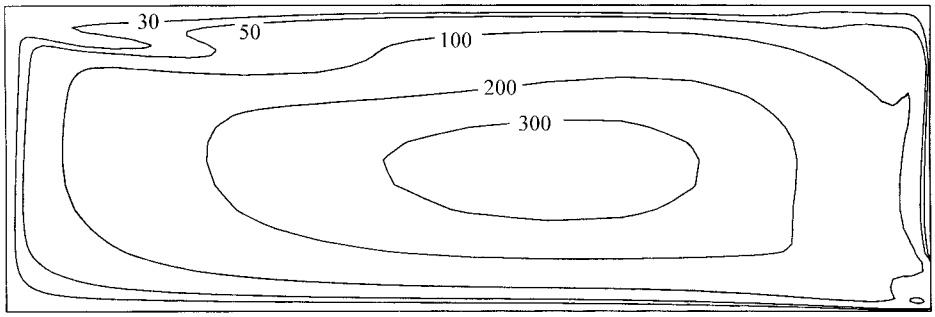

Figure 3.24 Viscosity distribution at $N=5h^{-1}$ in the empty room. The values represent the non-dimensional viscosity μ_{eff}/μ_l.

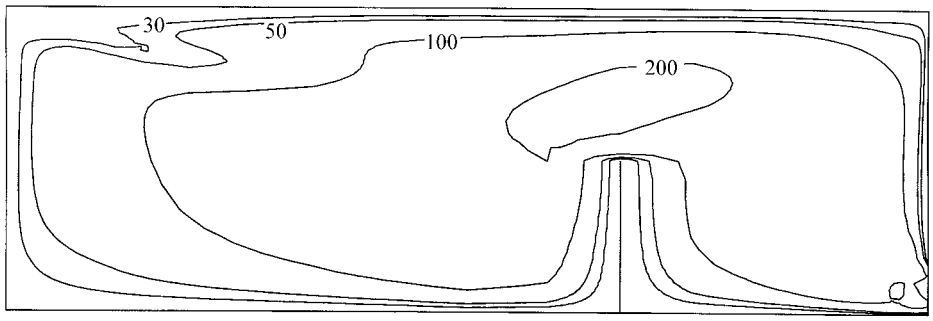

Figure 3.25 Viscosity distribution at $N=5h^{-1}$ in the room with a wall. The values represent the non-dimensional viscosity μ_{eff}/μ_l.

It is seen that at $N=2h^{-1}$ the flow is laminar as the viscosity corresponds to the laminar viscosity. At $N=5h^{-1}$ the flow can be considered fully turbulent in the entire room except for in a thin region close to the surfaces.

Based on the linear correlations of k_c and velocity (Figure 3.21), k_c can be expressed in terms of *Tu* at a given velocity. Assuming a linear correlation between k_c and *Tu* the solid lines in Figure 3.26 can be obtained. The figure also shows the results from the CFD calculations with the data grouped after velocity.

It is seen that for a given velocity the mass transfer coefficient is strongly influenced by both turbulence intensity and velocity. The figure also shows that accounting for those two parameters provides a reasonable basis for describing the mass transfer coefficient.

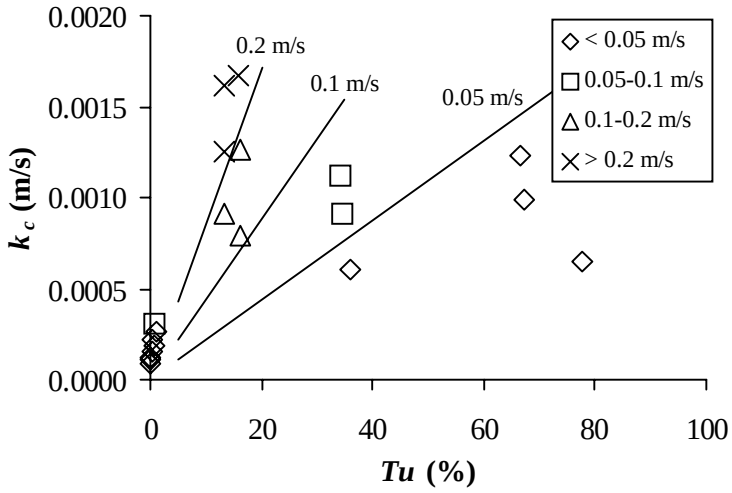

Figure 3.26 Relation between mass transfer coefficient and turbulence intensity with velocity as parameter. The solid lines are based on the linear correlations of k_c and velocity and the assumption of a linear correlation between k_c and Tu. The results from the CFD calculations have been grouped by velocity and not by set-up.

3.3.6 INFLUENCE OF SCALE

As the flow conditions over the emitting surface in a small-scale test chamber often differs from those found in a full-scale ventilated room the emission rates are also expected to be different for evaporative emission processes (see Figure 3.27).

It is appropriate to reproduce the actual flow conditions (in terms of velocity and turbulence) found in a full-scale ventilated room. However, this is often difficult as the velocity profile in a full-scale ventilated room has a maximum at some distance from the surface while the profile generated in a small-scale test chamber is often constant at the supply. Another important difference is the

scale of turbulence. In a full-scale ventilated room the size of the eddies correspond to the room height which can not be reproduced in a small-scale test chamber.

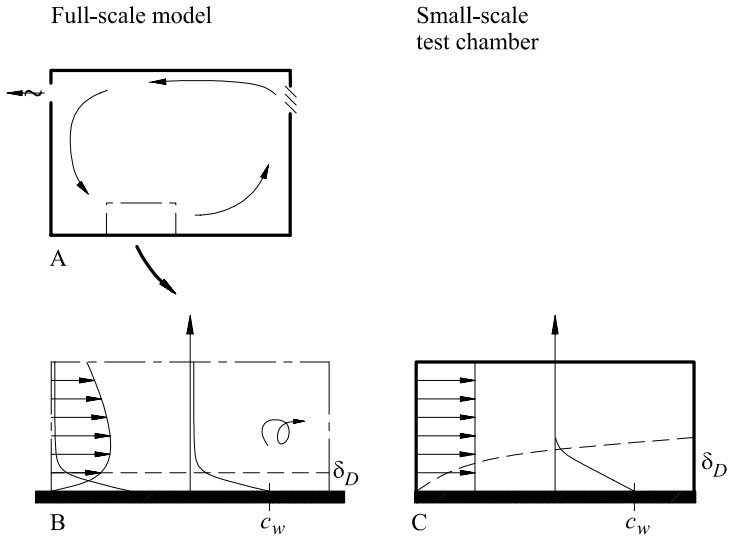

Figure 3.27 Comparison of flow conditions in a full-scale ventilated room and a small-scale test chamber. A: Recirculating flow in a mixing ventilated room. B: Enlargement of boundary layer flow at the floor. C: Small-scale test chamber for emission testing of materials.

In Figure 3.28 the mass transfer coefficient is plotted against velocity for both the small-scale test chamber and the full-scale test room. The inlet velocity is used as reference for the small-scale test chamber.

It is seen that different mass transfer coefficients are found in the two geometries at the same velocity. Materials should therefore not be tested at the velocity expected in the full-scale room but at the velocity corresponding to the mass transfer coefficient in the full-scale room. Say, a maximum velocity of 0.15 m/s is expected at the ceiling in the room without the wall then the material should be tested at 0.08 m/s to obtain the actual mass transfer coefficient of 0.0009 m/s.

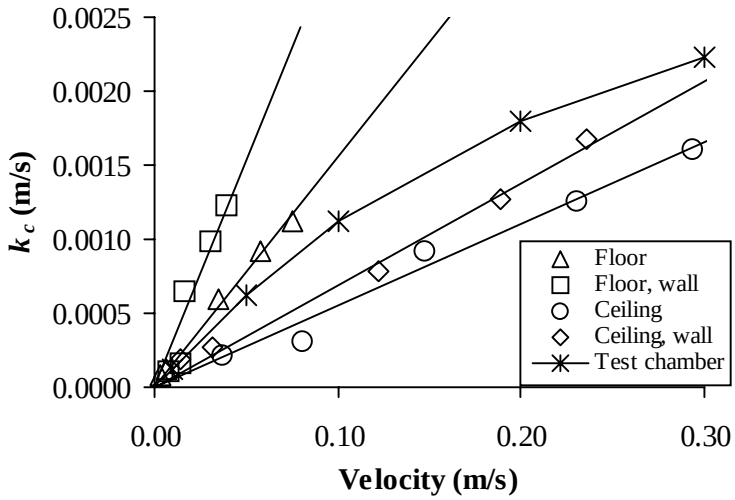

Figure 3.28 Relation between k_c and velocity for both the small-scale test chamber and the full-scale test room.

Figure 3.29 shows Sh_L versus Re_L for the full-scale test room as well as the small-scale test chamber described in Chapter 3.2.2. As both Sh_L and Re_L are based on the length, L, of the emitting surface the plot provides a better tool for comparison of data from different geometries.

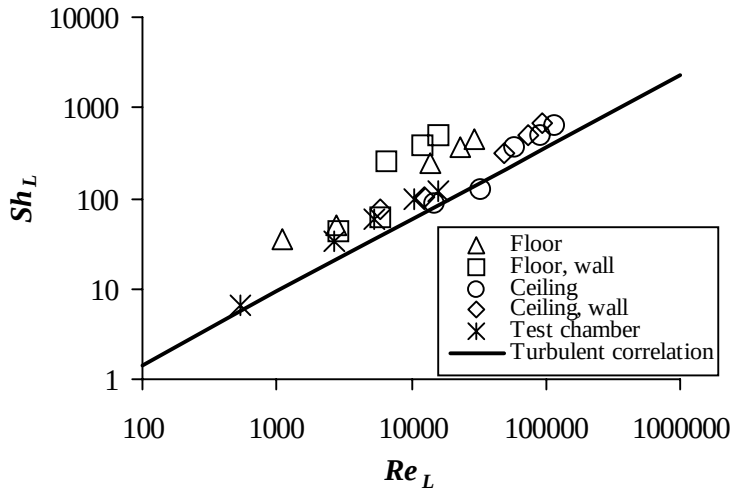

Figure 3.29 Relation between Sh_L and Re_L. The solid line represents the turbulent correlation for a Schmidt number of unity (White, 1991-a and Sissom and Pitts, 1972).

3.4 CONCLUSIONS

A series of CFD calculations for a two-dimensional full-scale geometry has been performed to investigate the influence of local airflow parameters such as velocity and turbulence intensity on the evaporative emission from a surface in a ventilated enclosure.

It was found that the emission rate varies along the emitting surface and is thus a function of the local airflow. When the air change rate is increased the emission rate goes up as a larger amount of VOCs is removed from the boundary layer flow and the results indicate a linear relationship between the emission rate and the air change rate.

The presence of an internal wall, that increases the level of turbulence, does not seem to have a significant influence on the emission rate for a given source location and air change rate. However, a difference is observed between the two source locations with the larger emission rate occurring at the ceiling.

The concentration distribution in the room strongly depends on the source location and the airflow pattern. If the source is located at the ceiling only a region close to the source and the end wall is contaminated. When the source is located at the floor the VOCs mix into a larger part of the room as they travel a longer path before they are exhausted from the room.

The emission rate can be conveniently expressed in terms of the mass transfer coefficient, k_c, or its non-dimensional equivalent, the Sherwood number. The results show that by increasing the velocity or the turbulence intensity in the boundary layer a proportional increase in the mass transfer coefficient is achieved.

It was found that the turbulent correlation between the Sherwood number and the Reynolds number, known from boundary layer theory, tends to underestimate the mass transfer coefficient. In addition, there is a difference between the individual set-ups indicating that the results can not be represented by one single correlation. The results indicate a linear relation between the mass transfer coefficient and the velocity for each set-up while boundary layer theory predicts k_c to be a function of $u^{0.8}$.

For a given set-up the turbulence intensity, Tu, is approximately constant except at low air change rates, while it differs from one set-up to another. It is thus concluded that the mass transfer coefficient is a function of both velocity and turbulence intensity. It is shown that linear relations between k_c and Tu and between k_c and u provide a reasonable description of the mass transfer coefficient.

CFD calculations were also performed for a small-scale test chamber to investigate the influence of scale. It was found that at a given velocity the mass transfer coefficient found in a small-scale test chamber differs from that found in a full-scale geometry. Different levels of turbulence cause this as the scale of turbulence found in a full-scale geometry can not be reproduced in small-scale experiments. A method for transferring results obtained from small-scale experiments to a full-scale ventilated room is proposed.

Chapter 4

FULL-SCALE EXPERIMENTS

4.1 INTRODUCTION

A series of experiments in a full-scale ventilated room have been performed to investigate the influence of local airflow on the evaporative emission from a surface (Topp et al. 1998). The experiments include velocity measurements and measurements of room air concentrations.

In the experiments the fresh airflow rate, temperature and relative humidity were kept fixed while the amount of recirculating air was varied.

All experiments were performed at the laboratories of the United States Environmental Protection Agency (EPA) in North Carolina, USA.

4.2 METHODS

As the interest has been focused on the influence of velocity on the emission rate all experiments have been performed at the same fresh air change rate, N, to keep the bulk concentration, c_∞, constant while the amount of recirculating air has been varied to generate different velocity levels. The air change rate, N^*, has been defined as the sum of the fresh air change rate and the recirculation air change rate

$$N^* = N + N_{re} \tag{4.1}$$

The temperature and relative humidity were monitored during the experiments and kept at 23°C ± 0.2°C and 48% ± 2%, respectively and the fresh air change rate was kept at $1h^{-1}$.

Duplicate experiments have been performed at three different air change rates. In Table 4.1 the experimental parameters are shown.

Experiment	N (h^{-1})	N^* (h^{-1})	M_0 (g/m^2)
1	1	5	44.0
2	1	5	39.0
3	1	2	35.7
4	1	2	34.8
5	1	3.5	34.9
6	1	3.5	39.9

Table 4.1 Experimental parameters. M_0 is the amount of VOC applied.

4.2.1 ROOM CHARACTERISTICS

The full-scale room contains a volume of 30 m^3 and is made of stainless steel to minimise sink effects. Four inlet slots provide supply air to the room, one at the foot of each wall while the return is located at the ceiling (se Figure 4.1). Three of the inlet slots (n, s, w) direct the flow upward along the wall and the fourth inlet slot (e) directs the flow along the floor. The pollutant source is located at the centre of the floor.

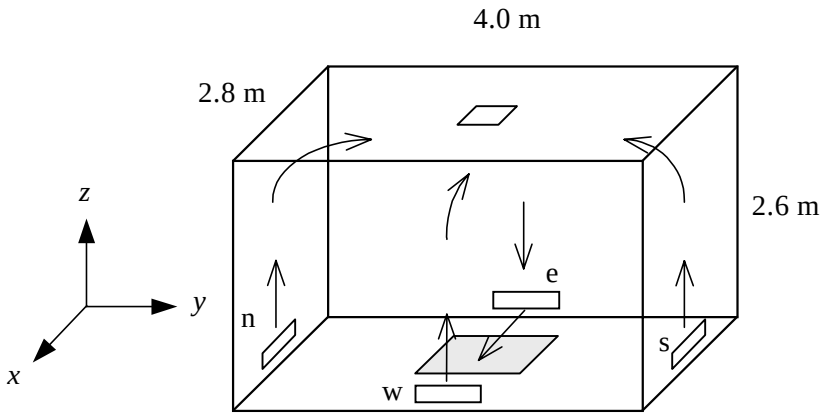

Figure 4.1 Outline of the full-scale ventilated room. Four inlet slots, one at the foot of each wall, provide supply air to the room while the return is located at the ceiling. The inlet slots are named east (e), west (w), north (n) and south (s). The pollutant source is located at the centre of the floor. The arrows indicate the airflow pattern.

At the starting point of the experiment the surface concentration of the pollutant source, c_w, equals the equilibrium vapour concentration, c_v, and as the surface ages the concentration decreases. From Tichenor, Guo and Sparks (1993) the surface concentration is assumed to be proportional to the amount of VOC remaining in the source

$$c_w = c_v \frac{M}{M_0} \tag{4.2}$$

As the VOC is being emitted from the source the concentration in the room air changes with time. The rate of change of concentration equals the emission rate minus the rate at which the VOC is leaving the room and the mass balance for the room is thus given by

$$V \frac{dc}{dt} = Ak_c (c_w - c) - Qc \tag{4.3}$$

The rate of change of VOC in the source equals minus the emission rate from the surface and the source mass balance yields

$$\frac{dM}{dt} = -k_c\left(c_w - c\right) \tag{4.4}$$

Equations 4.2 to 4.4 provide the full mass balance for the VOC and constitute the basis for the model developed by Tichenor, Guo and Sparks (1993). The model is applied further on for comparison.

Tracer gas (SF_6) experiments have been conducted to determine how well the air is mixed and to verify the fresh air change rate. The concentration of SF_6 in the exhaust was monitored and every three hours the supply air was dosed with SF_6 for five minutes at 60 ml/minute. The results are shown in Figure 4.2.

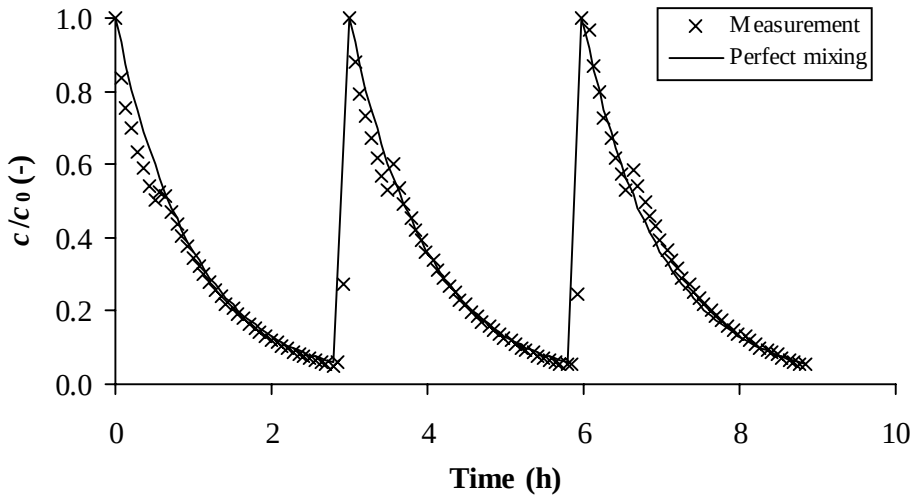

Figure 4.2 Dimensionless concentration versus time for the tracer gas experiments. The solid line corresponds to perfect mixing with a fresh air change rate of 1 h^{-1}.

It is seen that the measurements agree well with the prediction for perfectly mixed flow, all though some deviations occur. Henceforward the flow is considered perfectly mixed.

4.2.2 POLLUTANT SOURCE

The pollutant source consisted of pure decane ($C_{10}H_{22}$) applied to a board of plywood. Decane is a VOC with equilibrium vapour concentration c_v=12115 mg/m^3 and molecular diffusion coefficient D=5.75E-6 m^2/s.

In each experiment the pollutant source was located at the centre of the floor as seen in Figure 4.1. The amount of solution applied is shown in Table 4.1 and the area of the board is 1.48 m^2 (1.22 m by 1.22 m). The edges of the board were sealed to limit the VOC to emission from the top surface.

Experimental procedure:

1. Flush the room for at least 24 hours
2. Condition the board in the room for at least 48 hours
3. Apply the VOC to the board
4. Start the sampling

4.2.3 VELOCITY MEASUREMENTS

Due to the configuration of the inlet slots the flow over the pollutant source was parallel to the surface in a layer of approximately 0.15 m above the surface (visualised by smoke).

Velocity profiles were measured with an omni-directional thermal anemometer at five different locations to obtain detailed knowledge of the flow over the pollutant source (see Figure 4.3 and Figure 4.4).

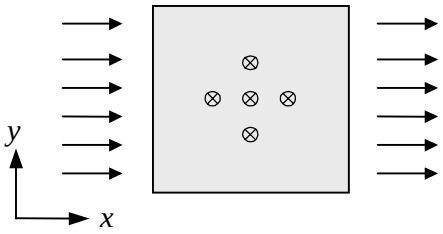

Figure 4.3 The flow over the pollutant source was parallel to the surface and in the direction from east to west. Velocity profiles were measured at five locations.

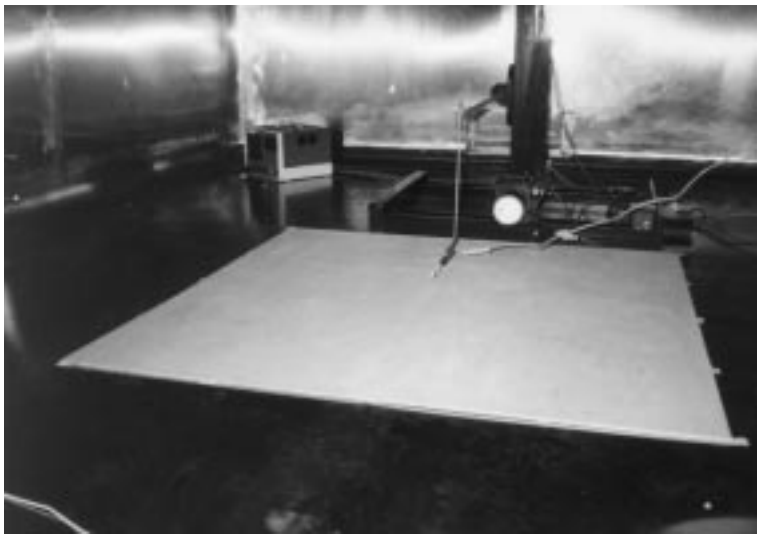

Figure 4.4 The velocity profiles over the pollutant source were measured with an omni-directional thermal anemometer mounted on a three-dimensional traverse system.

The profiles are named centre, east, west, north and south (see Table 4.2). As the anemometer only measures the magnitude of the velocity, i.e. the speed of the flow, the direction was verified by smoke experiments. Henceforward the measurements are referred to as velocities.

		***x* (m)**		
		-0.25	0	0.25
***y* (m)**	0.25		South	
	0	East	Centre	West
	-0.25		North	

Table 4.2 Coordinates for the velocity profiles. The locations are named centre, east, west, north and south.

Each profile consists of 7 measurement points (at z = 1, 2, 3, 4, 6, 10 and 15 cm).

4.2.4 CONCENTRATION MEASUREMENTS

As shown in Figure 4.2 the flow is well mixed and it is chosen to determine the concentration of decane from a single location in the room. The concentration was determined from samples of the room air taken at (x, y, z)=(0.3; 1.0; 1.3) m

By means of a vacuum pump and a mass flow controller the air samples were pulled through sorption tubes filled with activated charcoal. To keep the amount of decane in the individual samples above the detection limit the sampling flow rates and the sampling periods were varied. The sample volumes thus ranged from 1000 to 15000 cm^3 while the sample periods varied from 10 to 50 minutes.

Analytes were then extracted from the sorption tubes with carbon disulfide (CS_2) and the concentration of decane in the extract was determined by injecting a subsample of the extract onto the column of a gas chromatograph equipped with a mass selective detector.

4.3 RESULTS

4.3.1 VELOCITY

The velocity profiles over the pollutant source are shown in Figure 4.5 - Figure 4.7.

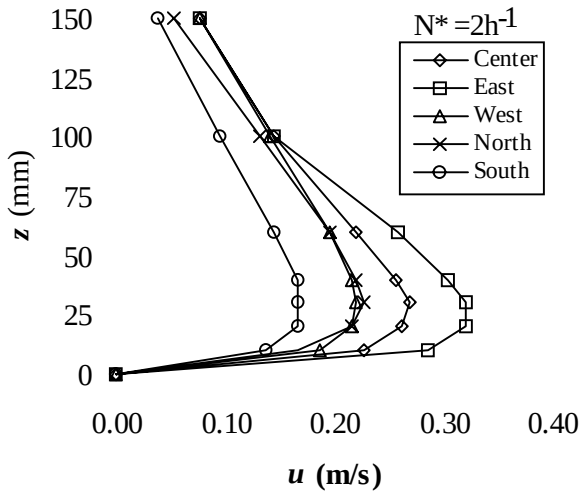

Figure 4.5 Velocity profiles over the pollutant source at N^*=2 h^{-1}.

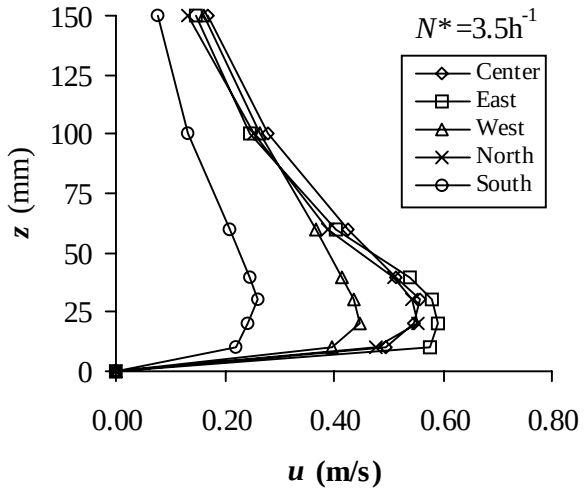

Figure 4.6 Velocity profiles over the pollutant source at N^*=3.5 h^{-1}.

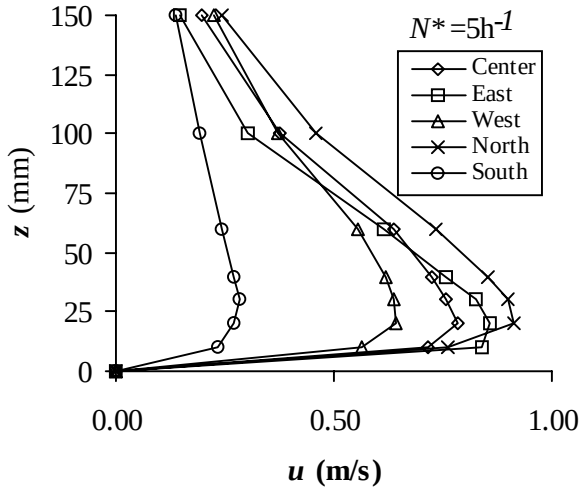

Figure 4.7 Velocity profiles over the pollutant source at N^*=5 h^{-1}.

It is seen that the profiles have a characteristic shape with the maximum velocity occurring 2-3 cm above the source. Further, the velocity level increases with N^* as expected.

Due to the configuration of the inlet slots the flow over the pollutant source is expected to be symmetrical along the y-axis, i.e. the profiles at north and south locations should be similar. This it is not the case however, as there is a difference between the north and south profiles that increases with N^* indicating that the flow from the east inlet slot is not distributed symmetrically.

The flow over the pollutant source is provided by the east inlet slot and acts like a wall jet. For a plane turbulent wall jet the velocity distribution of the entire jet has been found to be similar (Rajaratnam, 1976). Verhoff (1963) provides an empirical relation that describes the similarity

$$\frac{u}{u_{\max}} = 1.48 \left(\frac{z}{\delta_{1/2}} \right)^{1/7} \left[1 - erf\left(0.68 \frac{z}{\delta_{1/2}} \right) \right] \tag{4.5}$$

Despite the fact that the flow is not completely symmetrical along the *y*-axis the profiles express the similarity predicted by Verhoff (1963) as illustrated in Figure 4.8.

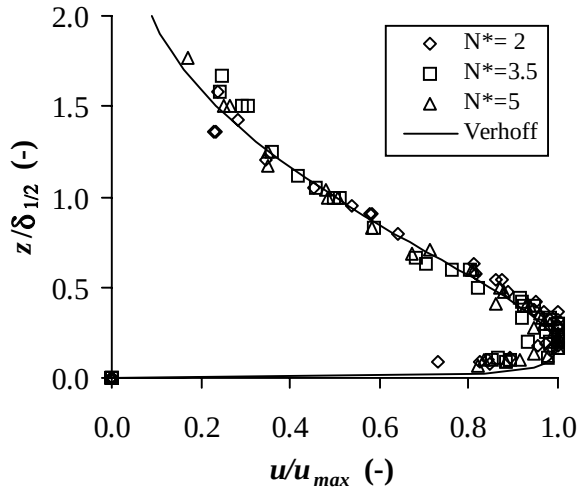

Figure 4.8 Non-dimensional velocity profiles over the pollutant source. The velocity, u, is non-dimensionalised by the maximum velocity, u_{max}, while the distance, z, is non-dimensionalised by $\delta_{1/2}$ defined as the distance from the wall where $u=u_{max}/2$. The solid line corresponds to the relation found by Verhoff (1963).

For reasons of simplification it is chosen to represent the flow over the pollutant source by the average of the profiles measured at the five locations. In the direction of the flow the velocity is seen to decrease proportional to the distance, x, and along the y-axis there is also a drop in velocity. It is thus believed that the average profiles provide a fair description of the flow over the source. The average profiles are shown in Figure 4.9.

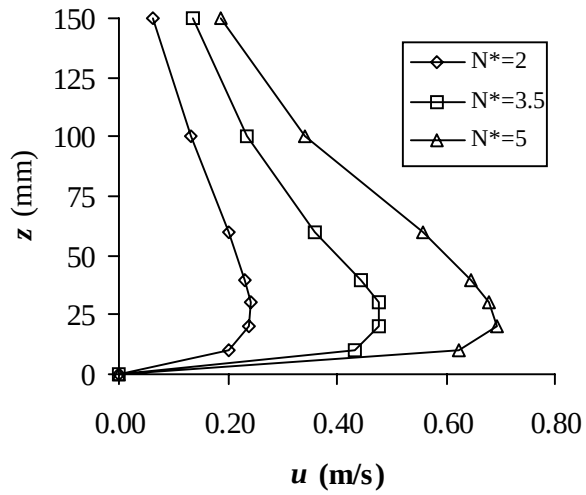

Figure 4.9 Average velocity profiles over the pollutant source.

It is seen that the maximum velocity increases from 0.24 m/s to 0.69 m/s as N^* increases from 2 h^{-1} to 5 h^{-1} while the boundary layer thickness is constant. The maximum velocity thus increases with approximately the same factor as N^*.

4.3.2 CONCENTRATION

The measured room concentrations are shown in Figure 4.10 - Figure 4.12 as well as model predictions (Tichenor, Guo and Sparks, 1993). Due to invalid samples within the first hour of experiments the model predictions for experiments 5 and 6 (N^*=3.5h^{-1}) include parameters estimated from the results of experiments 1-4. In general the model predictions agree well with the measurements but seems to underestimate the peak concentrations.

All profiles have the characteristic shape involving a rapid increase in concentration followed by a rapid decline within the first two hours. During this period there is a significant difference between concentrations from experiments with one N^* to another.

The concentration level is seen to increase with N^* as the emission rate increases with velocity over the source. A larger amount of VOC re-enter the room as N^* goes up and hence the emission rate is lower than if ventilating with the same amount of fresh air. After approximately two hours the concentration levels become similar as they approach zero.

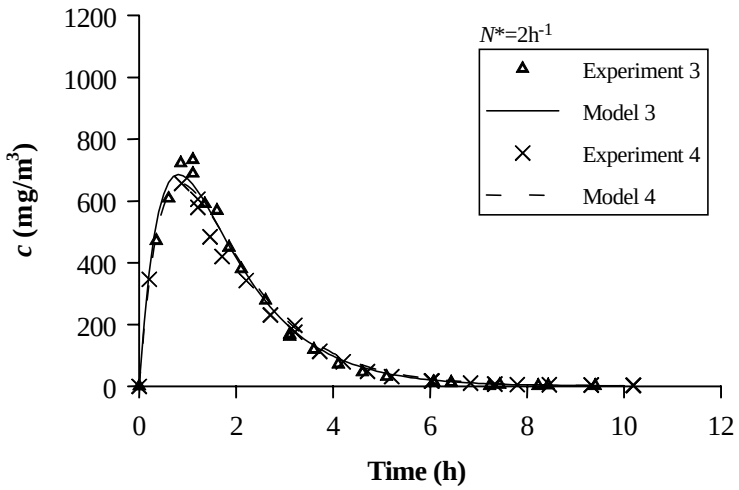

Figure 4.10 Room concentration at $N^*= 2h^{-1}$. The lines correspond to the model predictions by Tichenor, Guo and Sparks (1993).

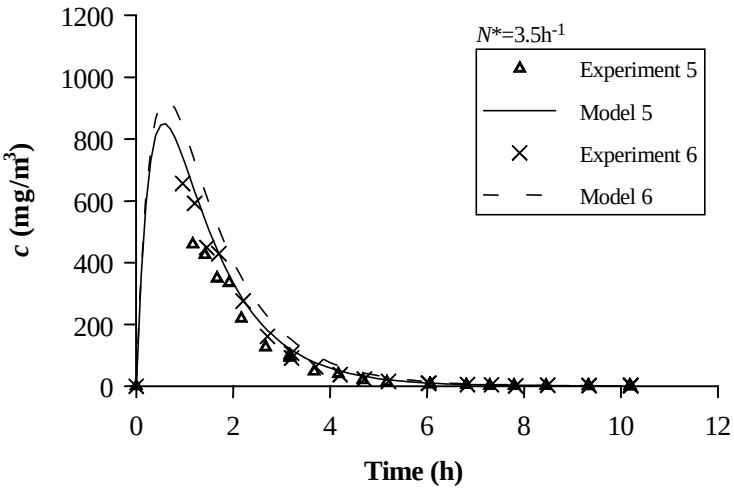

Figure 4.11 Room concentration at $N^*= 3.5h^{-1}$. The lines correspond to the model predictions by Tichenor, Guo and Sparks (1993).

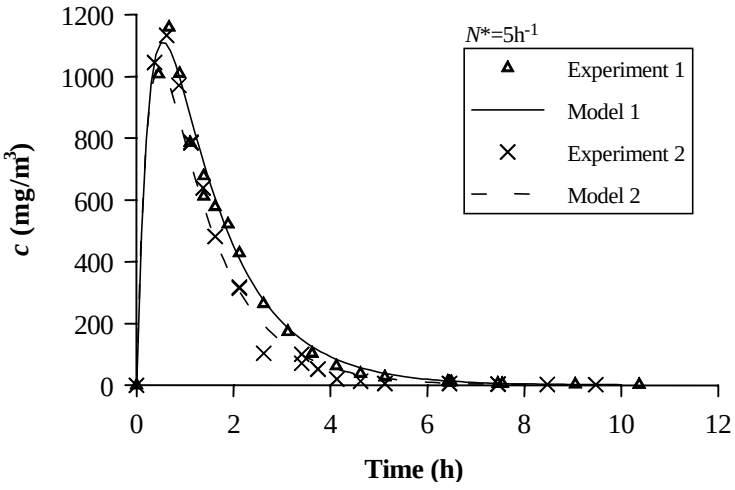

Figure 4.12 Room concentration at $N^*= 5h^{-1}$. The lines correspond to the model predictions by Tichenor, Guo and Sparks (1993).

It is further seen that the measurements from duplicate experiments are similar and the largest difference between peak concentrations is 10 % occurring at $N^*=2h^{-1}$. The initial amount of solution applied, M_0, differs up to 14 % within duplicate experiments but does not seem to have the same influence on the concentration measurements. Higher peak concentrations though, are found in the experiments with the largest amount of solution applied.

Due to the large variation in concentration it is difficult to evaluate the tail of the profiles from Figure 4.10 - Figure 4.12. The concentrations are therefore replotted in logarithmic scale (see Figure 4.13 - Figure 4.15).

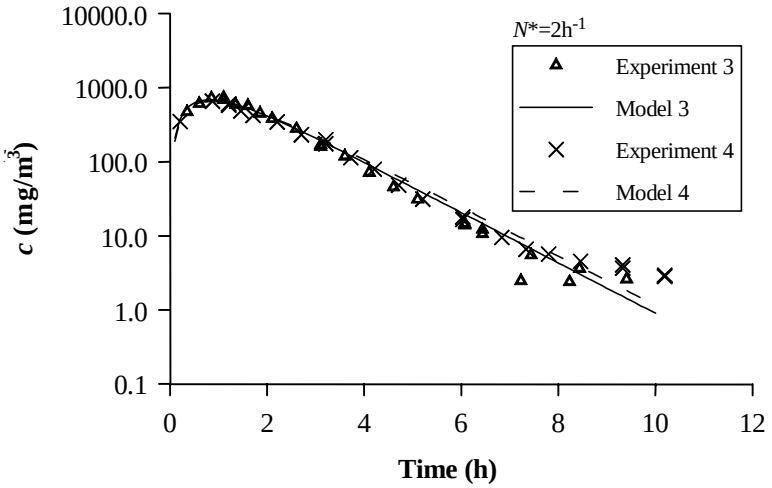

Figure 4.13 Room concentration in logarithmic scale at $N^*= 2h^{-1}$. The lines correspond to the model predictions by Tichenor, Guo and Sparks (1993).

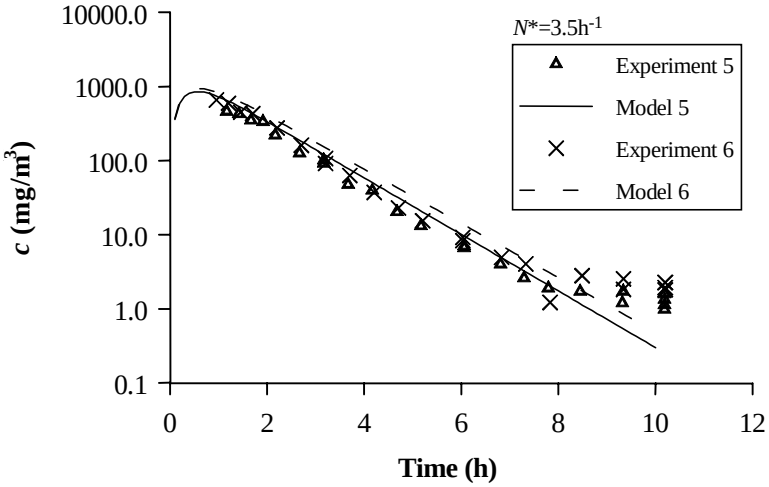

Figure 4.14 Room concentration in logarithmic scale at $N^*= 3.5h^{-1}$. The lines correspond to the model predictions by Tichenor, Guo and Sparks (1993).

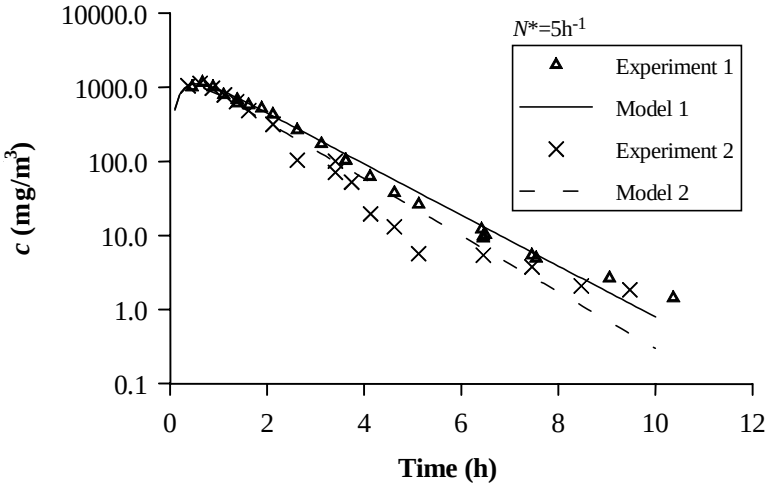

Figure 4.15 Room concentration in logarithmic scale at $N^*= 5h^{-1}$. The lines correspond to the model predictions by Tichenor, Guo and Sparks (1993).

After approximately 8 h the experiments show that the concentration decay rate becomes slower indicating that the emission process changes from evaporative to being controlled by internal diffusion.

The room air concentration changes rapidly with time during the evaporative phase as the boundary layer offers little resistance to the release of the VOC. When the emission becomes controlled by internal diffusion though, the gas molecules have to diffuse through the material before being released to the air and thus slow down the concentration decay rate. A solid material can hold a larger amount of VOC than air (expressed by the partition coefficient, K_p) and furthermore the ratio of the diffusion coefficients favours quicker diffusion in air.

The model predictions by Tichenor, Guo and sparks (1993) are valid for evaporative emissions only and therefore predicts no change in the concentration decay rate.

As mentioned previously the concentration profiles all have the characteristic shape involving a rapid increase in concentration and a rapid decline. It is thus plausible to believe that some similarity exist between the profiles. Assuming that the governing parameters are the maximum concentration, c_{max}, and the time, $t(c_{max})$ at which c_{max} occurs the profiles can be replotted in terms of the non-dimensional variables c/c_{max} and $t/t(c_{max})$. These profiles express similarity as illustrated in Figure 4.16 - Figure 4.17.

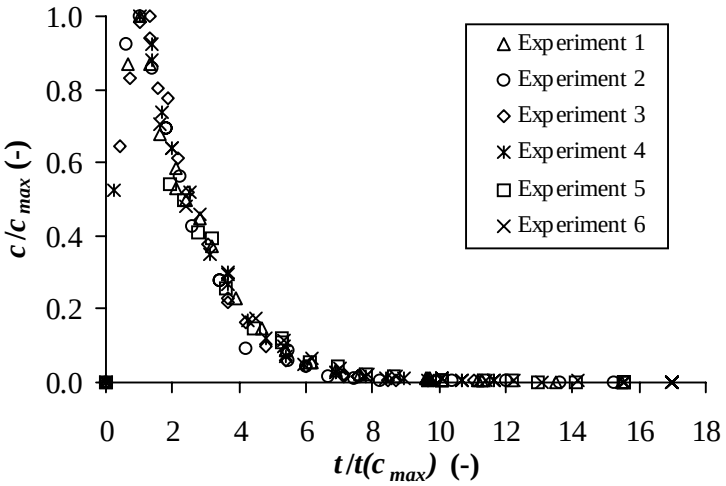

Figure 4.16 Non-dimensional concentration profiles. The concentration has been non-dimensionalised by the maximum concentration, c_{max}, while the time has been non-dimensionalised by the time, $t(c_{max})$, at which c_{max} occurs.

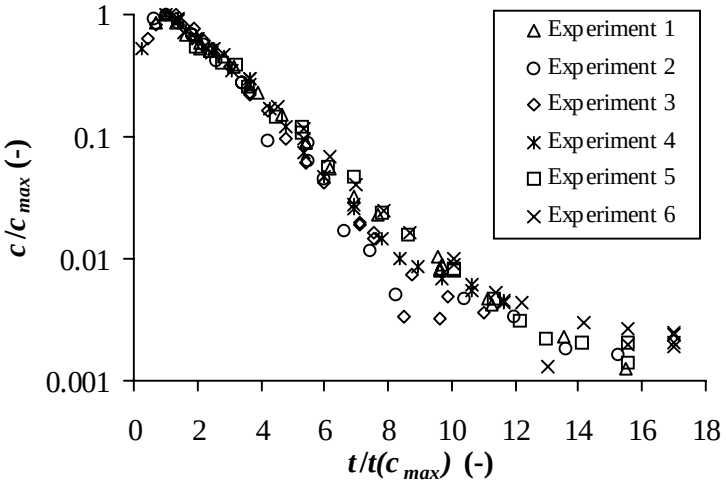

Figure 4.17 Non-dimensional concentration profiles in logarithmic scale. The concentration has been non-dimensionalised by the maximum concentration, c_{max}, while the time has been non-dimensionalised by the time, $t(c_{max})$, at which c_{max} occurs.

4.3.3 EMISSION

In the following the emission rates calculated are based on the VOC mass balance for the room (equation 4.3). The results are shown in Figure 4.18 - Figure 4.20.

It is seen that the emission rate drops rapidly within the first two hours and then the decline slows down. This is due to the fact that the concentration difference between the surface and the room air is the driving force for the emission of VOC from the surface. As the surface concentration drops from its initial value, c_v, the concentration difference becomes smaller and hence the emission rate reduces.

From the figures it is further seen that the initial emission rate increases with N^* while the duration of the rapid decline period reduces.

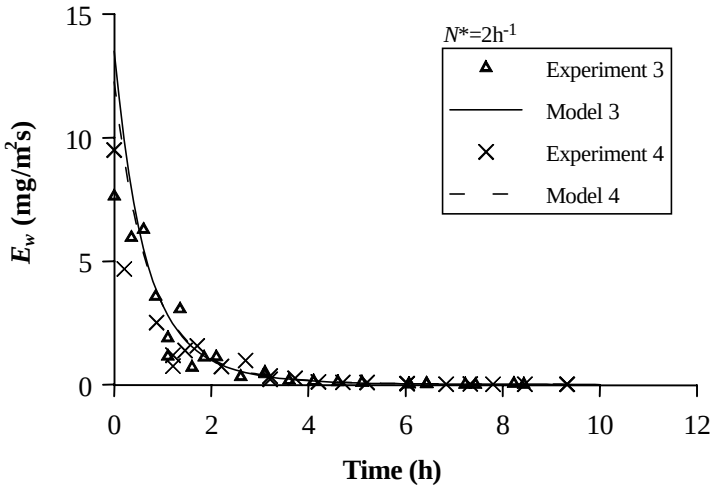

Figure 4.18 Emission rate at N^*=2h^{-1}. The lines correspond to the model predictions by Tichenor, Guo and Sparks (1993).

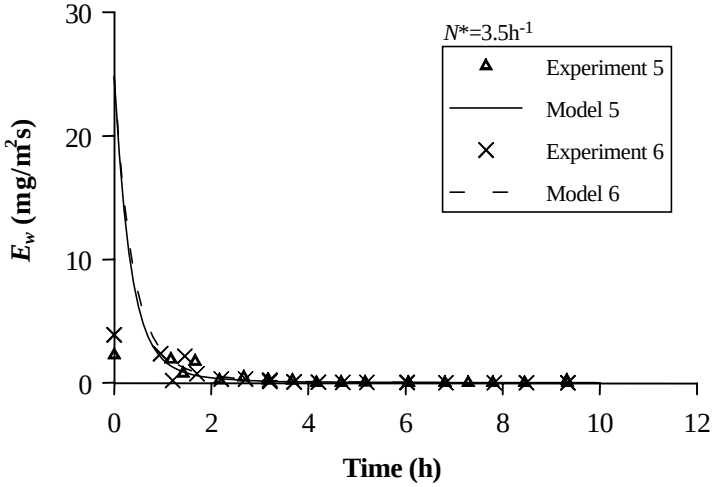

Figure 4.19 Emission rate at $N^*=3.5h^{-1}$. The lines correspond to the model predictions by Tichenor, Guo and Sparks (1993).

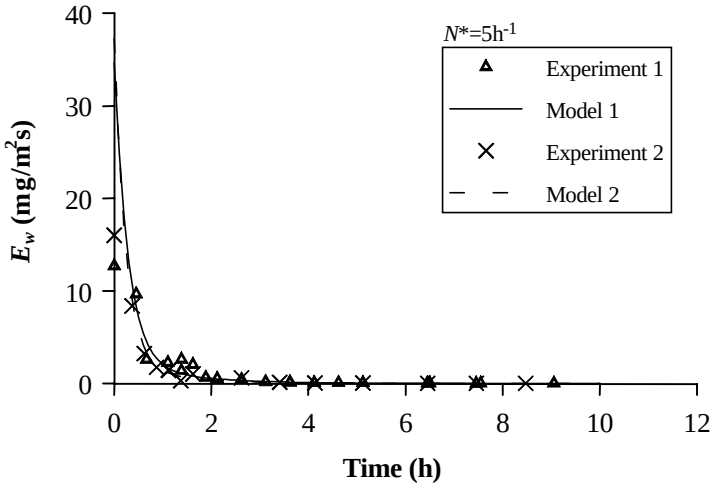

Figure 4.20 Emission rate at $N^*=5h^{-1}$. The lines correspond to the model predictions by Tichenor, Guo and Sparks (1993).

4.3.4 MASS TRANSFER COEFFICIENT

The model predictions (Tichenor, Guo and Sparks, 1993) for concentration and emission rate have been calculated by solving the VOC mass balance equations (4.2-4.4) leaving the mass transfer coefficient, k_c, as the only unknown parameter.

The mass transfer coefficient has then been obtained through non-linear regression by fitting the analytical solutions to the experimental data. For experiments 5 and 6 though, k_c has been estimated by knowledge of the results from experiments 1-4 due to invalid samples within the first hour of experiments. Table 4.3 shows the mass transfer coefficients for the experiments.

Experiment	N* (h^{-1})	k_c (m/s)
3	2	0.0011
4	2	0.0010
5*	3.5	0.0020
6*	3.5	0.0020
1	5	0.0029
1	5	0.0031

Table 4.3 Mass transfer coefficients obtained from non-linear regression. *k_c has been estimated by knowledge of the results from experiments 1-4.

In Figure 4.21 the mass transfer coefficient is plotted versus the average maximum velocity over the pollutant source. It is seen that the mass transfer coefficient depends strongly on the velocity over the source as an increase in velocity yields a proportional increase in mass transfer coefficient. The behaviour is expected as boundary layer theory predicts k_c to be a function of $u^{0.8}$.

For comparison the CFD results from the set-up with the pollutant source located at the ceiling and no wall are included in Figure 4.21. The experiments have been performed with a Schmidt number of Sc=2.6 while Sc=1.0 in the CFD calculations and the results in the figure thus only allows for qualitative comparison.

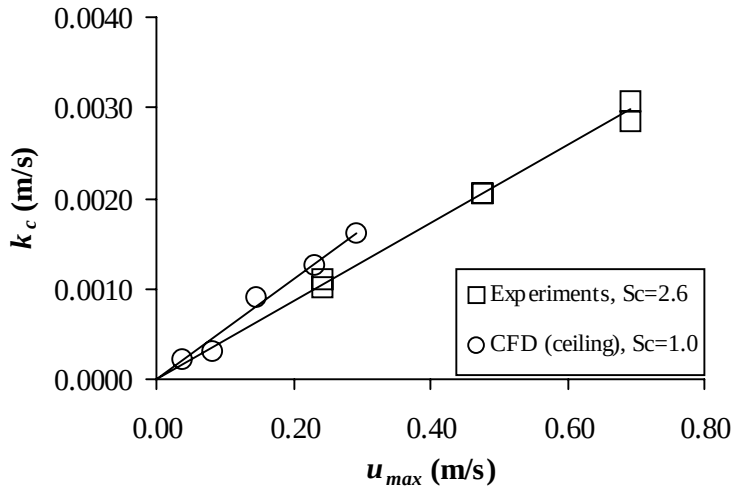

Figure 4.21 Relation between the mass transfer coefficient and the maximum velocity over the pollutant source. CFD results from the set-up with the pollutant source located at the ceiling and no wall are included

4.4 CONCLUSIONS

A series of experiments was performed in a full-scale ventilated room to investigate the influence of velocity on the emission rate from a surface. During the experiments the fresh air change rate, temperature and relative humidity were kept fixed while the amount of recirculating air was varied to generate different velocity levels over the source. The results are consistent with those obtained by Low et al. (1998) who studied the emission of VOCs from carpet-adhesive assemblies.

Duplicate experiments were performed at each velocity level and the results are similar indicating a high level of repeatability. Furthermore, the results show good agreement with model predictions (Tichenor, Guo and Sparks, 1993) for both concentration and emission, although the predictions seem to underestimate the peak concentrations.

A significant difference between concentrations from one velocity level to another was observed within the first two hours of experiments as the concentration levels increased with velocity. As the driving force for the emission is the concentration gradient between the surface and the bulk air, the experiments also exhibited higher emission rates at higher velocities in the early stage. After the first two hours concentrations as well as emissions became similar as they approached zero.

In addition it was found that the concentration decay rate slowed down after approximately 8 hours in all experiments. This indicates that the emission process changed towards being diffusion-controlled.

Consequently, it must be concluded that the velocity level has no influence on diffusion-controlled emissions. From an indoor air quality point of view this would have been desirable however, as long-term emissions are often controlled by internal diffusion.

When plotting concentration versus time in terms of non-dimensional variables c/c_{max} and $t/t(c_{max})$ the profiles are almost identical indicating that similarity exist between the experiments.

It was found that the mass transfer coefficient is a strong function of the velocity level over the surface as the mass transfer coefficient increases in proportion to the velocity which was also observed in the CFD calculations (Chapter 3). The results though, only allow for qualitative comparison as different Schmidt numbers were used in the experiments and the CFD calculations.

A source of error is introduced as the mass transfer coefficient has been obtained from a best-fit method. The standard deviation on the mass transfer coefficient is less than 12%.

Chapter 5

MODELLING INTERNAL DIFFUSION BY CFD

5.1 INTRODUCTION

In the previous chapters the interest has been focussed on the evaporative emission from a surface with known concentration, i.e. constant (Chapter 3) or modelled in terms of the amount of VOCs available (Chapter 4). However, most emission processes also involve diffusion through the source. For diffusion-controlled emission processes, the surface concentration becomes a function of material properties such as the diffusion coefficient and material structure.

The existing models are in general limited to either evaporation-controlled or diffusion-controlled emission and based on specific compounds and sources. Tichenor, Guo and Sparks (1993) developed a model for evaporative emission based on fundamental boundary layer theory. A model for diffusion-controlled emission based on experiments with vinyl floor covering was proposed by Clausen et al. (1993). Christiansson, Yu and Neretnieks (1993) developed a model for VOC emission from PVC floorings based on diffusion theory. Other diffusion models were proposed by Dunn (1987) and Little, Hodgson and Gadgil (1994). Yang, Chen and Bluyssen (1998) demonstrated a specific model based on CFD for VOC emission from a carpet. The model accounts for the internal diffusion through the carpet.

This chapter presents a general model by means of CFD that incorporates both internal diffusion in the material and evaporative emission from the material surface without prior knowledge of the surface concentration. The model provides detailed information on the concentration distribution in the air as well as in the source.

5.2 METHODS

Diffusion of VOCs through a solid material is a complex process as it involves both physical and chemical phenomena depending on material structure and material properties. To account for the internal diffusion in the CFD calculations the computational domain is expanded as the grid is extended into the material. Figure 5.1 outlines the concept of the approach.

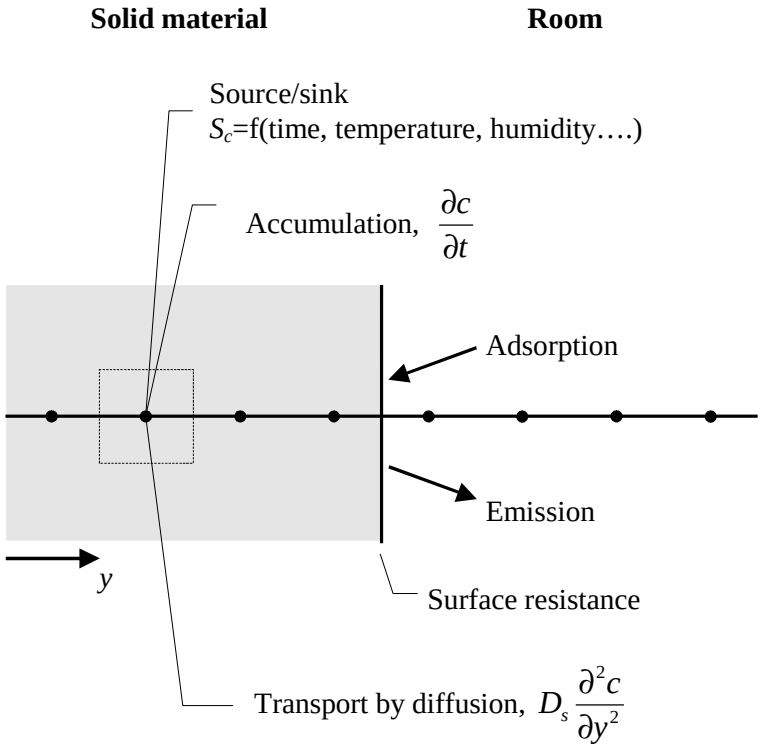

Figure 5.1 Outline of the numerical approach. The grid is extended into the solid material to account for internal diffusion.

The internal diffusion process tends toward a uniform distribution of compounds and molecules thus migrate from regions of high concentration to regions of low concentration. Initially the material contains an amount of compounds but compounds can also be generated or consumed within the

material through chemical reactions and the material thus behaves like a source or a sink. Furthermore, the material might have the capacity to accumulate VOCs.

At the surface-air interface the compounds undergo a change in phase as they assume a solid phase within the material and gas or vapour phase in the air. Both desorption and adsorption takes place at the surface and the emission rate is thus defined as the net flux of VOCs.

As there is zero or negligible fluid flow through the solid material all transport is by internal diffusion in analogue to heat conduction in a solid. Assuming diffusion in the *y*-direction only, Fick's laws for one-dimensional mass transfer defines the transport within the material

$$J = -D_s \frac{\partial c}{\partial y} \tag{5.1}$$

$$\frac{\partial c}{\partial t} = D_s \frac{\partial^2 c}{\partial y^2} + S_c \tag{5.2}$$

In CFD the equations for momentum and mass transfer are solved simultaneously for the airflow and the solid material.

The analogy between heat and mass transfer has been applied as the commercial CFD software package used allows for calculation of heat transfer in a solid but not for mass transfer. A Fortran routine was added to specify the source term, S_c.

5.3 CASE STUDY: DIFFUSION THROUGH SOLID MATERIAL

Meininghaus, Knudsen and Gunnarsen (1998) performed a series of experiments on diffusion through several indoor surface materials. In the following the numerical approach is compared to these experimental results.

The experimental set-up (Meininghaus, Knudsen and Gunnarsen, 1998) consisted of a pair of test chambers (CLIMPAQ, see Figure 3.3) with the

material in between (see Figure 5.2). The primary chamber had a constant supply of polluted air while the secondary chamber was ventilated by clean air.

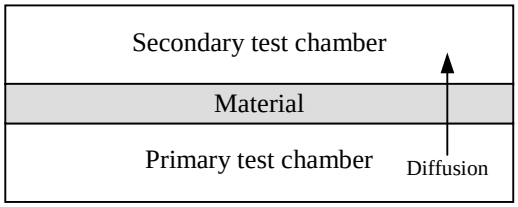

Figure 5.2 Outline of the experimental set-up used by Meininghaus, Knudsen and Gunnarsen (1998). The dimensions of one test chamber are (L, W, H)=(0.8, 0.21, 0.21) m.

Concentrations were measured in both chambers and due to an internal fan complete mixing was assumed. The calculation of the material diffusion coefficient was then based on the steady-state concentrations in the two chambers and thus neglecting any concentration gradient in the boundary layer.

5.3.1 CFD-MODEL

The simplified CFD model has been applied to the experimental set-up mentioned above. Figure 5.3 shows an outline of the CFD model.

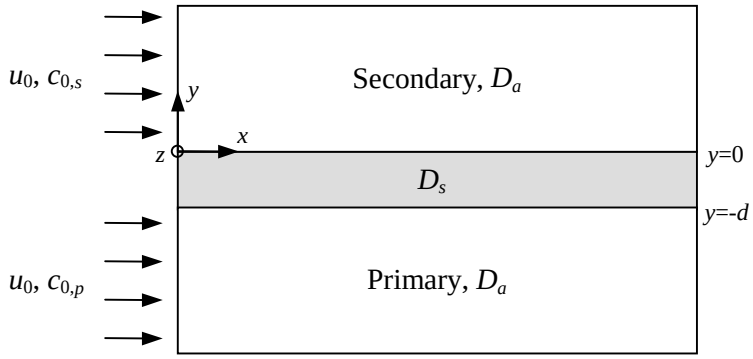

Figure 5.3 Outline of the CFD model.

In the secondary test chamber there is a large recirculation rate, which has been modelled in CFD by an inlet concentration, $c_{0,s}$.

The experiments by Meininghaus, Knudsen and Gunnarsen (1998) do not involve detailed velocity measurements and therefore the inlet velocity profile has been measured. Figure 5.4 shows the profiles measured 3 cm from the inlet.

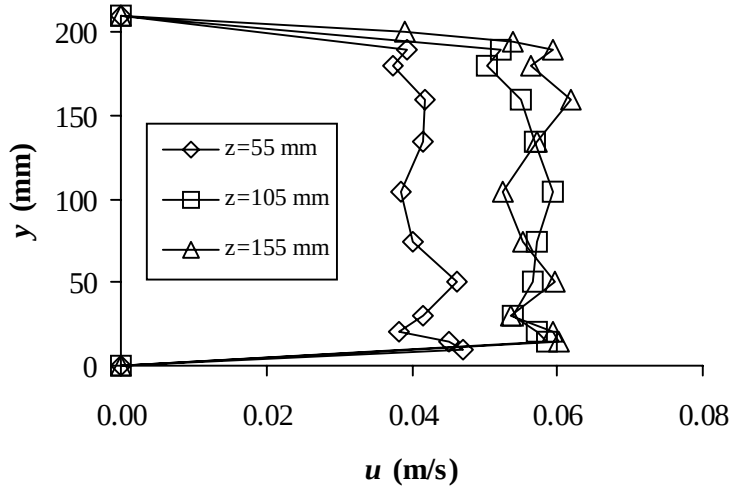

Figure 5.4 Inlet velocity profiles for the test chamber (CLIMPAQ). The profiles have been measured 3 cm from the inlet.

The inlet flow is not perfectly symmetrical along the *z*-axis and it is chosen to model the flow by a velocity, u_0, that ensures the same flow rate as found from the measurements.

Steady-state three-dimensional CFD calculations have been performed for diffusion of n-Octane through aerated concrete and brick wall with the parameters shown in Table 5.1. The material was resolved into 800 cells while each test chamber was resolved into 2000 cells thus yielding a total of 4800 cells.

	D_s (m^2/s)	D_a (m^2/s)	d (mm)	$c_{0,p}$ (mg/m^3)	$c_{0,s}$ (mg/m^3)	u_0 (m/s)
Aerated concrete	7.6E-7	6.0E-6	21	11.67	2.83	0.05
Brick wall	3.3E-7	6.0E-6	25	9.37	1.02	0.05

Table 5.1 Parameters for steady-state CFD calculations.

5.3.2 RESULTS

Figure 5.5 shows the concentration profiles at x=0.4 m and z=0.105 m from the CFD calculations.

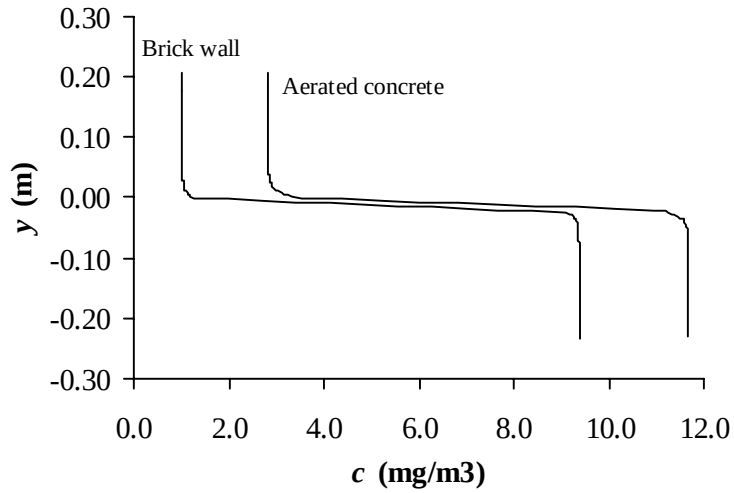

Figure 5.5 Steady-state concentration in the test chambers at x=0.4 m and z=0.105 m for diffusion of n-Octane through aerated concrete and brick wall. It should be noticed that the material surface in the secondary chamber is at y=0 and that the materials have different thickness.

It is seen that there exists a boundary layer along the material surface as the concentration changes from its surface value to the bulk concentration with in a thin layer.

As the concentration gradients through the material are similar it is further seen that the flux in the brick wall is larger than in the aerated concrete due to the larger diffusion coefficient. Therefore, the surface emission from the brick wall is larger and thus generating a thinner boundary layer.

In the experiments by Meininghaus, Knudsen and Gunnarsen (1998) the test chambers were assumed to be completely mixed and the concentration was measured in the exhaust only. Table 5.2 compares the concentrations in the exhaust from the secondary chamber.

	Exhaust concentration	
	Experiment (mg/m^3)	CFD (mg/m^3)
Aerated concrete	2.86	2.85
Brick wall	1.03	1.03

Table 5.2 Comparison of exhaust concentrations for the secondary test chamber obtained from experiments (Meininghaus, Knudsen and Gunnarsen, 1998) and CFD calculations.

Good agreement between the measured and predicted exhaust concentrations from the secondary chamber have been achieved as seen in the table. It should be noticed though, that the CFD predictions are based on source diffusion coefficients and inlet concentrations obtained from the experiments.

5.4 SIMPLIFIED MODEL

A simplified model for two-dimensional steady-state conditions is proposed (see Figure 5.6). The pollutant source is modelled as a solid body, i.e. no convective transport takes place within the source.

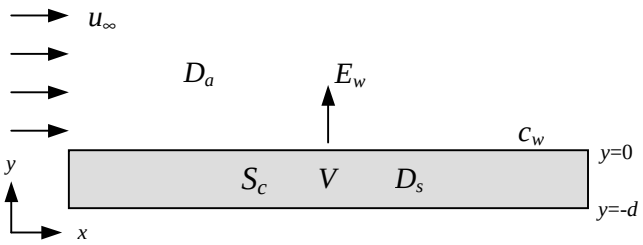

Figure 5.6 Outline of the simplified model.

The source term within the pollutant source is assumed constant per unit volume and there is mass transfer across the boundary at y=0 only.

5.4.1 ANALYTICAL SOLUTION

In the following an analytical expression for the concentration distribution within the pollutant source is derived.

For steady-state the left hand-side of equation 5.2 cancels out and Fick's second law reduces to

$$S_c = -D_s \frac{\partial^2 c}{\partial y^2} \tag{5.3}$$

The concentration at the surface and the flux at the lower boundary provide the boundary conditions

$$c\big|_{y=0} = c_w \tag{5.4}$$

$$-D_s \frac{\partial c}{\partial y}\bigg|_{y=-d} = 0 \tag{5.5}$$

As the source term is constant the emission rate is given by

$$E_w = S_c d \tag{5.6}$$

The analytical solution for the concentration distribution within the source thus yields

$$c = -\frac{S_c}{2D_s} y^2 - \frac{E_w}{D_s} y + c_w \qquad for - d \le y \le 0 \tag{5.7}$$

The concentration distribution within the source is given in terms of gas-phase concentration as c_w is expressed as a gas-phase concentration. Alternatively c_w can be adjusted according to the adsorption isotherm to obtain the solid-phase concentration within the source. For reasons of simplification the concentration within the source is henceforward expressed as gas-phase concentration.

Figure 5.7 shows the concentration distribution within the source for S_c=1 mg/m^{3}s, d=0.02 m, D_s=1e-7 m^{2}s and u_∞=0.2 m/s. The surface concentration in the analytical expression is found from the CFD calculation.

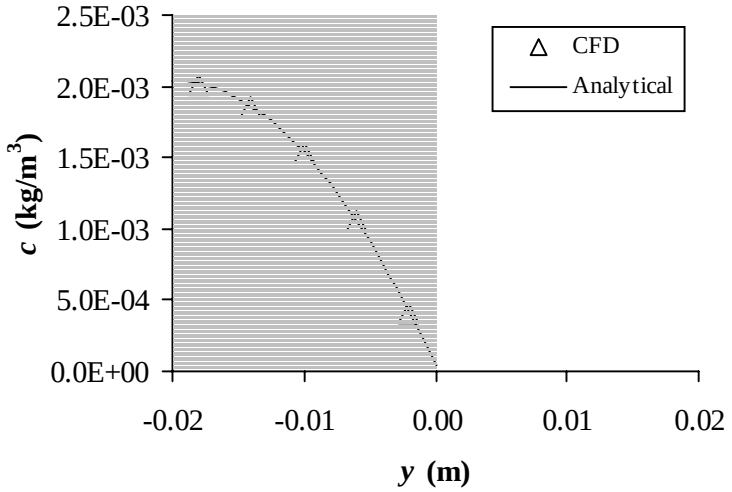

Figure 5.7 Concentration distribution within the source for S_c=1 mg/m^{3}s, d=0.02 m, D_s=1e-7 m^{2}s and u_∞=0.2 m/s.

It is seen that the CFD results and the analytical solution are identical and the numerical approach thus provides a method for further calculations.

5.4.2 RESULTS

A series of CFD calculations have been performed for different combinations of free stream velocity and source diffusion coefficient. In all calculations the diffusion coefficient in air have been kept fixed at D_a=15.1E-6 m^2/s while the source term has been fixed at S_c=1 mg/m^3s. The thickness of the source is d=0.02 m.

The diffusion coefficients determines whether the emission process is diffusion-controlled or evaporation-controlled and as D_a has been kept fixed D_s is the governing parameter. If $D_s>>D_a$ the emission is evaporative as transport in air will be much slower than within the source and therefore be the limiting process. For $D_s<<D_a$ the emission is controlled by internal diffusion as transport within the source is the limiting process.

Figure 5.8 - Figure 5.10 shows the concentration distribution for different free stream velocities with the source diffusion coefficient as parameter. It should be noticed that the concentrations are plotted in logarithmic scale as large variations occur.

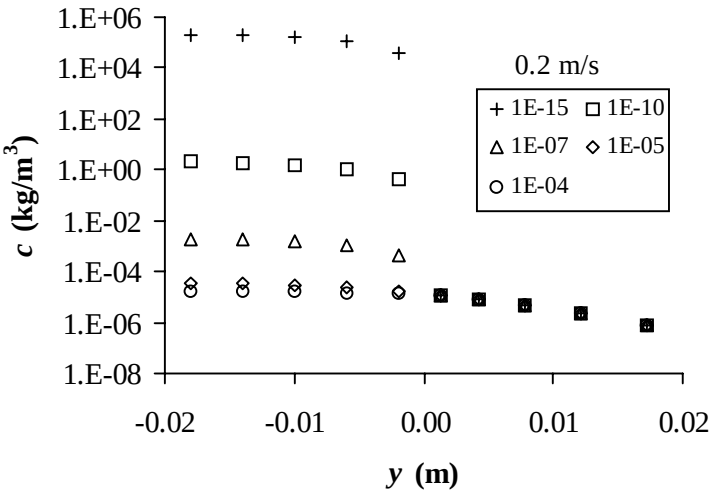

Figure 5.8 Concentration distribution in logarithmic scale for u_∞=0.2 m/s. The parameter is the source diffusion coefficient, D_s.

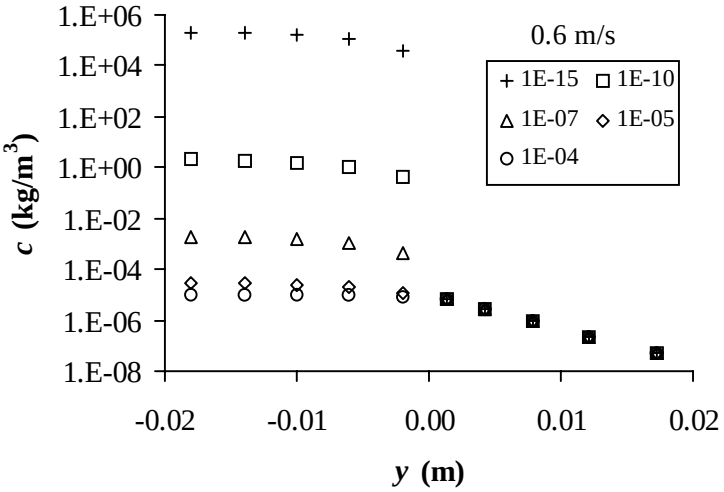

Figure 5.9 Concentration distribution in logarithmic scale for u_∞=0.6 m/s. The parameter is the source diffusion coefficient, D_s.

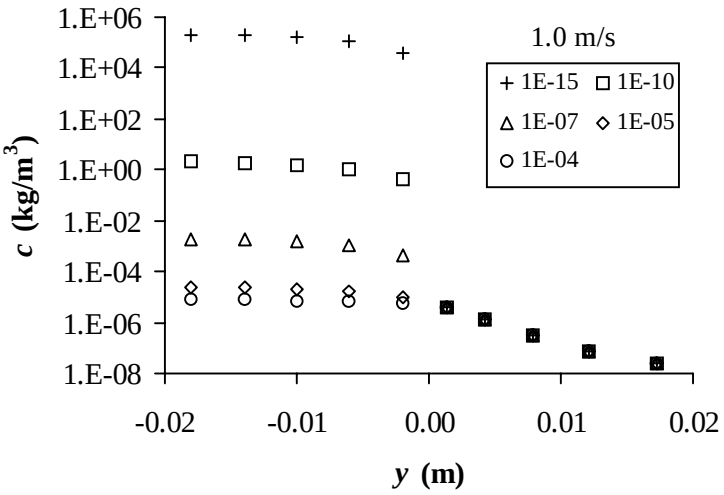

Figure 5.10 Concentration distribution in logarithmic scale for u_∞=1.0 m/s. The parameter is the source diffusion coefficient, D_s.

It is seen that large concentration variations occur within the source while the concentration distribution in the boundary layer is identical at a given free stream velocity.

For low values of D_s, i.e. diffusion-controlled emission, the transport of VOCs through the material is slow and the concentration level is higher than in case of evaporative emission. In case of evaporative emission there is no significant drop in concentration at the surface as VOCs diffuse quickly through the source.

The situation corresponds to heat conduction in a solid with constant thermal load. For low thermal conductivity (low diffusivity) the temperature in the solid will be higher than in a solid with high thermal conductivity.

In Figure 5.11 and Figure 5.12 the concentration distributions at different free stream velocities are compared for typical diffusion-controlled (D_s=1E-10 m^2/s) and evaporative emissions (D_s=1E-4 m^2/s).

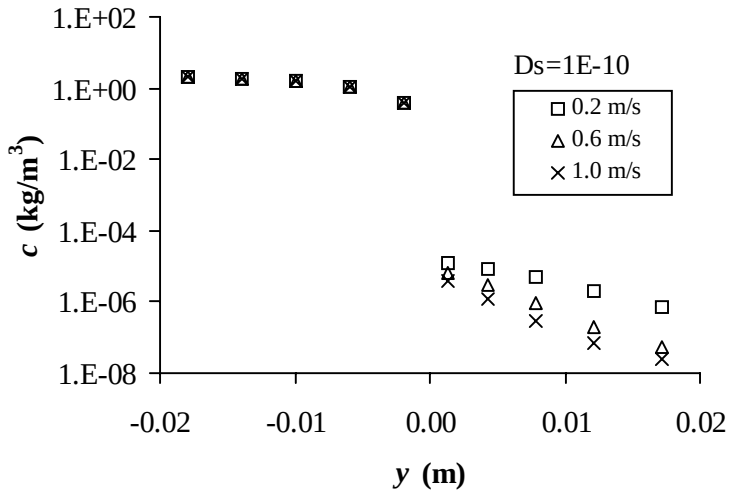

Figure 5.11 Concentration distribution in logarithmic scale for different free stream velocities for a typical diffusion-controlled emission process, D_s=1E-10 m^2/s.

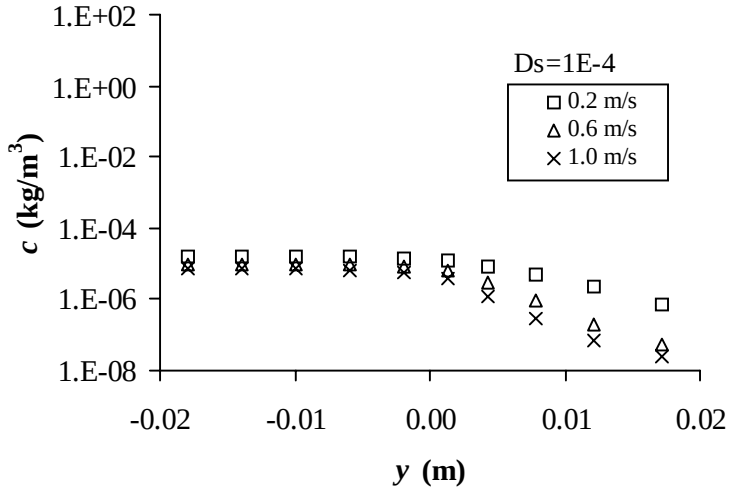

Figure 5.12 Concentration distribution in logarithmic scale for different free stream velocities for a typical evaporative emission process, D_s=1E-4 m^2/s.

For the diffusion-controlled emission process (D_s=1E-10 m^2/s) it is seen that the concentration distributions within the source are identical while the concentration in the boundary layer changes with velocity.

In case of evaporative emission the source concentration changes significantly with velocity. This is clearer from Figure 5.13 where the concentration is plotted in a linear scale.

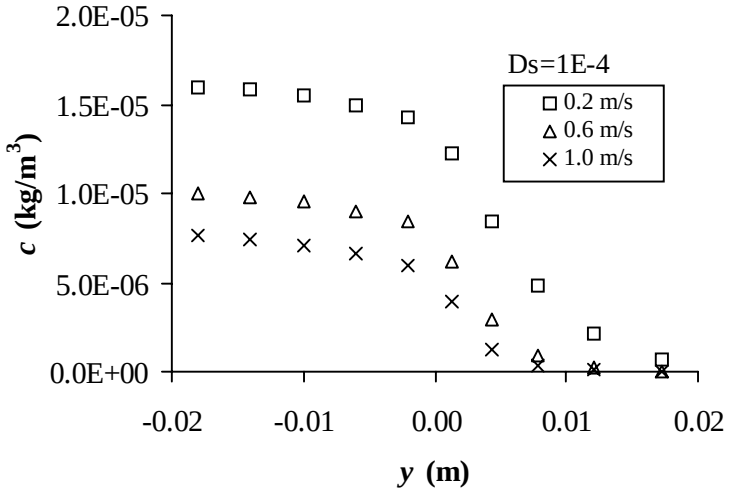

Figure 5.13 Concentration distribution in linear scale for different free stream velocities for a typical evaporative emission process, D_s=1E-4 m^2/s.

As steady-state conditions are considered for a constant source term per unit volume, S_c, the surface emission, E_w, is constant in all calculations. The mass transfer coefficient though, changes as the surface concentration changes. In Figure 5.14 the mass transfer coefficient is plotted versus the free stream velocity.

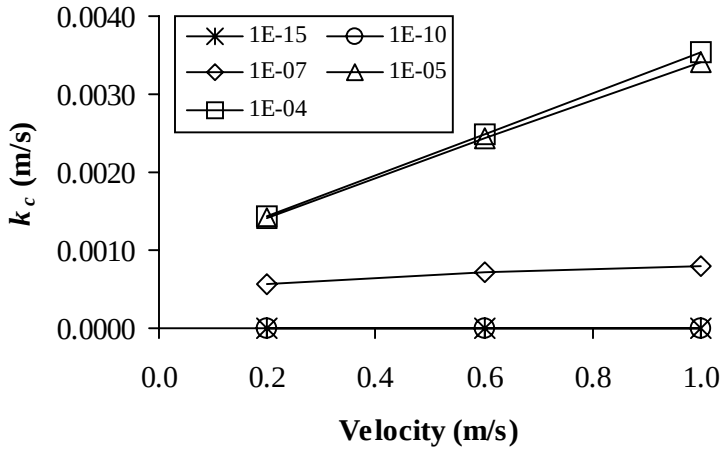

Figure 5.14 Mass transfer coefficient versus free stream velocity. The parameter is the source diffusion coefficient.

The figure shows that for low values of D_s the mass transfer coefficient is constant with the free stream velocity and as D_s increases the mass transfer coefficient becomes dependent of the velocity. In other words, the mass transfer coefficient is unaffected by velocity for diffusion-controlled emission but is strongly affected by the velocity when the emission is evaporative.

5.5 CONCLUSIONS

A model by means of CFD for prediction of emission from pollutant sources in ventilated enclosures has been proposed. Existing models are in general limited to either evaporation-controlled emissions or diffusion-controlled emissions and based on specific sources and compounds. The model proposed in this work is generally applicable as it accounts for both pollutant transport across the boundary layer and diffusion through the source without prior knowledge of which is the limiting process. In addition, the model is based on physical properties of the source and the airflow.

CFD calculations were compared to the results from an experimental investigation by Meininghaus, Knudsen and Gunnarsen (1998) on diffusion through a solid material between two test chambers. The CFD calculations were based on parameters obtained from the experiments and good agreement was achieved between the measured and the predicted exhaust concentrations. This illustrates the potential of the model and shows that the model is valid.

The model has also been applied to a series of CFD calculations for steady-state conditions to investigate the influence of air velocity and source diffusion coefficient. A constant production of pollutants per unit volume within the source was assumed.

The results show that the concentration of pollutants in the boundary layer is independent of the source diffusion coefficient for a given velocity. In the source large concentration variations occur as the pollutants diffuse quickly towards the surface at large source diffusion coefficients. The concentration level in the source is thus higher when the emission is controlled by internal diffusion than in case of evaporation being the limiting process. As expected, the boundary layer concentration decreases when the velocity is increased.

When the emission is controlled by diffusion through the source, the source concentration is independent of velocity as pollutants are released from the source as quick as they are supplied to the surface. The source concentration is a function of velocity for evaporation-controlled emission as pollutants are released from the source at the rate at which they are removed from the boundary layer. The mass transfer coefficient increases in proportion to the velocity for evaporative emissions, while it is independent of velocity when the emission is controlled by internal diffusion.

Chapter 6

GENERAL DISCUSSION AND CONCLUSIONS

Nowadays people spend the majority of their time in an indoor environment and it is thus of great importance that buildings provide a healthy and comfortable indoor environment. Building materials have been identified as major sources of indoor air contamination (Haghighat and Donini, 1993, Wolkoff, 1995 and Fanger et al., 1988) due to the large surface area and permanent exposure to indoor air.

This thesis provides a general investigation on the influence of local airflow (velocity and turbulence intensity) on the evaporative emission from surfaces in a ventilated enclosure. In addition, by means of CFD, a generally applicable model for prediction of emission from surfaces has been developed.

6.1 INFLUENCE OF LOCAL AIRFLOW ON THE EMISSION

CFD calculations as well as full-scale experiments have been used to investigate the influence of local air velocity and turbulence intensity on the evaporative emission in a ventilated room. It was found that the emission is a strong function of local airflow as it increases in proportion to both velocity and turbulence intensity.

The investigations show that the evaporative emission increases with the air change rate. This was expected as a larger amount of pollutants is removed from the boundary layer flow when the air change rate goes up. Both the CFD calculations and the full-scale experiments show a linear relation between the emission and the air change rate.

Different velocity and turbulence levels were generated for a given air change rate in the CFD calculations as the influence of an interior wall was investigated. The results show that the emission is only affected if the wall changes the local airflow conditions.

During the full-scale experiments the room air concentration versus time profiles were obtained for different air change rates, while the supply rate of fresh air was kept unchanged to investigate the influence of velocity. The results are consistent with those of Low et al. (1998) and model predictions by Tichenor, Guo and Sparks (1993) although the model seems to underestimate the peak concentrations.

In the early stage of the experiments the results show that the emission increases with velocity. After a couple of hours though, the difference is reduced as the emission approaches zero. The results express the behaviour of diffusion-controlled emission at the end of the experiments. It is thus concluded that the evaporation-controlled emission is a strong function of velocity while, the velocity has no substantial influence when the emission is controlled by internal diffusion.

The emission has further been evaluated in terms of the mass transfer coefficient, k_c, given by

$$E_w = k_c (c_w - c_\infty) \tag{2.22}$$

The results from the CFD calculations as well as the full-scale experiments show that the mass transfer coefficient is a strong function of the velocity, u, as they indicate a linear relationship between k_c and u, while boundary layer theory predicts k_c to be a function $u^{0.8}$. In addition, it was found from the CFD calculations that linear relations between k_c and Tu and between k_c and u provide a reasonable description of the mass transfer coefficient.

CFD calculations were also performed for a small-scale test chamber to investigate the influence of scale. It was found that at a given velocity the mass transfer coefficient found in a small-scale test chamber differs from that found in a full-scale geometry. Different levels of turbulence cause this as the scale of turbulence found in a full-scale geometry can not be reproduced in small-scale experiments. A method for transferring results obtained from small-scale experiments to a full-scale ventilated room is proposed.

6.2 MODEL DEVELOPMENT

By means of CFD a generally applicable model for prediction of emission from surfaces has been developed. The model is based on physical properties of the pollutant source and the airflow. Furthermore, it accounts for mass transfer across the boundary layer as well as diffusion through the source.

The interior walls of a room traditionally bound the computational domain in CFD, when dealing with ventilation problems. The model presented in this work expands the computational domain into the pollutant source, i.e. the building material, so that the governing equations are solved simultaneously in the source and the room.

CFD calculations were compared to the results from an experimental investigation by Meininghaus, Knudsen and Gunnarsen (1998) on diffusion through a solid material between two test chambers. The CFD calculations were based on parameters obtained from the experiments and good agreement was achieved between the measured and the predicted exhaust concentrations. This illustrates the potential of the model and shows that the model is valid.

With a simplified version of the model (steady state, constant production of pollutants in the source) the influence of air velocity and source diffusion coefficient on the concentration distribution has been investigated. The results show that the boundary layer concentration is independent of source diffusion coefficient for a given velocity, while the concentration decreases as the velocity is increased. The boundary layer concentration is therefore always a function of velocity.

When the emission is evaporative the mass transfer coefficient increases in proportion to the velocity, while for diffusion-controlled emissions the mass transfer coefficient is independent of velocity. These observations are consistent with those obtained from the CFD calculations on the full-scale geometry and the full-scale experiments.

6.3 RECOMMENDATIONS

It is recommended that the model proposed be further developed so those more complicated problems can be accounted for.

The generation of pollutants within the source has been modelled as a constant rate per unit volume, which is believed to be a far to simple approximation. The description of the source term should thus be extended, as the generation of pollutants is a complex process involving several parameters such as temperature, humidity, concentration, chemical reactions and time.

For validation purposes the model predictions should be compared to existing results as well as further experiments could be performed.

This extended model would further allow for investigation of the influence of local airflow parameters such as velocity, turbulence temperature and concentration on time-dependent emission processes.

Appendix A

COMPUTATIONAL FLUID DYNAMICS (CFD)

A.1 TURBULENCE MODELS

The time averaged conservation equations (Chapter 2.5) involves the unknown turbulent correlations $\overline{u_i' u_j'}$ and $\overline{u_j' c'}$. These are assumed proportional to the velocity and concentration gradients, respectively and thus necessitate a description of the eddy properties by a turbulence model.

The two models considered in the present work are introduced in the following

A.1.1 THE STANDARD K-ε MODEL

The standard k-ε turbulence model is a two-equation model that makes use of the eddy viscosity concept and relates the eddy viscosity to the turbulent kinetic energy, *k*, and the turbulent dissipation, ε (Rodi 1984)

$$\mu_t = C_\mu \rho \frac{k^2}{\varepsilon} \tag{A.1}$$

To close the set of equations two additional equations are introduced. These are the transport equations of turbulent kinetic energy (Wilcox, 1994)

$$\rho \overline{u_i} \frac{\partial k}{\partial x_i} = \frac{\partial}{\partial x_i}\left(\mu_l + \frac{\mu_t}{\sigma_k}\frac{\partial k}{\partial x_i}\right) + \mu_t \frac{\partial \overline{u_i}}{\partial x_j}\left(\frac{\partial \overline{u_i}}{\partial x_j} + \frac{\partial \overline{u_j}}{\partial x_i}\right) - \rho\varepsilon \tag{A.2}$$

and turbulent dissipation

$$\rho\overline{u_i}\frac{\partial\varepsilon}{\partial x_i}=\frac{\partial}{\partial x_i}\left(\mu_l+\frac{\mu_t}{\sigma_\varepsilon}\frac{\partial\varepsilon}{\partial x_i}\right)+C_{1\varepsilon}\mu_t\frac{\varepsilon}{k}\frac{\partial\overline{u_i}}{\partial x_j}\left(\frac{\partial\overline{u_i}}{\partial x_j}+\frac{\partial\overline{u_j}}{\partial x_i}\right)-C_{2\varepsilon}\rho\frac{\varepsilon^2}{k} \quad \text{(A.3)}$$

The transport equations contain the five empirical constants C_μ, σ_k, σ_ε, $C_{1\varepsilon}$ and $C_{2\varepsilon}$. Standard values for these constants are shown in Table A.1 (Wilcox, 1994).

C_μ	$C_{1\varepsilon}$	$C_{2\varepsilon}$	σ_k	σ_ε
0.09	1.44	1.92	1.0	1.3

Table A.1 Empirical constants for the standard k-ε model (Wilcox, 1994).

The model is applicable to fully turbulent flows and is therefore not valid close to walls where viscous forces dominate. Wall functions (see Chapter 2.3) are then used to describe the flow in the near-wall region and fewer grid points are needed.

A.1.2 THE LOW REYNOLDS NUMBER (LRN) K-ε MODEL

Another way of handling the near wall region is by using the Low Reynolds Number (LRN) formulation of the k-ε model. The model accounts for the damping effect of the wall and ensures that viscous stresses dominate at low Reynolds numbers, i.e. in the near wall region. In the present work the LRN model proposed by Launder and Sharma (1974) has been used.

The equations of the LRN model are given by (Launder and Sharma, 1974)

$$\mu_t = f_\mu C_\mu \rho\frac{k^2}{\varepsilon} \quad \text{(A.4)}$$

$$\rho\overline{u_i}\frac{\partial k}{\partial x_i}=\frac{\partial}{\partial x_i}\left[\left(\mu_l+\frac{\mu_t}{\sigma_k}\right)\frac{\partial k}{\partial x_i}\right]+\mu_t\frac{\partial\overline{u_i}}{\partial x_j}\left(\frac{\partial\overline{u_i}}{\partial x_j}+\frac{\partial\overline{u_j}}{\partial x_i}\right)-\rho\varepsilon-D \quad \text{(A.5)}$$

$$\rho\overline{u_i}\frac{\partial\varepsilon}{\partial x_i}=\frac{\partial}{\partial x_i}\left[\left(\mu_l+\frac{\mu_t}{\sigma_\varepsilon}\right)\frac{\partial\varepsilon}{\partial x_i}\right]+C_{1\varepsilon}\mu_t\frac{\varepsilon}{k}\frac{\partial\overline{u_i}}{\partial x_j}\left(\frac{\partial\overline{u_i}}{\partial x_j}+\frac{\partial\overline{u_j}}{\partial x_i}\right)-f_2C_{2\varepsilon}\rho\frac{\varepsilon^2}{k}+E \quad \text{(A.6)}$$

The five empirical constants C_μ, σ_k, σ_ε, $C_{1\varepsilon}$ and $C_{2\varepsilon}$ assume the values given in Table A.1 while the functions f_μ, f_2, D and E are defined by (Launder and Sharma, 1974)

$$f_\mu=exp\left(\frac{-3.4}{(1+R_t/50)^2}\right) \quad \text{(A.7)}$$

$$f_2=1-0.3exp\left(-R_t^2\right) \quad \text{(A.8)}$$

$$D=2\mu_l\left(\frac{\partial k^{\frac{1}{2}}}{\partial x_i}\right)^2 \quad \text{(A.9)}$$

$$E=2\frac{\mu_l\mu_t}{\rho}\left(\frac{\partial\overline{u_i}}{\partial x_i}\right)^2 \quad \text{(A.10)}$$

$$R_t=\frac{\rho k^2}{\mu_l\varepsilon} \quad \text{(A.11)}$$

As the model requires a high resolution of the near-wall region it is more expensive in terms of computational time than the standard k-ε model.

A.2 GRID DISTRIBUTION IN THE NEAR-WALL REGION

The turbulence models are based on different assumptions on the level of turbulence and therefore require different grid distributions to cope with the damping effect of nearby wall.

A series of CFD calculations have been performed to investigate the influence of the grid distribution. The case considered is flow over a flat plate (see Figure A.1).

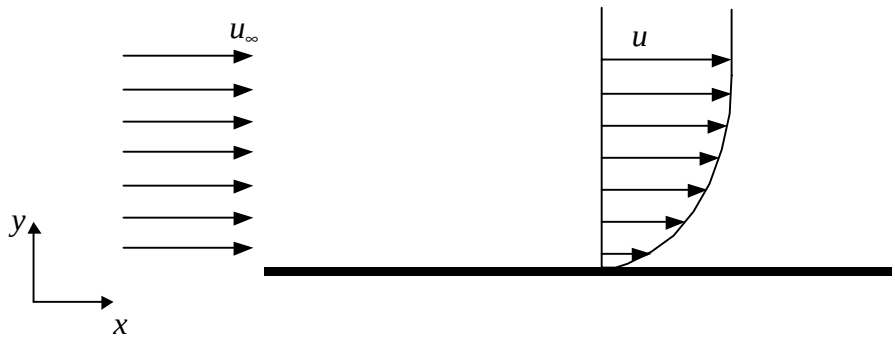

Figure A.1 Flow over flat plate.

The boundary layer has an initial laminar section but due to instability it becomes turbulent as the Reynolds number increases. The critical Reynolds number regarding instability is $Re_{x,crit} \approx 100000$ (Versteeg and Malalasekera, 1996 and White, 1991-a). At $Re_x \approx 500000$ the boundary layer can be considered as fully turbulent (White, 1991-a).

A.2.1 THE STANDARD K-ε MODEL

As the standard k-ε model neglects the damping effect of a nearby wall it is important that the k-ε computations are begun at a point in the fully turbulent region of the boundary layer. For the model to work properly the grid points should therefore be no closer to the wall than $y^+ \approx 11$. The wall functions then describe the variables close to the wall and connect the wall boundary conditions to the properties in the fully turbulent region.

In Figure A.2 the non-dimensional velocity profiles in the boundary layer flow over a flat plate calculated by the standard k-ε model are compared to the universal velocity profile for different grid distributions and Reynolds numbers.

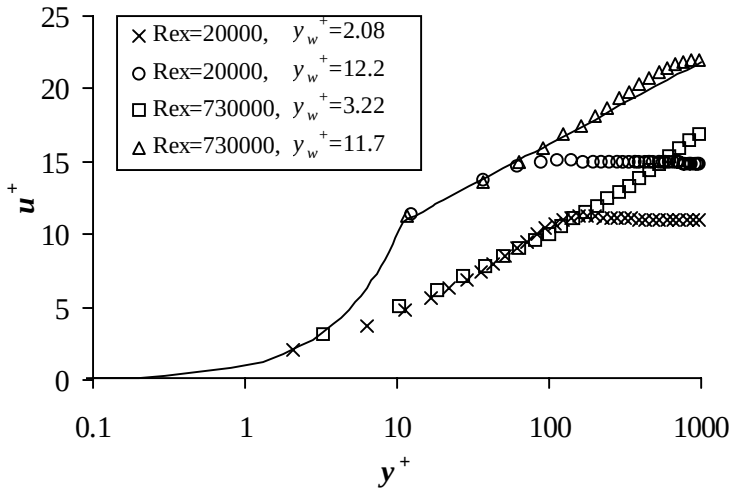

Figure A.2 Non-dimensional velocity profiles in the boundary layer flow calculated by the standard k-ε. The solid line represents the universal velocity profile.

It is seen that good agreement between the CFD calculations and the universal velocity profile is achieved for Re_x =730000 provided the first grid point is located in the fully turbulent region of the boundary layer.

The flow is fully laminar at Re_x =20000. However, the standard k-ε model wrongly predicts the transition from laminar to turbulent flow. This is due to the fact that the wall function applied is valid for fully turbulent flow only.

A.2.2 THE LOW REYNOLDS NUMBER (LRN) K-ε MODEL

The LRN model accounts for the damping effect of a nearby wall and the computations should thus begin at a point where the turbulent forces are absent, that is in the viscous or laminar sublayer. The laminar sublayer is extremely

thin, that is $y^+<5$ (Versteeg and Malalasekera, 1996 and White, 1991-b) and hence a high resolution of this region is necessary.

In Figure A.3 the non-dimensional velocity profiles in the boundary layer flow over a flat plate calculated by the LRN model are compared to the universal velocity profile for different grid distributions and Reynolds numbers.

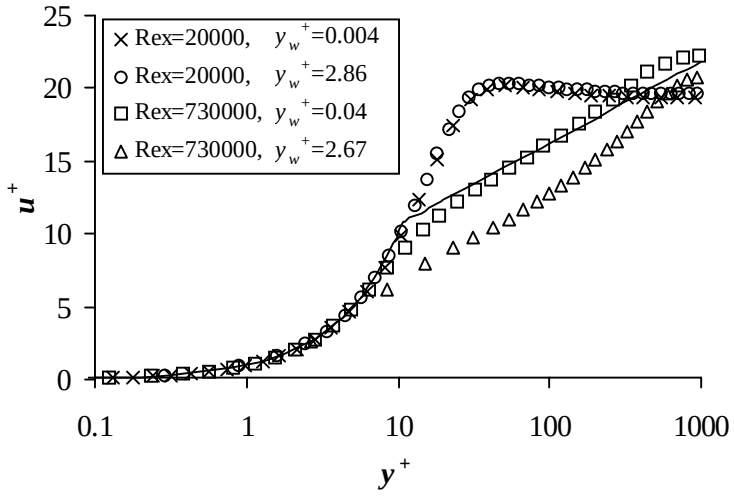

Figure A.3 Non-dimensional velocity profiles in the boundary layer flow calculated by the LRN model. The solid line represents the universal velocity profile.

For Re_x =730000 the model calculates the expected velocity profile in the laminar sublayer as well as in the fully turbulent layer provided the first grid point is located sufficiently close to the wall.

In case of a pure laminar boundary layer (Re_x =20000) the location of the first grid point is unimportant for the velocity profile as there are no turbulent forces in the boundary layer.

A.2.3 WALL SHEAR STRESS

The difference between the velocity profiles calculated at different grid distributions is due to the wall shear stress, τ_w, which is grid sensitive. In the boundary layer the shear stress can be approximated by (White, 1991-b)

$$\tau \approx \mu \frac{\partial u}{\partial y} \tag{A.12}$$

As the velocity gradient in the laminar sublayer is assumed constant the wall shear stress is given by

$$\tau_w \approx \left(\mu \frac{\partial u}{\partial y} \right)_{y=0} \tag{A.13}$$

In Table A.2 the calculated wall shear stresses are shown for the CFD calculations.

	Standard k-ε model		**LRN k-ε model**	
Re_x (-)	y_w^+ (-)	τ_w (N/m^2)	y_w^+ (-)	τ_w (N/m^2)
20000	2.08	9.27E-4	0.004	2.92E-4
20000	12.2	4.90E-4	2.86	2.85E-4
730000	3.22	3.61E-2	0.04	2.22E-2
730000	11.7	2.26E-2	2.67	2.53E-2

Table A.2 Wall shear stresses at different Reynolds numbers and grid distributions.

It is seen that for Re_x =730000 the two models calculate similar wall shear stresses provided the first grid point is located properly.

At Re_x =20000 there is a significant difference between the models due to the fact that the standard k-ε model wrongly predicts the transition from laminar to turbulent flow.

For the LRN model there is no significant difference in wall shear stress for the two grid distributions at Re_x =20000 as the first grid point in both cases is located in a region where viscous shear dominate.

The wall shear stress is not constant along the surface as the velocity gradient changes and hence y_w^+ is a function of x. This is illustrated in Figure A.4.

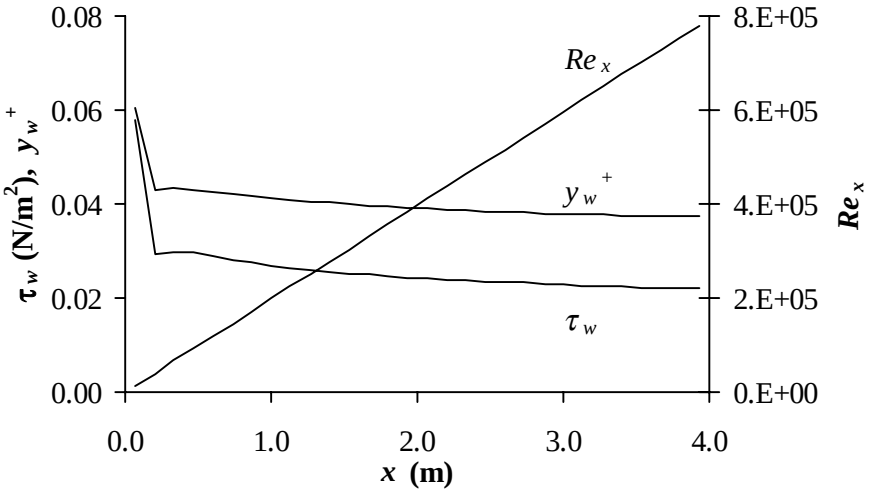

Figure A.4 Typical curves for τ_w, y_w^+ and Re_x along the surface. The curves shown are calculated by the LRN model.

Appendix B

CFD RESULTS FROM THE TWO-DIMENSIONAL FULL-SCALE ROOM

B.1 COMPARISON OF VELOCITIES

In Figure B.1 - Figure B.4 velocity profiles from the CFD calculations are compared to the measurements reported by Nielsen (1990). The profiles shown have been obtained at N=10h^{-1}.

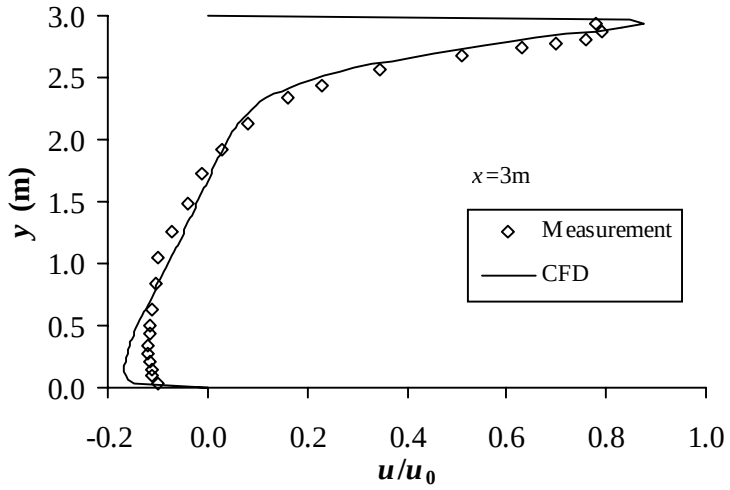

Figure B.1 Velocity profiles at x=3m, N=10h^{-1}.

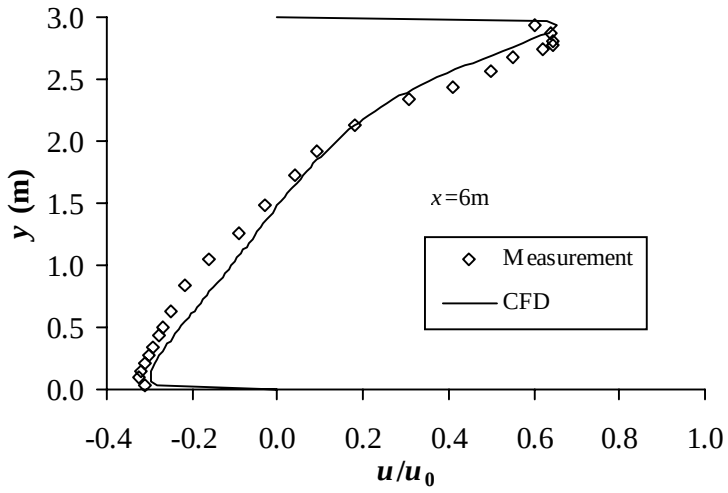

Figure B.2 Velocity profiles at x=6m, N=10h^{-1}.

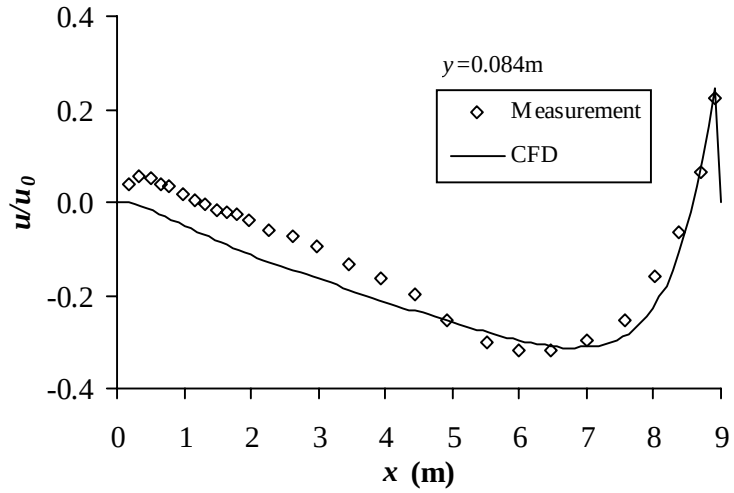

Figure B.3 Velocity profiles at y=0.084m, N=10h^{-1}.

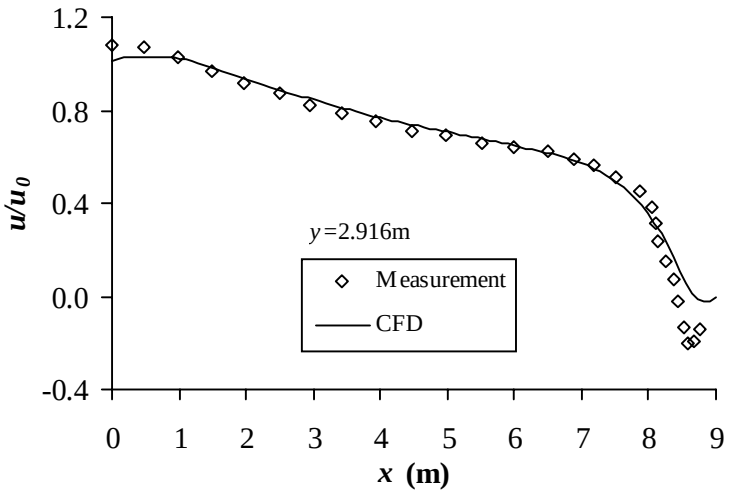

Figure B.4 Velocity profiles at y=2.916m, N=10h^{-1}.

B.2 AIR FLOW PATTERN

The airflow pattern is shown for the different set-ups and air change rates in Figure B.5 - Figure B.14. It should be noticed that different scale parameters have been used for obtaining the vectorplots. Plots for different air change rates therefore allow for a qualitatively comparison only, i.e. comparison of airflow patterns. In addition it should be recalled that the length of the room is 9 m while the height is 3 m.

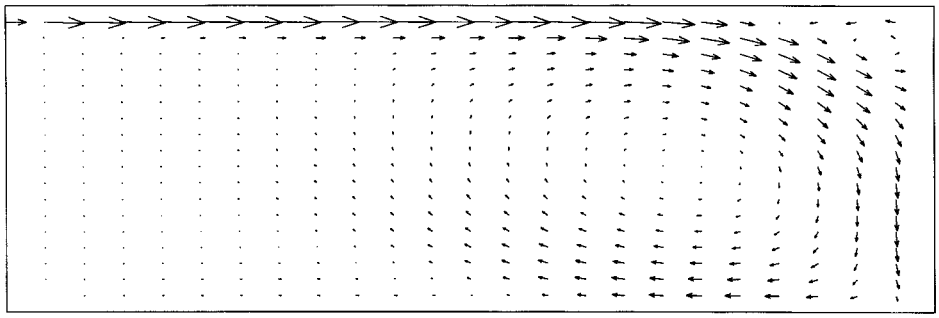

Figure B.5 Airflow pattern at N=1h^{-1}. A vector of 1 m in the geometry corresponds to a velocity of 0.1 m/s.

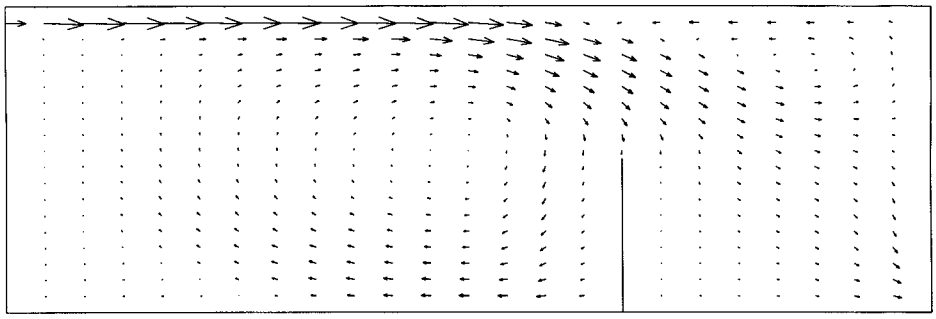

Figure B.6 Airflow pattern at N=1h^{-1}. A vector of 1 m in the geometry corresponds to a velocity of 0.1 m/s.

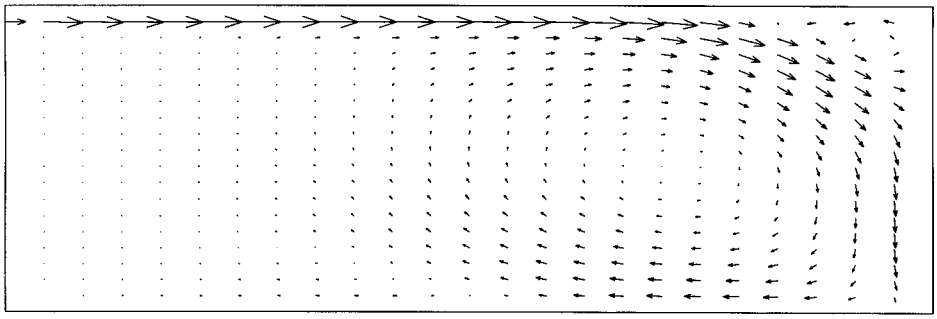

Figure B.7 Airflow pattern at N=2h^{-1}. A vector of 1 m in the geometry corresponds to a velocity of 0.2 m/s.

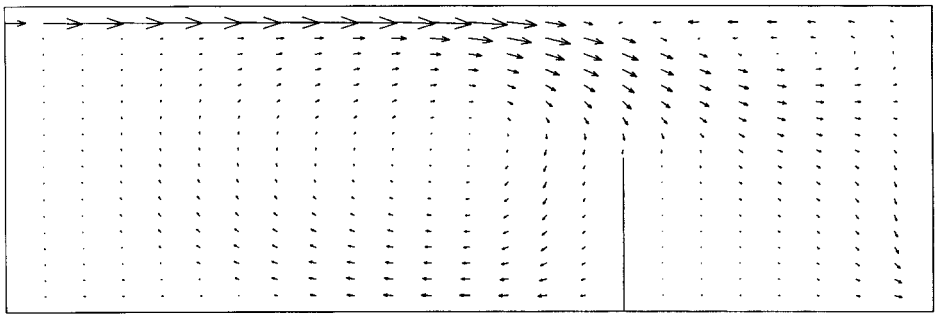

Figure B.8 Airflow pattern at N=2h^{-1}. A vector of 1 m in the geometry corresponds to a velocity of 0.2 m/s.

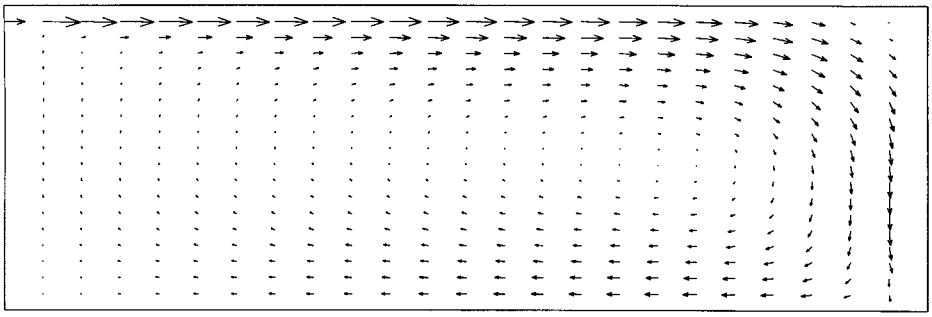

Figure B.9 Airflow pattern at N=5h^{-1}. A vector of 1 m in the geometry corresponds to a velocity of 0.5 m/s.

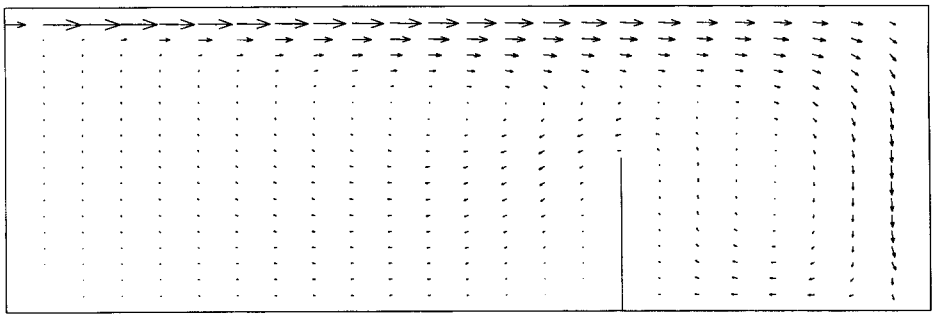

Figure B.10 Airflow pattern at N=5h^{-1}. A vector of 1 m in the geometry corresponds to a velocity of 0.5 m/s.

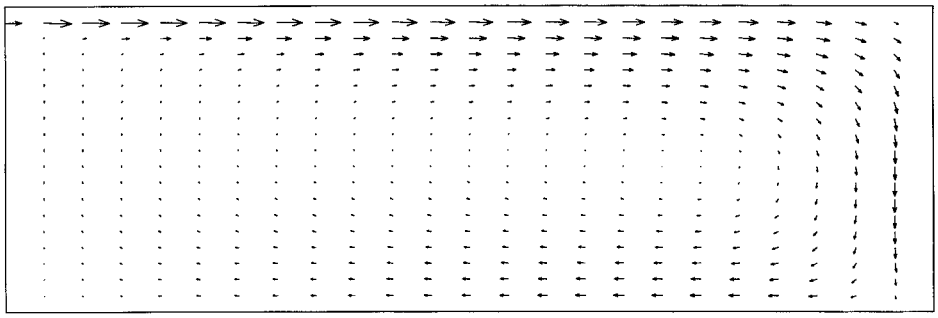

Figure B.11 Airflow pattern at N=8h^{-1}. A vector of 1 m in the geometry corresponds to a velocity of 1.0 m/s.

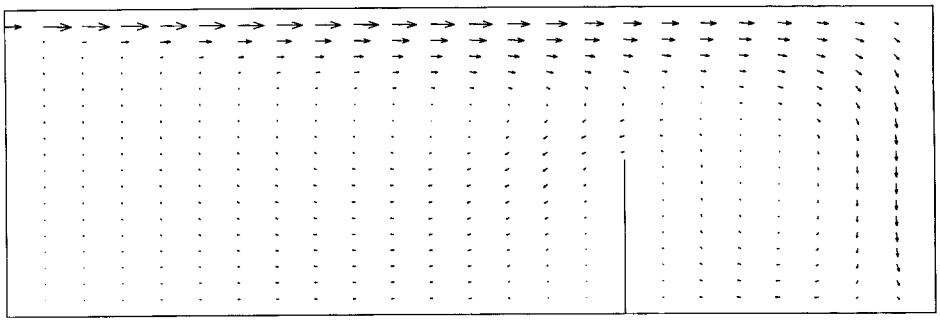

Figure B.12 Airflow pattern at N=8h^{-1}. A vector of 1 m in the geometry corresponds to a velocity of 1.0 m/s.

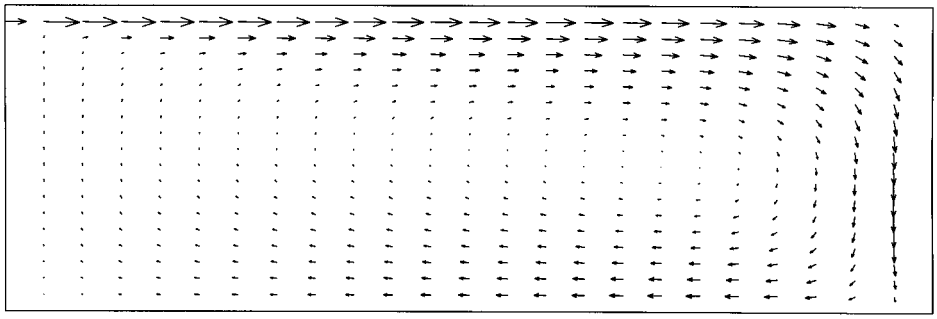

Figure B.13 Airflow pattern at N=10h^{-1}. A vector of 1 m in the geometry corresponds to a velocity of 1.0 m/s.

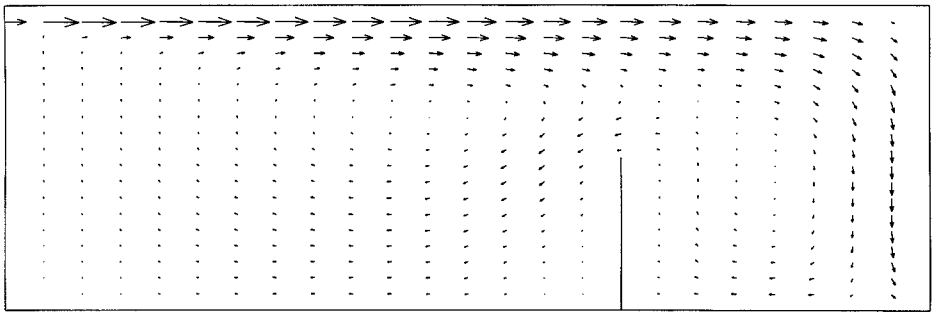

Figure B.14 Airflow pattern at N=10h^{-1}. A vector of 1 m in the geometry corresponds to a velocity of 1.0 m/s.

B.3 CONCENTRATION DISTRIBUTION

The concentration distributions for the four different set-ups at N=1h^{-1} are shown in Figure B.15 - Figure B.18.

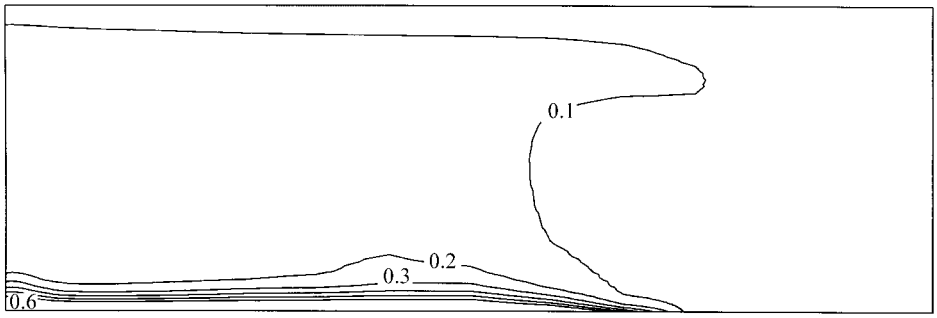

Figure B.15 Concentration distribution at N=1h^{-1} in the empty room and the source located at the floor

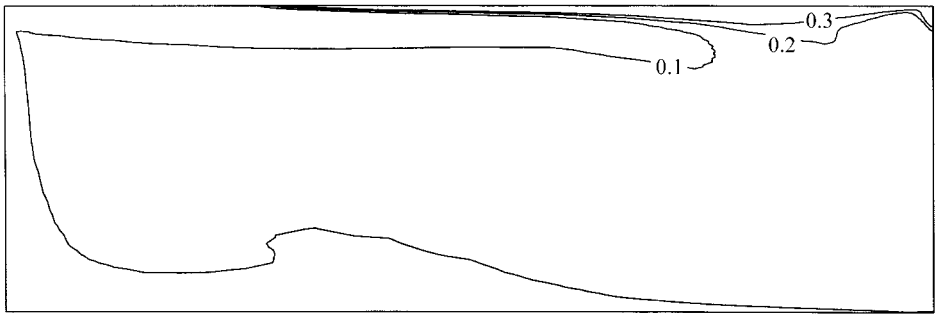

Figure B.16 Concentration distribution at N=1h^{-1} in the empty room and the source located at the ceiling.

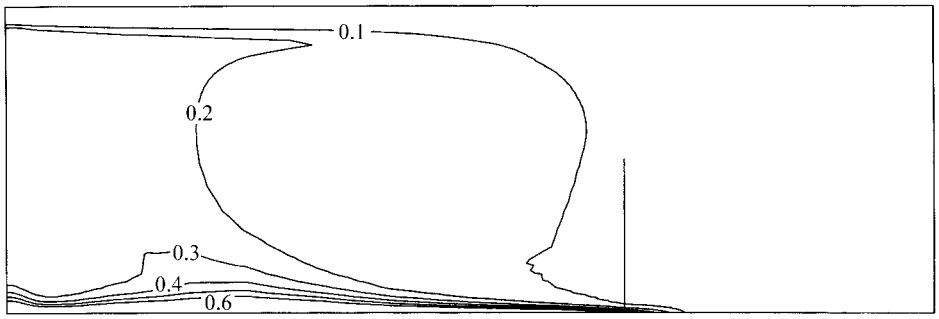

Figure B.17 Concentration distribution at N=1h^{-1} in the room with the wall and the source located at the floor.

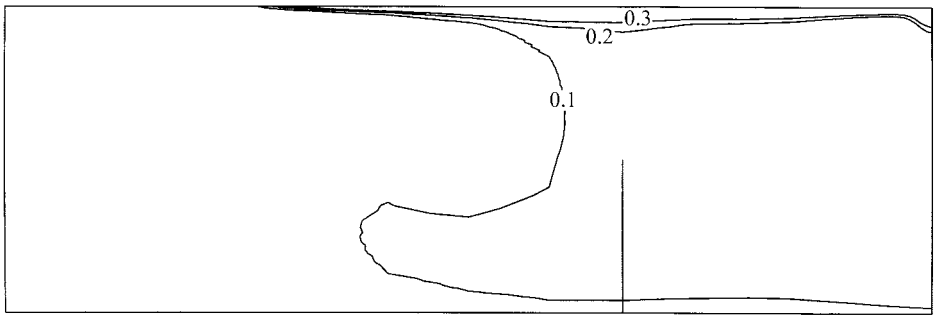

Figure B.18 Concentration distribution at N=1h^{-1} in the room with the wall and the source located at the ceiling.

DANSK SAMMENDRAG

De fleste mennesker opholder sig indendørs i størstedelen af deres levetid, og det er derfor vigtigt, at bygninger leverer et godt og sundt indeklima. Brugere af nye bygninger oplever dog ofte en forringet luftkvalitet som følge af dårlig ventilation, øget tæthed af bygningen og en mere udbredt anvendelse af syntetiske materialer. Emission af flygtige organiske forbindelser fra netop byggematerialer er blevet udpeget (Haghighat and Donini, 1993, Wolkoff, 1995 and Fanger et al., 1988) som en stor kilde til forurening af indeluften på grund af materialernes store overflade og permanente eksponering.

Emission fra byggematerialer som fx maling, gulvbelægning, tæpper og fugemasse er en kædeproces, som involverer diffusion gennem materialet, fordampning fra overfladen, transport gennem grænselaget og opblanding med rumluften. Emissionen karakteriseres ofte som værende diffusions- eller fordampningsstyret afhængig af den begrænsende proces. Diffusionsstyret emission er afhængig af materialets struktur, temperatur og fugtighed, mens fordampningsstyret emission afhænger af strømningsforholdene ved overfladen og koncentrationsforskellen mellem overfladen og rumluften. Hvad enten emissionen er styret af diffusion eller fordampning, så involverer den transport gennem grænselaget.

Denne Ph.D. afhandling omhandler emission fra overflader i et ventileret lokale. Indflydelsen på emissionen af de lokale strømningsforhold over en forureningskilde er undersøgt ved hjælp af CFD (computational fluid dynamics) og fuldskalaforsøg. Der er endvidere opstillet en generel emissionsmodel i CFD.

INDFLYDELSE AF LOKALE STRØMNINGSFORHOLD

Der er udført numeriske beregninger med CFD samt fuldskalaforsøg for at undersøge indflydelsen af lokale strømningsforhold, over en forureningskilde, på den fordampningsstyrede emission i et ventileret lokale. CFD beregningerne er foretaget ved forskellige luftskifter og opstillinger. Fuldskalaforsøgene er ligeledes udført ved forskellige luftskifter dog med konstant friskluftskifte.

Resultaterne viser, at emissionen stiger proportionalt med luftskiftet, hvilket var ventet, da et øget luftskifte medfører, at en større mængde forurening fjernes fra grænselagsstrømningen. Endvidere fremgår det af CFD beregningerne, at tilstedeværelsen af en skillevæg kun har betydning for emissionen, hvis skillevæggen ændrer de lokale strømningsforhold over forureningskilden.

Under forsøgene var der i begyndelsen højere emission ved højere luftskifte, men efter et par timer var forskellen ikke væsentlig. Mod slutningen ændrede rumluftkoncentrationen sig kun langsomt, hvilket er karakteristisk for diffusionsstyret emission.

Emission udtrykkes ofte i form af masseovergangstallet, k_c, som er proportionalitetsfaktoren mellem emissionen og koncentrationsgradienten

$$E_w = k_c (c_w - c_\infty) \tag{2.22}$$

Der er fundet forskellige lineære sammenhænge mellem masseovergangstallet og hastigheden over forureningskilden for de forskellige opstillinger i CFD beregningerne. Dette indikerer, at k_c ikke kan beskrives som funktion af hastigheden alene. Masseovergangstallet stiger også med turbulensintensiteten, *Tu*, og CFD beregningerne viser, at k_c kan beskrives som en lineær funktion af både hastighed og turbulensintensitet. Forsøgene viser ligeledes en lineær sammenhæng mellem masseovergangstal og hastighed.

Ved sammenligning af resultater fra fuldskalamodellen og en model i lille skala er der fundet store forskelle i masseovergangstallet ved en given hastighed. Forskellen skyldes, at der i fuldskalamodellen findes en turbulens med meget stor skala, som ikke kan genskabes i den lille model.

EMISSIONSMODEL

Der er opstillet en generel emissionsmodel i CFD, som er baseret på fysiske egenskaber for forureningskilden (materialet) og rumluften. Modellen er i stand til at beregne såvel diffusionsstyret som fordampningsstyret emission.

I CFD beregninger for ventilerede lokaler afgrænses beregningsområdet traditionelt af lokalets begrænsningsflader. I den opstillede model er bereg-

ningsområdet udvidet, således at de bestemmende ligninger løses både i materialet og i luften.

Modellens resultater er sammenlignet med forsøgsresultater af Meininghaus, Gunnarsen og Knudsen (1998), som undersøgte diffusionen gennem et fast materiale mellem to testkamre. Der blev opnået god overensstemmelse mellem modellen og forsøgsresultaterne, hvilket bekræfter modellens gyldighed og potentiale.

Der blev udført en række CFD beregninger med en simplificeret version af modellen, dvs. under stationære forhold og med en konstant produktion af forurening i materialet, for at undersøge indflydelsen af lufthastigheden og materialets diffusionskoefficient på koncentrationsfordelingen.

Resultaterne viser, at koncentrationen i grænselaget er uafhængig af materialets diffusionskoefficient ved en given hastighed, mens koncentrationen falder når, hastigheden øges. Ved fordampningsstyret emission blev det fundet, at masseovergangstallet stiger proportionalt med hastigheden, samt at hastigheden ikke har nogen betydning, når emissionen er diffusionsstyret.

REFERENCES

Ashley, S. (1986). Sick Buildings. *Building Services,* Vol. 8, February.

Axley, J.W (1993). Modeling Sorption Transport in Rooms and Sorption Filtration Systems for Building Air Quality Analysis. *Indoor Air,* Vol. 3, pp. 298-309.

Bird, B.R., Stewart, W.E. and Lightfoot, E.E. (1960). *Transport Phenomena*. John Wiley & Sons, Inc.

Bishop, V.L., Custer, D.E. and Vogel, R.H. (1985). The Sick Building Syndrome: What It Is, and How To Prevent It. *National Safety and Health News,* Vol. 132, pp. 31-338.

Bjørn, E. and Nielsen, P.V. (1996). Exposure due to Interacting Air Flows Between Persons. *Proceedings of ROOMVENT '96*, Yokohama, Japan, Vol. 1, pp. 107-114.

Bjørn, E. and Nielsen, P.V. (1998). CFD Simulations of Contaminant Transport Between Two Breathing Persons. *Proceedings of ROOMVENT '98*, Stockholm, Sweden, Vol. 2, pp. 133-140.

Brohus, H. (1997). Personal Exposure to Contaminant Sources in Ventilated Rooms. *Ph.D.-Thesis*, Aalborg University, Denmark, ISSN 0902-7953 R9741.

Chang, J.S. and Guo, Z. (1992). Characterization of Organic Emissions from a Wood Finishing Product - Wood Stain. *Indoor Air,* Vol. 2, pp. 146-153.

Christiansson, J., Yu, J-W. and Neretnieks, I. (1993). Emission of VOC's from PVC-floorings - models for predicting the time dependent emission rates and resulting concentrations in the indoor air. *Proceedings of INDOOR AIR '93*, Helsinki, Finland, Vol. 2, pp. 389-394.

Clausen, P.A. (1993). Emission of Volatile and Semivolatile Organic Compounds from Waterborne Paints - the Effect of the Film Thickness. *Proceedings of INDOOR AIR '93,* Helsinki, Finland, Vol. 2, pp. 567-572.

Clausen, P.A., Laursen, B., Wolkoff, P., Rasmussen, E. and Nielsen, P.A. (1993). Emission of Volatile Organic Compounds from a Vinyl Floor Covering. *Modeling of Indoor air Quality and Exposure,* ASTM STP 1205, Niren L. Nagda, Ed., American Society for Testing and Materials, Philadelphia, pp. 3- 13.

De Bellis, L. and Haghighat, F. (1996). The Impact of Environmental Conditions on Material Emission Rate. *Proceedings of INDOOR AIR '96,* Nagoya, Japan, Vol. 2, pp. 441-446.

De Bortoli, M. and Colombo, A. (1993). Determination of VOCs emitted from indoor materials and products. Interlaboratory comparison of small chamber measurements. *Commission of the European Communities, Joint Research Center - Environment Institute,* Ispra, Italy, Report No. 13.

Dunn, J.E. (1987). Models and statistical Methods for Gaseous Emission Testing of Finite Sources in Well-Mixed chambers. *Atmospheric Environment,* Vol. 21, No. 2, pp. 425-430.

Fanger, P.O., Lauridsen, J., Bluyssen, P. and Clausen, G. (1988). Air Pollution Sources in Offices and Assembly Halls, Quantified by the olf Unit. *Energy and Buildings,* Vol. 12, pp. 7-19.

Girman, J.R. (1989). Volatile Organic Compounds and Building Bake-Out. *Occupational Medicine: State of the Art Reviews,* Vol. 4, No. 4, pp. 695-712.

Girman, J.R., Alevantis, L.E., Kulasingam, G.C., Petreas, M.X. and Webber, L.M. (1989). The bake-out of an office building: a case study. *Environment International,* Vol. 15, pp. 449-453.

Gunnarsen, L. (1997). The Influence of Area-specific Ventilation Rate on the Emissions from Construction Products. *Indoor Air, Vol. 7, pp. 116-120.*

Gunnarsen, L.Nielsen, P.A. and Wolkoff P. (1994). Design and Characterization of the CLIMPAQ, Chamber for Laboratory Investigations of Materials, Pollution and Air Quality. *Indoor Air,* Vol. 4, pp. 56-62.

Guo, Z., Tichenor, B.A., Krebs, K.A. and Roache, N. (1996). Considerations on Revisions of Emissions Testing Protocols. *Characterizing Sources of Indoor Air Pollution and Related Sink Effects*, ASTM STP 1287, Bruce A. Tichenor, Ed., American Society for Testing and Materials, pp. 225-236.

Haghighat, F. and De Bellis, L. (1998). Material Emission Rates: Literature Review, and the Impact of Indoor Air Temperature and Relative Humidity. *Building and Environment*, Vol. 33, No. 5, pp. 261-277.

Haghighat, F. and Donnini, G. (1993). Emissions of Indoor Pollutants from Building Materials - State of the Art Review. *Architectural Science Review*, Vol. 36, pp. 13-22.

Larsen, A., Funch, L.W. and Mortensen P. (1995). A New Approach to Label the Emission of VOCS from Building Products. Part IV: Experiences with the Carpet and Ceiling Product Industry. *Proceedings of Healthy Buildings '95*, Milan, Italy, Vol. 2, pp. 905-910.

Larsen, A., Wolkoff, P. and Nielsen, P.A. (1995). A New Approach to Label the Emission of VOCs from Building Products. Part V: The Present Status and Organization in Denmark. *Proceedings of Healthy Buildings '95*, Milan, Italy, Vol. 2, pp. 911-916.

Launder, B.E. and Sharma, B.I. (1974). Application of the energy-dissipation model of turbulence to the calculation of flow near a spinning disc. *Letters in heat and mass transfer*, Vol. 1, No. 2, pp. 131-138.

Little, J.C. and Hodgson, A.T. (1996). A Strategy for Characterizing Homogeneous, Diffusion Controlled, Indoor Sources and sinks. *Characterizing Sources of Indoor Air Pollution and Realated Sink Effects*, ASTM STP 1287, Bruce A. Tichenor, Ed., American Society for Testing and Materials, pp. 294-304.

Little, J.C., Hodgson, A.T. and Gadgil, A. (1994). Modeling Emissions of Volatile Organic Compounds from New Carpets. *Atmospheric Environment*, Vol. 28, No. 2, pp. 227-234.

Low, J.M., Zhang, J.S., Plett, E.G. and Shaw, C.Y. (1998). Effects of Airflow on Emissions of Volatile Organic Compounds from Capet-Adhesive Assemblies. *ASHRAE Transactions*, Vol. 104, part 2, pp. 1281-1288.

Meininghaus, R., Knudsen, H.N. and Gunnarsen, L. (1998). Diffusion and sorption of volatile organic compounds in indoor surface materials. *Proceedings of EPIC '98, Second European conference on Energy Performance and Indoor Climate in Buildings and Third International Conference on Indoor Air Quality, Ventilation and Energy Conservation in Buildings,* Lyon, France, Vol. 1, pp. 33-38.

Nielsen, P.A. and Wolkoff P. (1995). A New Approach to Label the Emission from Building Products Part III: The Total Concept. *Proceedings of Healthy Buildings '95,* Milan, Italy, Vol. 2, pp. 899-904.

Nielsen, P.V. (1990). Specification of a Two-Dimensional Test Case. *IEA Annex 20 Report,* Aalborg University, ISSN 0902-7513 R9040.

Nielsen, P.V. (1995). Healthy Buildings and Air Distribution in Rooms. *Proceedings of Healthy Buildings '95,* Milan, Italy, Vol. 2, pp. 923-928.

Nielsen, P.V. (1998). The selection of turbulence models for prediction of room airflow. *ASHRAE Transactions,* Vol. 104, part 1B, pp. 1119-1127.

Patankar, S.V. (1980). *Numerical Heat Transfer and Fluid Flow*. Hemisphere Publishing Corporation.

Rajaratnam, N. (1976). *Turbulent jets*. Elsevier, Amsterdam.

Robertson, A.S., Burge, P.S., Hedge, A., Sims, J., Gill, F.S., Finnegan, M., Pickering, C.A. and Dalton, G. (1985). Comparison of health problems related to work and environmental measurements in two office buildings with different ventilation systems. *British medical journal,* Vol. 291, pp. 373-376.

Rodi, W. (1984). *Turbulence Models and their Application in Hydraulics - A State of the Art Review*. University of Karlsruhe, Ger*many*.

Ruthven, D.M. (1984). *Principles of Adsorption and Adsorption Processes*. John Wiley & Sons, Inc.

Sissom, L.E. and Pitts, D.R. (1972). *Elements of Transport Phenomena*. McGraw-Hill, Inc.

Skov, P., Valbjørn, O., Pedersen, B.V. and the Danish Indoor Climate Study Group (1990). Influence of indoor climate on the sick building syndrome in an office environment. *Scandinavian Journal of Work, Environment & Health,* Vol. 16, pp. 363-371.

Slejko, F.L. (1985). *Adsorption Technology: A Step-by-Step Approach to Process Evaluation and Application*. Marcel Dekker, Inc.

Sparks, L.E., Tichenor, B.A., Chang, J. and Guo, Z. (1996). Gas-Phase Mass Transfer Model for Predicting Volatile Organic Compound (VOC) Emission Rates from Indoor Pollutant sources. *Indoor Air,* Vol. 6, pp. 31-40.

Tichenor, B.A., Guo, Z. and Sparks, L.E. (1993). Fundamental Mass Transfer Model for Indoor Air Emissions from Surface Coatings. *Indoor Air,* Vol. 3, pp. 263-268.

Tichenor. B.A. and Guo, Z. (1991). The effect of ventilation on emission rates of wood finishing materials. *Environment International,* Vol. 17, pp. 317-323.

Topp, C., Nielsen, P.V. and Heiselberg, P. (1997). Evaporation Controlled Emission in ventilated Rooms. *Proceedings of Healthy Buildings/IAQ '97,* Washington DC, USA, Vol. 3, pp. 557-562.

Topp, C., Nielsen, P.V., Heiselberg, P., Sparks, L.E., Howard, E.M. and Mason, M. (1998). Experiments on Evaporative Emissions in Ventilated Rooms. *Proceedings of ROOMVENT '98,* Stockholm, Sweden, Vol. 1, pp. 499-505.

Van der Wal, J.F., Hoogeveen, A.K. and Wouda, P. (1997). The Influence of Temperature on Emission of Volatile Organic Compounds from PVC flooring, Carpet, and Paint. *Indoor Air,* Vol. 7, pp. 215-221.

Verhoff, A. (1963). *The two-dimensional turbulent wall jet with and without an external stream.* Report No 626, Princeton University, Department of Aeronautical Engineering.

Versteeg, H.K. and Malalasekera, W. (1996*). An introduction to Computational Fluid Dynamics*. Addison Wesley Longman Ltd.

White, F.M. (1991-a). *Heat and Mass Transfer*. Addison-Wesley.

White, F.M. (1991-b). *Viscous Fluid Flow*. McGraw-Hill, Inc.

Wilcox, D.C. (1994). *Turbulence Modeling for CFD*. DCW Industries, Inc.

Wolkoff, P. (1995). Volatile Organic Compounds - Sources, Measurements, Emissions, and The Impact on Indoor Air Quality. *Indoor Air*, Supplement No. 3.

Wolkoff, P. (1996). Characterization of Emissions from Building Products: Long-Term Chemical Evaluation. The Impact of Air Velocity, Temperature, Humidity, Oxygen and Batch/Repeatability in the FLEC. *Proceedings of INDOOR AIR '96*, Nagoya, Japan, Vol. 1, pp. 579-584.

Wolkoff, P. (1998). Impact of air velocity, temperature, humidity and air on long-term VOC emissions from building products. *Atmospheric Environment*, Vol. 32, No. 14/15, pp. 2659-2668.

Wolkoff, P. and Nielsen, P.A. (1995-a). A New Approach to Label the Emission of VOCs from Building Products. Part I: The Technical Background. *Proceedings of Healthy Buildings '95*, Milan, Italy, Vol. 2, pp. 887-892.

Wolkoff, P. and Nielsen, P.A. (1995-b). A New Approach to Label the Emission of VOCs from Building Products. Part II: Assumptions, Limitations and Indoor Comfort Evaluation. *Proceedings of Healthy Buildings '95*, Milan, Italy, Vol. 2, pp. 893-898.

Yaglou, C.P., Riley, E.C. and Coggins, D.I. (1936). Ventilation requirements. *ASHVE Transactions*, Vol. 42, pp. 133-162.

Yang, X., Chen, Q. and Bluyssen, P.M. (1998). Prediction of Short-Term and Long-Term VOC Emissions from SBR Bitumen-Backed Carpet Under Different Temperatures. *ASHRAE Transactions*, Vol. 104, part 2, pp. 1297-1308.

Zhang, J.S., Shaw, C.Y., Kanabus-Kaminska, J.M., MacDonald, R.A., Magee, R.J., Lusztyk, E. and Weichert, H.J. (1996). Study of Air Velocity and Turbulence Effects on Organic Compound Emissions From Building Materials/Furnishings Using a New Small Test Chamber. *Characterizing Sources of Indoor Air Pollution and Realated Sink Effects*, ASTM STP 1287,

Bruce A. Tichenor, Ed., American Society for Testing and Materials, pp. 184-199.

Zhang, Y. and Haghighat, F. (1996). A Small Velocity-Controlled Test Chamber for Emission Studies. *Characterizing Sources of Indoor Air Pollution and Realated Sink Effects*, ASTM STP 1287, Bruce A. Tichenor, Ed., American Society for Testing and Materials, pp. 23-33.

Zhang, Y. and Haghighat, F. (1997). The impact of Surface Air Movement on Material Emissions. *Building and Environment*, Vol. 32, No. 6, pp. 551-556.

LIST OF SYMBOLS

The list of symbols is divided into three parts: English symbols, Greek symbols and constants.

ENGLISH SYMBOLS

A	Source area (m^2)
c	Concentration (kg/m^3)
$\bar{c}$	Mean value of concentration (kg/m^3)
c_∞	Concentration in bulk flow (kg/m^3)
c^+	Dimensionless concentration (-)
c_a	Concentration in air at gas phase (kg/m^3)
c_0	Inlet concentration (kg/m^3), initial concentration (kg/m^3)
$c_{0,p}$, $c_{0,s}$	Inlet concentration in primary and secondary test chamber, respectively (kg/m^3)
c_{max}	Maximum concentration (kg/m^3)
c_p	Specific heat (J/kgK)
c_s	Solid phase concentration (kg/m^3)
c_{s0}	Solid phase concentration corresponding to complete surface coverage in Langmuir model (kg/m^3)
c_v	Equilibrium vapour concentration (kg/m^3)
c_w	Concentration at surface (kg/m^3)
d	Thickness of pollutant source (m)
D	Molecular diffusion coefficient (m^2/s), Function in LRN turbulence model
D	Function in LRN turbulence model
D_{AB}	Molecular diffusion coefficient for diffusion of component A into component B (m^2/s)
D_{eff}	Effective molecular diffusion coefficient (m^2/s)
D_t	Turbulent molecular diffusion coefficient (m^2/s)
erf	The error function, $erf(x) = \frac{2}{\sqrt{\pi}} \int_0^x e^{-t^2} dt$
E	Function in LRN turbulence model

E_w	Emission from wall (kg/m^{2}s)
E_x	Local emission (kg/m^{2}s)
E^*	Non-dimensional emission (E_x/E_w)
f_2	Function in LRN turbulence model
f_μ	Function in LRN turbulence model
g_i	Gravity component (m/s^2)
h_{in}	Height of inlet opening (m)
h_{out}	Height of outlet opening (m)
J	Species flux (kg/m^{2}s)
J_0	Species flux at time zero (kg/m^{2}s)
k	Species flux decay constant (s^{-1}), Turbulent kinetic energy (J/kg)
k_c	Convective mass transfer coefficient (m/s)
k_0	Turbulent kinetic energy at inlet (J/kg)
K_L	Langmuir adsorption coefficient (m^3/kg)
K_p	Linear partition coefficient (-)
L	Characteristic length (m)
M	Amount of VOCs left in the source (kg/m^2)
M_0	Amount of VOCs applied (kg/m^2)
N	Fresh air change rate (h^{-1})
N_{re}	Recirculation air change rate (h^{-1})
N^*	Air change rate (h^{-1})
$\overline{p}$	Mean value of pressure (N/m^2)
Pr	Prandtl number (ν/α)
Pr_t	Turbulent Prandtl number (ν_t/α_t)
q_w	Wall heat flux (W/m^2)
Re_L	Reynolds number (uL/ν)
Re_x	Local Reynolds number (ux/ν)
$Re_{x,crit}$	Critical Reynolds number $(ux/\nu)_{crit}$ regarding instability
R_t	Turbulent Reynolds number ($\rho k^2/\mu_l\varepsilon$)
Sc	Schmidt number (ν/D)
S_c	Source term in concentration equation (kg/m^{3}s)
Sc_t	Turbulent Schmidt number (ν_t/D_t)
S_m	Source term in momentum equation (N/m^3)
S_T	Source term in temperature equation (°C/s)

Sh_L	Sherwood number ($k_c L/D$)
T	Temperature (°C)
Tu	Turbulence intensity (%)
t	Time (s)
$t(c_{max})$	Time at which c_{max} occurs (h)
T_∞	Temperature in bulk flow (°C)
T^+	Dimensionless temperature (-)
T_w	Temperature at wall surface (°C)
u	Velocity component in main flow direction (m/s)
u_τ	Shear velocity or wall friction velocity (m/s)
u_∞	Velocity component in bulk flow (m/s)
u^+	Dimensionless velocity (-)
u_i, u_j	Velocity component (m/s)
$\overline{u_i}, \overline{u_j}$	Mean value of velocity component (m/s)
u_0	Inlet velocity (m/s)
$\overline{u_i' u_j'}$	Turbulent stress (m^2/s^2)
$\overline{u_i' c'}$	Turbulent transport of species (kg/m^2s)
V	Volume of full-scale room (m^3)
x	Co-ordinate (m)
x_i, x_j	Co-ordinate (m)
y	Co-ordinate (m)
y^+	Dimensionless distance (-)
$y_w{}^+$	Dimensionless distance from the wall to the first grid point (-)
z	Co-ordinate (m)

GREEK SYMBOLS

α	Thermal diffusion coefficient (m^2/s)
α_t	Turbulent thermal diffusion coefficient (m^2/s)
δ_c	Thickness of concentration boundary layer (m)
δ_D	Thickness of diffusion boundary layer (laminar sublayer) (m)
δ_{ij}	Kronecker delta (=1 for $i=j$ and =0 for $i \neq j$)
δ_T	Thickness of temperature boundary layer (m)

δ_u	Thickness of velocity boundary layer (m)
$\delta_{1/2}$	Distance from the wall where $u=u_{max}/2$ (m/s)
ε	Dissipation rate of turbulent kinetic energy (J/kgs)
ε_0	Dissipation rate of turbulent kinetic energy at inlet (J/kgs)
μ	Dynamic viscosity (kg/ms)
μ_{eff}	Effective dynamic viscosity (kg/ms)
μ_l	Laminar dynamic viscosity (kg/ms)
μ_t	Turbulent dynamic viscosity (kg/ms)
ν	Kinematic viscosity (m^2/s)
ν_t	Turbulent kinematic viscosity (m^2/s)
ρ	Density (kg/m^3)
τ_w	Wall shear stress (N/m^2)

CONSTANTS

B	Constant in universal velocity profile ($\approx$5.0)
$C_{1\varepsilon}$	Constant in k-ε turbulence model (=1.44)
$C_{2\varepsilon}$	Constant in k-ε turbulence model (=1.92)
C_μ	Constant in k-ε turbulence model (=0.09)
κ	Kármán constant ($\approx$0.41)
σ_k	Constant in k-ε turbulence model (=1.0)
σ_ε	Constant in k-ε turbulence model (=1.44)

PH.D.-THESES ON INDOOR ENVIRONMENTAL ENGINEERING

THESIS No. 1: P. Heiselberg: *Strømningsforhold i lokaler ventileret efter opblandings- og fortrængningsprincippet.* ISSN 0902-7513 R9015.

THESIS No. 2: P. Kofoed: *Thermal Plumes in Ventilated Rooms*. ISSN 0902-7513 R9156.

THESIS No. 3: M. Skovgaard: *Turbulent Flow in Rooms Ventilated by the Mixing Principle*. ISSN 0902-7513 R9145.

THESIS No. 4: L. Germann: *REEXS - Reinforced Exhaust System* (in Danish). ISSN 0902-7513 R9154.

THESIS No. 5: H. Overby: *Vertikale temperaturgradienter i rum med konvektive strømninger*. ISSN 0902-7513 R9312.

THESIS No. 6: T. V. Jacobsen: *Airflow and Temperature Distribution in Rooms with Displacement Ventilation*. ISSN 0902-7513 R9328.

THESIS No. 7: U. Madsen: *Numerical Prediction of Dispersion and Local Exhaust Capture of Gaseous and Particulate Contaminants in Indoor Environment*. ISSN 0902-7513 R9419.

THESIS No. 8: P. S. Vinzents: *Assessment of Occupational Exposure to Dust and Other Selected Air Pollutants based on Measurements in Large Sturdy Populations*. ISSN 1395-7513 R9530.

THESIS No. 9: H. Brohus: *Personal Exposure to Contaminant Sources in Ventilated Rooms*. ISSN 0902-7953 R9741.

THESIS No. 10: J. Richter Nielsen: *The Influence of Office Furniture on the Air Movements in a Mixing Ventilated Room*. ISSN 1395-7953 R9837.

THESIS No. 11: Claus Topp: *Diffusion and Evaporation-Controlled Emission in Ventilated Rooms.* ISSN 1395-7953 R9917.

ISSN 1395-7953 R9917

Dept of Building Technology and Structural Engineering
Aalborg niversity September 1999
Sohngaardsholmsve 57 D -9 Aalborg Denmar
hone 5 9 35 a 5 9 1 3
http iee civil auc d